Study on Performance Improvement of GaN-based Light Emitting Diodes Grown on Silicon (111) Substrate

シリコン(111)基板上窒化ガリウム系

発光ダイオードの特性改善に関する研究

March 2012

Youhua Zhu (朱　友華)

Contents

Chapter 1

Introduction

1.1 Background of This Research

In the last century, many progress in silicon fabrication technology has been created to information society in industry. These progress in information technology industry further has been demanded for immediate and low-latency access for a large volume of date, which then has merged into information and communication technology (ICT). Worldwide spreading of internet is the core factor, which has already pushed rapid development in the industry. Moreover, since the early 21st century, a new ubiquitous society has started to be born through the advancement in ICT industry. In ubiquitous society, access to information is anytime, anywhere, with anyone and with anything [1].

As a result for information accessibility in this society, copper-based cable communication can no longer serve the large volume of information at low-latency, which then pushed for optical-based communication like fiber-optics. Cell phone previously a medium for voice communication has emerged into smart phone, which can carry voice, video, and date communications, demanding for more base stations with more efficient use of wavelength to serve the growing volume of date transmission. Radio and video broadcast through analog wave signal need to be converted into digital signal to significantly improve radio wave utilization, while at the same time broadcasting more imformation with better quality to the audiences. Vehicles previously a solely mechanical products with combustion engine, have emerged into smart vehicles with mechanical-electrical hybrid engine, supported by intelligent transportation system

for improved safety, security and efficiency in surface transportation system.ubiquitous society has demanded for enormous utilization of resources and electricity. The vast amounts of date also need to be efficiently stored and archived, which demanded for higher density date storage [1].

Fortunately for the material system, III-nitride-based materials can be applied in wide area of optoelectronics and electronics products. As shown in Fig. 1.1, the wide bandgap energy of III-nitride alloys from 0.7 eV for InN to 6.2 eV for AlN can cover the whole light spectrum from deep ultra-violet until IR regin.

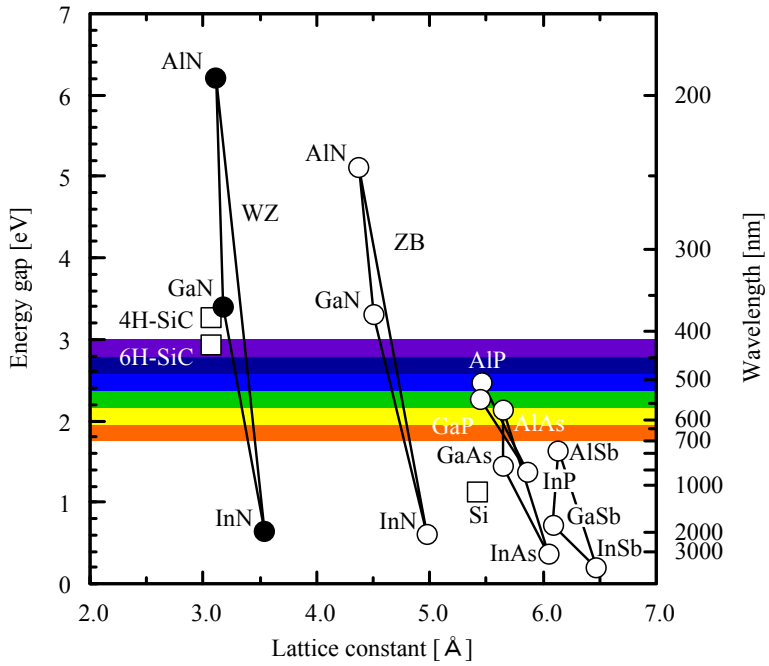

Fig. 1.1. Band-gap energy as a function of lattice constant for common semiconductor materials including III-nitride alloys.

Nowaday, the new history will be written in the 21 century. During the course of society developing, human will be confused when meeting some more serious problems, such as water, food, environment and so on. It is believed that the most important problem should be limitation of resource, especially, regarding energy problem, the corresponding measures must be immediately taken into accounted in the

future. The world-wide photo, which was taken from satellite in the sky for the electrical light in the night, is shown in the Fig. 1.2. Based on this figure, comparing the different area, it is obvious that energy consumption is losing its balance because of technology and economy gap. Nevertheless, the responsibility of saving engery will become to be more and more significant in the following years. Consequently, it can be expected that the development of wide band-gap nitride-based material research would give its contribution for solving or relieving these scoiety problems.

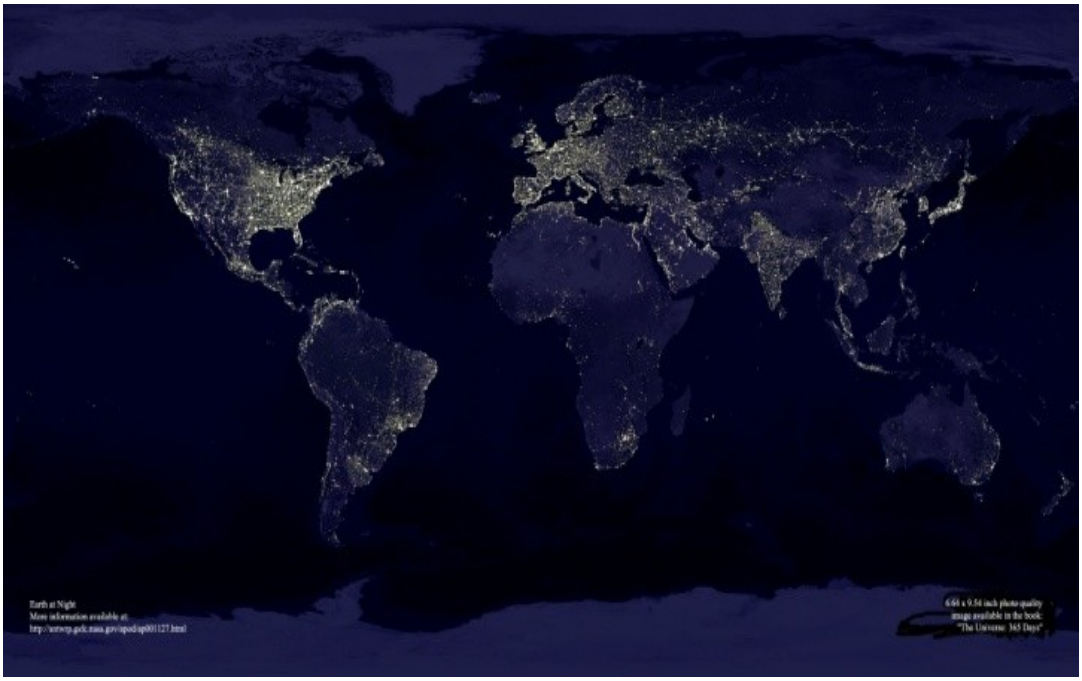

Fig. 1.2.The world-wide satellite photo of electrical light in the night [2].

Actually, gallium nitride technology was once deemed too expensive to replace silicon technology. However, if some successes can be made in the growing high qulity GaN on a silicon wafer, which would make the technology more economical. In terms of the Si substrate, the substrate costs around fifty cents per square centimetre, which is much cheaper than the usual substrates, such as sapphire or SiC, which cost about five dollars, or even twenty dollars/cm^2 in the case of SiC. Moreover, using silicon, large wafers measuring thirty centimetres in diameter can be produced, which is not possible

with sapphire and SiC.

However, because GaN and silicon have different material properties, it is difficult to combine the two materials on a wafer, cracks may form during heating, for instance, as the materials expand to a different degree. Recenty, lots of rearch group, including our group, have found ways to grow high qulity GaN on silicon and solved around this problem. As aforementioned, most transistors in the world are still based on silicon. This semiconductor does not just serve as a substrate, but also the base material of transistors and chips. That is, pretty much everything in electronics is still made of silicon. It's a fabulous material. Unfortunately, silicon also has its drawbacks. At high temperatures above 200°C silicon-based components begin to malfunction. On the other hand, the present popular and active research target, that is, GaN transistors, can withstand temperatures of up to 1000°C, which makes the material attractive for building sensors in car engines.

Moreover, GaN can withstand electrical fields that are up to fifteen times stronger than in silicon, the electrons also move more quickly in GaN than in silicon, which enables faster circuitry. In fact, this is especially important for telecommunications since the information is processed more rapidly and efficiently. Thanks to its heat resistance, power electronics made of GaN barely requires cooling. If the base stations of mobile communications installations were equipped with GaN transistors, for instance, the providers would not need power-guzzling cooling systems. In addition, conventional base stations require ten kilowatts input to emit just one kilowatt. Therefore, a lot of energy is thus wasted, which ultimately costs the environment and consumers dearly. If silicon electronics were to be replaced with GaN-Si electronics, a lot of energy could be saved. As well known, gallium nitride is

therefore just the ticket for use in many areas of electronics, especially power electronics. Herein, it should be noted that GaN can help to save energy in lighting, which is currently responsible for a fifth of the global electricity consumption. A five-watt LED lamp based on GaN, however, generates the same amount of light as a conventional sixty-watt bulb, which makes enormous energy savings possible. The same also goes for voltage conversion in appliances. When plugging a PC into a 230-volt socket, a converter inside the appliance provides the right voltage to the chips, such converters can be more efficient with GaN technology. Experts have already estimated that the global energy consumption could be reduced by a quarter if the energy were used intelligently at the place of consumption. One of the most important things is, that GaN transistors have shown to be lightning-fast and allow frequencies of up to 205 gigahertz, it is more than enough to make computers, mobile phones, and power electronics quicker, smaller and more economical [3].

General speaking, everything is there to help this technology make a break through. What's lacking is an industrial partner that wants to launch gallium nitride silicon electronics on the market. At the same time, just why telecommunications companies did not already convert to GaN technology, the answer is very clear, because the conversion costs a huge sum of money. In the ideal scenario, silicon components could be replaced with GaN power electronics when required. Consequently, it can be imagined that support for the changeover will come from the political arena: introducing a strict CO_2 emission guidelines, for instance, would encourage companies to reduce their energy costs. This would incite telecommunications companies for example to invest in greener technologies and to reduce CO2 emissions. Also, people can look forward to realizing the almost ultimate dream some day.

1.2 Development of Wide Band-gap Nitride-based Light Emitting Diodes

As well known, stupendous progress has been made in development of the III-nitride AlN, GaN, InN, and their family of material alloys for optoelectronics and electronics applications since last century [4-5]. Wurtite InN, GaN, and AlN have direct room-temperature bandgaps of 0.7 eV, 3.4 eV, and 6.2 eV respectively [6] The entire spectral region, from infrared to ultraviolet, can be covered, which is impossible with the other III-V materials system, such as gallium Arsenic (GaAs)-based and phosphide (P)-based alloys. It makes the nitride system be attractive for optoelectric device applications, such as light-emitting diodes (LED), laser diodes (LD), and detectors, in particular, the combination of GaN-based blue and green LEDs with GaAs-based red LEDs forms for full-color displays and solid-state white light illumination. At present, incandescent bulbs and fluorescent lamps are used as light sources and many applications, which have poor reliability, durability, and a low luminous efficiency. By using a solid-state white light source to replace the conventional incandescent bulbs or fluorescent lamps would provide not only a longer life time, but also reduce the power consumption. Also, III-nitride materials are promising for high temperature/high power/high breakdown field applications.

On the other hand, the first electroluminescence from GaN was announced at the Radio Corporation of America (RCA) in the summer of 1971 by Jacques Pankove et al. At that time, the sample consisted of an insulating Zn-doped layer which was contacted with two surface probes, and blue light centered at 475 nm was emitted [7] as presented in Fig. 1.3. Then, they made a device consisting of a metal-insulator -semiconductor (MIS) diode. This was the first current-injection GaN light emitter [8].

In April 1972, the RCA team (Paul Maruska et al.) decided that magnesium (Mg) might be a better choice of p-type dopant than zinc. They began growing Mg-doped GaN films using the Halide Vapor Phase Epitaxy (HVPE) technique, and on July 7, 1972, got a blue and violet emission at 430 nm [9]. These devices were inefficient due to lack of p-type conductivity, even though they were Mg doped, the luminescence in these films was probably mediated by minority carrier injection or impact ionization in the high-field insulating region of the films. Unfortunately, at the beginning of 1974, the RCA Corporation was collapsing as revenues plunged. Therefore, the corresponding blue LED project was cancelled. In the years subsequent to the collapse of RCA, work on GaN virtually ceased everywhere, and in 1982 only a handful of papers were published world-wide on this material.

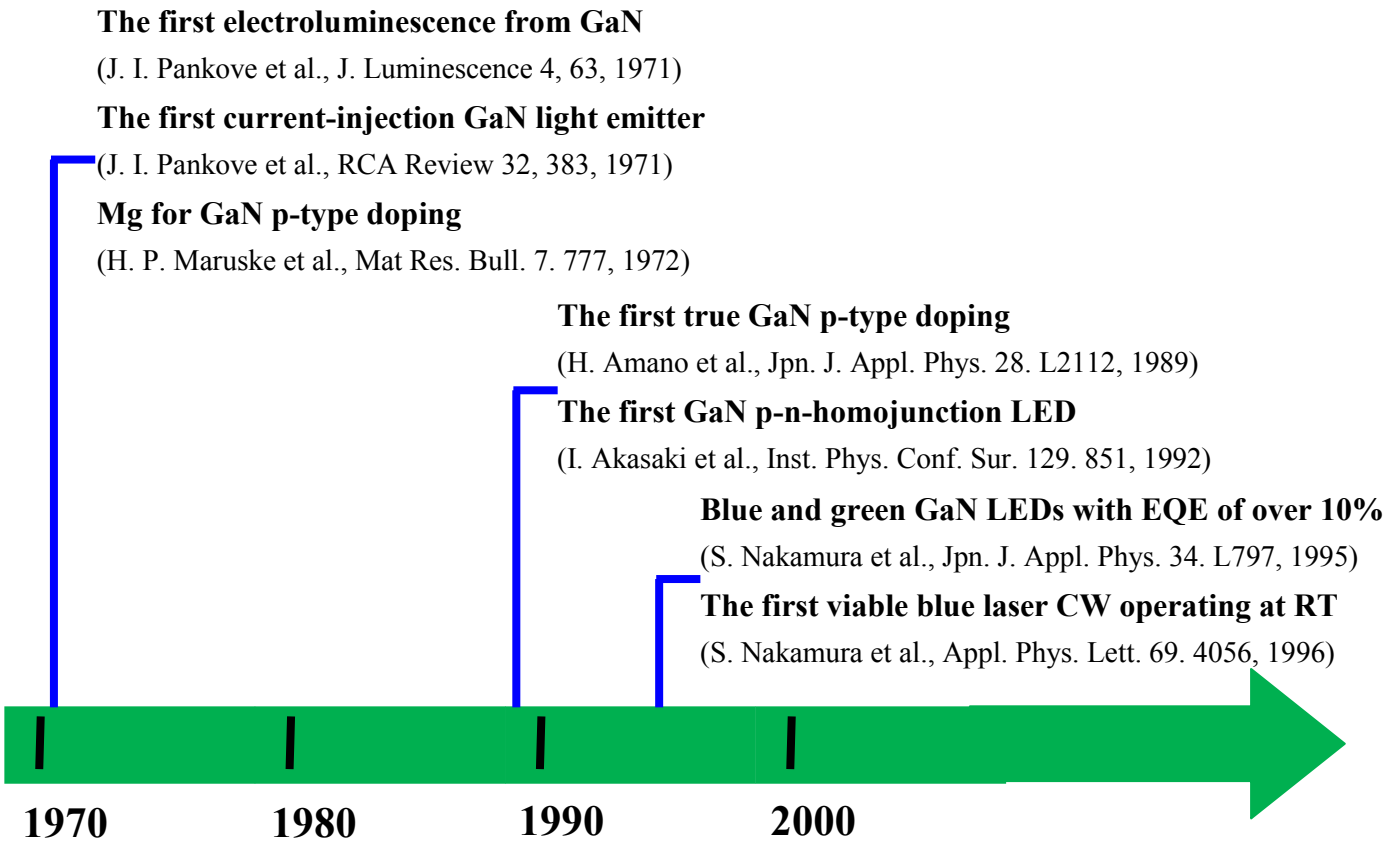

Fig. 1.3. Evolution of III-nitride-based semiconductor.

However, Isamu Akasaki and co-workers Amano et al. in Nagoya of Japan didn't want to give up. They succeeded in growing the first high quality GaN single crystal in the world by using the LT-AlN buffer layer in 1985 [10], and finally in 1989, they continued to demonstrate the first true p-type doping, with achieving conducting material with electron-beam annealed Mg-doped GaN [11]. In 1992, the first GaN p-n-homojunction LED was reported by Akasaki et al [12]. The efficiency of the LED is approximately 1%, which is not affected by dislocations in the same adverse manner as III-V As-based and P-based light emitters. In 1992, p-type GaN was also produced by thermal annealing of Mg-doped GaN grown with the LT-GaN buffer layer by Nakamura et al. at Nichia Chemical Industries [13]. In 1995 they developed blue and green GaN hetero-structure LEDs with the efficiencies of exceeding 10% [14] and demonstrated the first viable blue laser pulse and CW operating at room temperature in 1996 [15]. With these technique developments and achievements, much progress is expected in the area of solid-state lighting. The history of improvement in the efficiency for light emitting diodes is shown in Fig. 1.4, from which the trend of LEDs can also be judged. And, some data about the incandescent and fluorescent lamp are also presented.

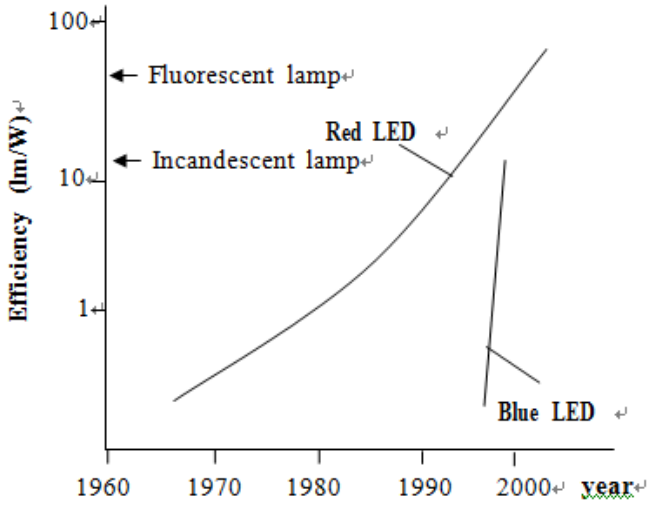

Fig. 1.4. The history of improvement in the efficiency for LED.

1.3 Brief Introduction of This Dissertation

This research focuses on improving the characteristics of GaN-based light emitting diodes grown on Si(111) substrate, by using the 3C-SiC/Si(111) templet substrate and increasing the thickness of n-GaN. These approaches have resluted in a significant improvement in controlling threading dislocation density (TDD), electrial and optical properties. Herein, it is worthy noting that the corresponding purpose of this study is to impove the performance of the LEDs grown on Si substrate. In additon, during the epitaxial growth of LEDs on 4-inch Si substrate, it is important to understand the evolution of GaN epilayer strain. These study topics will be discussed in this thesis.

The dissertation composes of seven chapters and each of them is summarized as following:

Chapter 1 gives brief introduction about the technological progress, which demands for a more cost efficient electronic and optoelectronic devices, such as in high-density storage, light emitting diodes, etc. Then, some explanations on the development of GaN research is also described.

In chapter 2, a few established growth techniques are described for GaN-based epitaxy on conventional substrates, such as Si, sapphire, SiC, GaN free-standing substrate. Also, further detailed growth mechanism for GaN hetero-epitaxy on Si(111) substrate is discussed, it is the fundamental subject for this study, Needing for GaN-based electronic and optoelectronic devices grown on low cost Si substrate is eager to match the challenging progress of the industry.

Chapter 3 presents major characterization method essential for GaN-based

epitaxial crystalline and devices, such as, X-ray diffraction (XRD), transmission electron microscopy (TEM), and device characterization measurement. It should be noted that samples in these studies have been grown by means of MOCVD system.

Demonstration on GaN-based light emitting diodes grown on 3C-SiC/Si(111) is described in chapter 4. This study suggests that using the 3C-SiC interlayer is one of effective approaches to improve the performance of GaN-based LEDs grown on Si substrate.

In chapter 5, regarding to the mechanism on the improvement of GaN-based LEDs by inceasing the n-GaN thickness is presented. It is worth noting that the size of the Si substrate is 4 inches. On the other hand, stain evolution in GaN-based LEDs with different n-GaN thickness is discussed in chaper 6.

The conclusions of these studies are summarized in chapter 7. In addition, suggestions for further improvements in epitaxial quality and LEDs performance are also proposed in the same chapter.

Finally, acknowledgements are presented. Also, in the ending of this dissertation, some information of the publication and conference is listed.

References

[1] B. A. B. Ahmad Shuhaimi, *Research on Improvement of GaN-based Light Emitting Devices Grown on Silicon (111) Substrate*. Ph. D. Thesis, ch.1 March, (2010).

[2] R. E. Smalley, Energy & Nano Technology, Conference, Rice University. May. 3, (2003).

[3] Compound Semiconductor, "GaN-on-silicon transistors are faster and smaller", Sept. 27, (2011).

[4] S. Nakamura, and S. F. Chichibu, *Introduction to Nitride Semiconductor Blue Lasers and Light Emitting Diodes*. London: Taylor & Francis, ch.1(2000).

[5] S. J. Peraton, C. R. Abernathy, and F. Ren, *Gallium Nitride Processing for Electronics, Sensors and Spintronics. London*: Springer-Verlag, ch. 3 (2006).

[6] H. Morkoc, *Handbook of Nitride Semiconductors and Devices*. Weinheim: Wiley-VCH, , ch. 1(2008).

[7] J. I. Pankove, E. A. Miller, D. Richman, and J. E. Berkeyheiser, J. Lumin. **4**, 63 (1971).

[8] J. I. Pankove, E. A. Miller, D. Richman, and J. E. Berkeyheiser, RCA Review, **32**, 383(1971).

[9] H. P. Maruska, W. C. Rhines, and D. A. Stevenson, Mat. Res. Bull. **7**, 777 (1972).

[10] H. Amano, N. Sawaki, I. Akasaki, and T. Toyoda, Appl. Phys. Lett. **48**, 353 (1986).

[11] H. Amano, M.Kito, K. Hiramatsu, and I. Akasaki, Jpn. J. Appl. Phys. **28**, L2112 (1989).

[12] I. Akasaki, H. Amano, K. Itoh, N, Koide, and K. Manabe, GaAs and Related Compounds conference, Inst. Phys. Conf. Ser.,**129**, 851 (1992).

[13] S. Nakamura, T. Mukai, M. Senoh and N. Iwasa, Jpn. J. Appl. Phys. **31**, L139 (1992).

[14] S. Nakamura, M. Senoh, N. Iwasa, and S. Nagahama, Jpn. J. Appl. Phys. **34**, L797 (1995).

[15] S. Nakamura, M. Senoh, S. Nagahama, N. Iwasa, T. Yamada, T. Matsushita, Y. Sugimoto, and H. Kiyoku, Appl. Phys. Lett. **69**, 4056 (1996).

Chapter 2

Ⅲ-Nitride Epitaxial Growth by MOCVD

2.1 Introduction

Nowaday, it is believed that one of the hottest research areas is in the GaN-based material system , which has always been actively studied because of many applications in high-performance device, such as high-density optical data storage, light emitting diodes for illumination and power electronics. However, the biggest hindrence in the early starting years of GaN-based epitaxty growth is no nutural GaN substrate, which has incited researchers to depend on epitaxial growth using different substrate materials, that is called to hetero-epitaxy. Therefore, the corresponding substrate, at least, whose constants in the lattice and themeal expansion coefficient should be nearly matched to the ones of GaN. Normally, Si, sapphire, SiC, and GaN substrates have been employed in the research.

2.2 Substrate Comparison for GaN Epitaxial Growth

GaN-based materials have been usually grown on sapphire substrate due to its considerably good properties and variable applications. However, sapphire has a few limitations, such as its native physical property as an insulator, it prevents fabrication of device with vertical-type electrode structure. Also, sapphire has a relatively low thermal conductivity, which restricts thermal dissipation in high-power devicess. On the other hand, maximum diameter size for sapphire wafer is limited to 4 inches, it will hinder commercial mass production of GaN.

Hetero-epitaxy of GaN on 6H-SiC has been tremendously investigated by several groups [5,6], with the successful fabrication of electronic and optoelectronic devices, such as high electron mobility transistor (HEMT) [7], light emitting diode (LED) [8], and laser diode (LD) [9,10]. However, 6H-SiC substrate has limited availability, restricted to small diameter size and relatively far more expensive than sapphire and silicon substrate, which limits mass production quantity and interests for device fabrication.

As well known, homo-epitaxy of GaN on free-standing GaN substrate has reached dislation density as low as 10^6 cm^{-2} [11]. In addition, such substrate has maximum diameter size of only 2 inches and very limited availability, which leads to its price to become extremely expensive. Therefore, it is only employed in high-performance devices, for which the corresponding low disloction density is significant necessary such as blue-violet LD.

While epitaxy growth technology of GaN on sapphire, 6H-SiC and GaN free-standing substrate can be already considered well established, there are lots of demands for the other breakthrough for GaN-based epitaxy on silicon (Si) substrate. Regarding the Si substrate, there are many charming points, for instance, excellent availability, large diameter size of up to 12 inches, and very low cost. The best advantage in successful growth of GaN-based devices with well-established Si-based electronic device, for example, integrated-circuits, photo-detector, and so on, allowing fabrication of multi-fuction hybrid device on a single wafer.

Comparing with sapphire substrate, Si is a native semiconductor, its electrical conductivity can be controlled by doping, allowing the fabrication of devices with

vertical-type electrode structure. Si has better thermal conductivity than sapphire, which improves thermal dissipation, in particular, for high-temperature device operation. Some parameters can be referred in the Table II-I.

Table II-I: Comparison of substrate for GaN epitaxial growth [1-4].

			GaN	AlN	Si(111)	6H-SiC	sapphire
lattice constant	a	(Å)	3.189	3.11	5.43	3.08	4.758
	c	(Å)	5.185	4.98	-	15.12	12.991
thermal conductivity		(W./cmK)	1.3	2.85	1～1.5	3.0～3.8	0.5
thermal expansion	in-plane	($\times 10^6$/K)	5.59	4.2	2.59	4.2	7.5
lattice mismatch GaN/substrate		(%)	-	2.4	-16.9	3.5	-16
thermal mismatch GaN/substrate		(%)	-	33	116	33	-25

However, GaN epitaxy on Si substrate is more challenging than that of on sapphire or SiC substrates. Large thermal coefficient mismatch of 116% between the GaN and Si is thought as the main reason for cracks(as shown in Fig. 2.2-b) to occur during cooling down after growth, even though lattice constant mismatich for GaN/Si(111) of -17% is almost similar to GaN/sapphire of 16% as shown in Fig. 2.1. At the same time, the mechanism of strain happening is shown in the Fig. 2.1. On the other hand, GaN-Si reaction during growth causes amorphous meltback-etching layer (Fig. 2.2-c) when using conventional growth technology (Fig. 2.2-a). Then, Si gas from the substrate caused low-doping density in p-type GaN epitaxial layer. These growth challenges have been presented by many approaches of buffer layer techniques to obtain high quality GaN epitaxy on Si substrate.

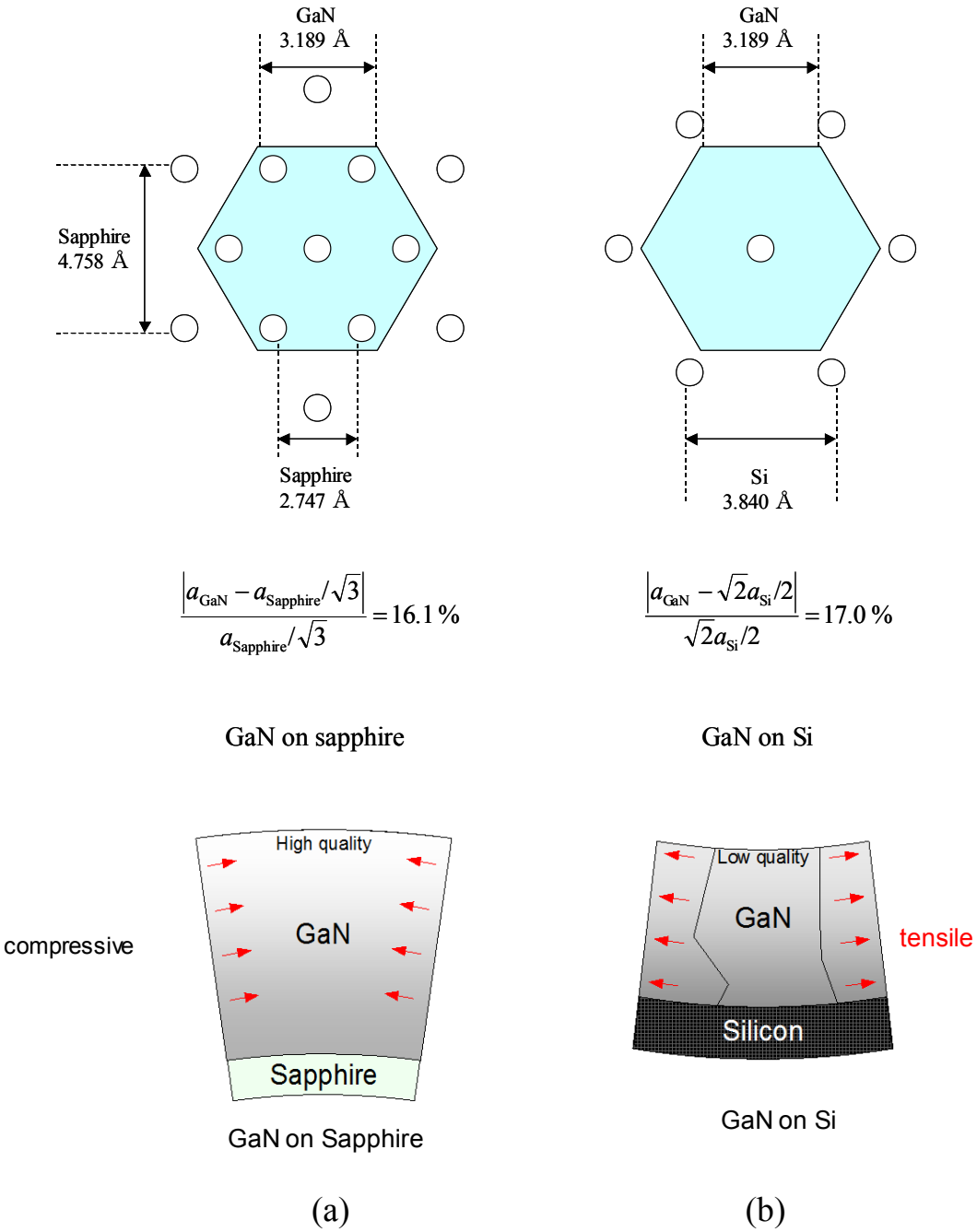

Fig. 2.1. Mechanism of lattice mismatch and strain happening in GaN grown on (a) sapphire substrate and (b) Si (111) substrate.

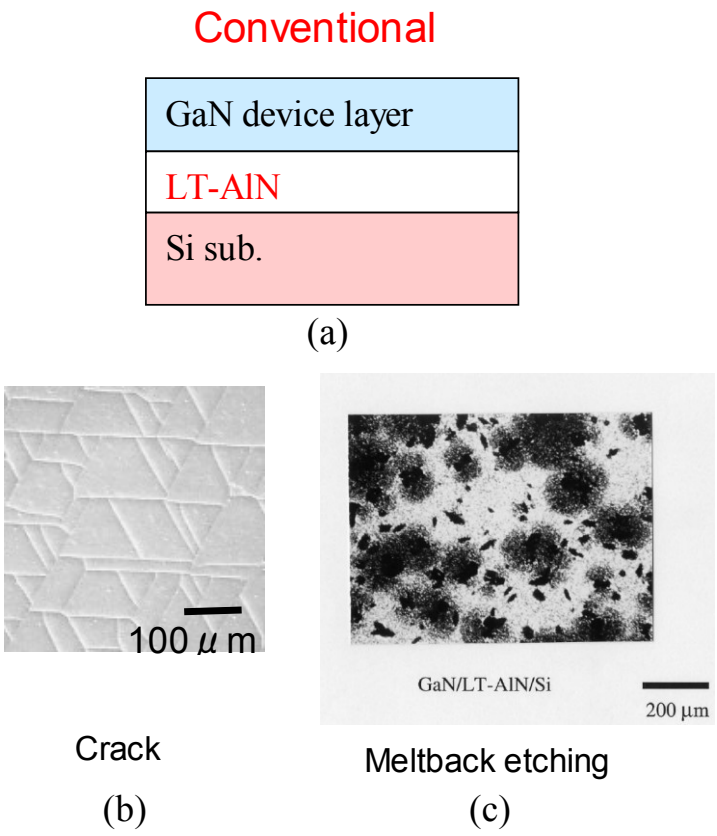

Fig. 2.2. (a) Conventional GaN epitaxial growth method, (b) Some cracks have occurred on the surface, and (c) image of meltback etching.

GaN epitaxy on Si substrate has typical dislocation density of around 10^{9}-10^{11} cm^{-2} [12], and can still be improved by optimizing its growth techniques. However, as shown in Fig. 2.2, GaN grown on Si with low-temperature AlN layer is more prone to cracks when the growth temperature is cooled down to room temperature (RT), which results from the large thermal expansion difference and lattice mismatch. In the case of sapphire substrate, GaN epilayer undergos compressive strain when growth temperature is returned to RT. In contrast, GaN epilayer grown on Si substrate suffers tensile stress when growth temperature is cooled down to RT making Si substrate more prone to cracks comparing with sapphire sustrate, especially, when the GaN thickness is over 1 μm.

This research concentrates on GaN epitaxy on Si substrate grown with high-temperature AlN nucleation layer and AlN/GaN strained-layer superlattice (SLS), Further improvement on material and optical properties have been realized by using the template of 3C-SiC/Si(111) and increasing the n-GaN thickness to 2 μm.

2.3 GaN Epitaxial Technique Grown on Si Substrate

Buffer and intermediate layers have been extensively investigated by many research groups for GaN growth on Si substrate, such as Al/AlGaN buffer and AlN/GaN SLS [13-16], AlN interlayer [17] and Si_xN_{1-x} interlayer [18]. This research focuses on crystalline quality improvement for GaN epitaxy on Si substrate by using the template of 3C-SiC/Si(111) and increasing the n-GaN thickness to 2 μm. Variable buffer and/or intermediate layer growth techniques as aforementioned above, including epitaxial lateral overgrowth (ELO) [19] and pendeo epitaxial overgrowth (PEO) [20], are not discussed in this dissertation.

2.3.1 AlN/AlGaN Buffer Layer

AlN/AlGaN layer is used to prevent formation of meltback-etching when GaN epilayer is grown on Si substrate. It also acts as intermediate layer to create a high density nucleation growth. In the growth of sapphire substrate, high density nucleation growth is achieved by low-temperature GaN buffer layer. However, in the case of growth on Si substrate, low-temperature GaN buffer can not be used because of GaN-Si reaction, which has been already explained in the above section. Therefore, materials such as AlN and AlGaN, which are stable at high temperature are preferred for high density nucleation growth. Usage of AlN layer as nucleation layer for GaN growth on Si

substrate has been reported by many group [21-26]. While, this approach suffers poor surface flatness, it influences the subsequent layer growth. It is presented that 170 nm GaN layer has grown on the initial AlN nucleation layer [27], In addition, it depends on the Al composition, AlGaN has relatively better coating property and it easier to grow [28]. Consequently, AlGaN is considered as one of good candiates for intermediate layer. Our research group has presented AlN/AlGaN buffer layer to take advantage of the combined material properties [13-16]. That is, AlN layer which is stable at high-temperature is initially grown on Si substrate to create a high density nucleation layer, followed by AlGaN layer to obtain a layer with good smooth surface.

2.3.2 AlN/GaN Strained-layer Superlattice (SLS)

Multilayer and/or strained-layer superlattice (SLS) growth technology is significant to control crack generation in III-nitride-based semiconductor layer growth. In III-nitride layer growth on Si substrate, reactor temperature ramp-down to RT generates concave wafer curvature, and cracks on the epitaxial layer due to the difference of thermal expansion coefficient between III-nitride epitaxial layer and Si substrate, leading to the difficulty of thick GaN epitaxial layer, Thus, optimization in the epitaxial structure is necessary to successfully grow high quality crack-free thick GaN-based layer on Si substrate. The importance of growing thick epitaxial GaN layer can be expressed in the device structure, it is fortunate that improving the material quality can be realized as using AlN/GaN SLS in controlling wafer curvature and cracks. SLS is also effective to reduce misfit dislocations resulted from lattice mismatch of GaN-based epitaxial layer and the underlying Si substrate. Threading dislocation (TDs) can be modulated to prevent them from penetrating to the surface using SLS, an

approach which has already been used previously in GaAs-based growth on Si substrate [27,29-30]. When a stack of two types of material with different lattice constant is grown coherently, lattice strain is built upon the interface of the two different materials giving a strong strain when they are accumulated together. Therefore, TDs which reach the interface are bent by the strain, and reaction between inclined TDs will create dislocation close-loop, eliminating the TDs from penetrating vertically into the epitaxial surface. The SLS structure creates multiple bulit-up interface strain for TDs inclination, thus, it is possible to control penetrations of TDs into the subsequent epitaxial layers. If the lattice strain is weak, it is not possible to bend the treading dislocations causing it to penetrate through the SLS. Moreover, if the lattice strain is too large, new misfit dislocation might be built due to the strain. In this research, a SLS consisting of periodes of AlN and GaN stacks with respective layer thickness optimized values of 5 and 20 nm is employed as the fundamental intermediate layer, followed by further optimization in the succeeding layer.

2.4 MOCVD Equipment in This Study

In this reseach, a commercial MOCVD reactor system (Nippon Sanso SR-4000) has been used for the epitaxial growth of InGaN-based multiple-quantum wells (MQWs) LEDs structure. The photo of outward appearance is shown in Fig. 2.3. At the same time, Figure 2.4 shows the design schematics of the corossponding MOCVD reactor. Herein, it should be noted that epitaxial growth in our system can be used for one 4-inch or three 2-inch wafer. Also, the growth pressure can be easily controlled automatically in the range from low (100-300 torr) to normal air pressure (760 torr).

Fig. 2.3. The appearance of Nippon Sanso SR-4000 MOCVD system.

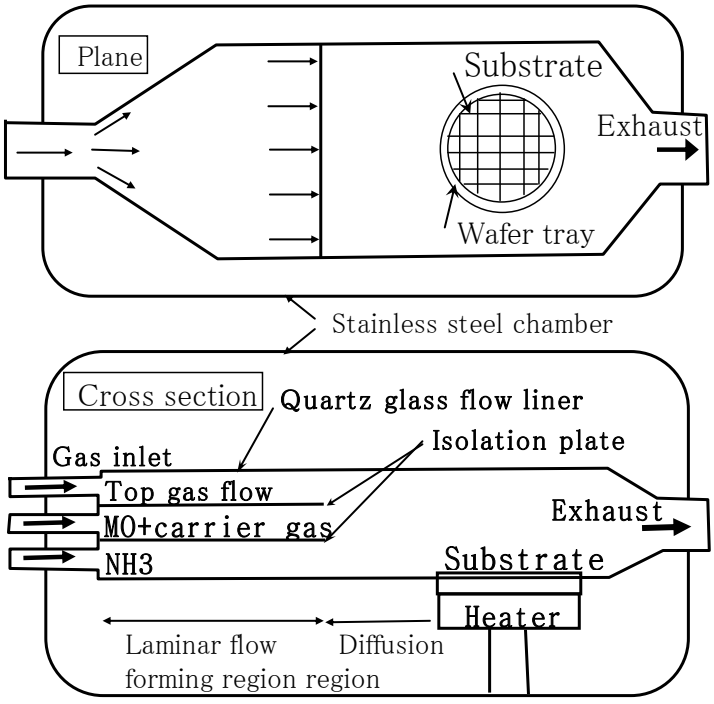

Fig. 2.4. The design schematics of the above MOCVD reactor.

2.5 Conclusions

This chapter describes buffer and intermediate layer growth techniques and their mechanism in improving crystalline quality for GaN epitaxy on Si substrate. In our GaN growth appoach on Si substrate, firstly, a thin AlN nucleation layer is grown initially on the substrate to prevent meltback-etching due to Ga-Si reaction, then, a little thick AlGaN layer is grown to improve surface routhness. Subsequently, a stack of AlN/GaN SLS is grown to suppress TDs, resulting in a high quality GaN epitaxy in the succeeding layer. The techniques described here is the basic techniques for further improvement carried out through this reasearch.

References

[1] S. Nakamura, S. Pearton, and G. Fasol, *The Blue Laser Diode,* Springer-Verlag, Berlin, Germany (2000)

[2] S. Nakamura, and S. F. Chichibu, *Introduction to Nitride Semiconductor Blue Lasers and Light Emitting Diodes*. Taylor & Francis, New York, USA (2000).

[3] J. Piprek, *Nitride Semiconductor Devices Principles and Simulation,* Wiley-VCH Verlag, Weinheim, Germany (2007).

[4] K. Takahashi, *Wide-Gap Semiconductor Optical and Electronic Device* , Morikita Publishing, Tokyo, Japan (2006).

[5] M. A. L. Johnson, S. Fujita, W. H. Rowland, K. A. Bowers, W. C. Hughes, Y. W. He, N. A. El-Masry, J. W. Cook, J. F. Schetzina, J. Ren, and J. A. Edmond, J. Vac. Sci. Technol. B. **14**, 2349 (1996).

[6] J. T. Torvik, M. Leksono, J. I. Pankove, B. V. Zeghbroeck, H. M. Ng, and T. D. Moustakas, Appl. Phys. Lett. **72**, 1371 (1998).

[7] J. Bernát, M. Wolter, A. Fox, M. Marso, J. Flynn, G. Brandes, and P. Kordoš, Electron Lett. **40**, 78 (2004).

[8] H. S. Kong, M. Leonard, G. Bulman, G. Negley, and J. Edmond, Mat. Res. Soc. Symp. Proc. **395**, 903 (2005).

[9] A. Kuramata, K. Hirino, and K. Domen, Fujitsu Sci. Tech. J. **34**, 191 (1998).

[10] J. Edmond, A. Abare, M. Bergman, J. Bharathan, K. L. Bunker, D. Emerson, K. Haberern, J. Ibbetson, M. Leung, P. Russel, and D. Slater, J.Cryst. Growth **272**, 242 (2004).

[11] S. Hashimoto, Y. Yoshizumi, T. Tanabe, and M. Kiyama, J. Cryst. Growth **298**, 871 (2006).

[12] Y. B. Pan, Z. J. Yang, Z. T. Chen, Y. Lu, T. J. Yu, X. D. Hu, K. Xu, and G. Y. Zhang, J. Cryst. Growth **286**, 255 (2006).

[13] T. Egawa, B. Zhang, N. Nishikawa, H. Ishikawa, T. Jimbo, and M. Umeno, J. Appl. Phys. **91**, 528 (2002).

[14] H. Ishikawa, K. Asano, B. Zhang, T. Egawa, and T. Jimbo, Phys. Stat. Sol. A **201**, 2653 (2004).

[15] T. Egawa, B. Zhang, and H. Ishikawa, IEEE Elect. Dev. Lett. **26**, 169 (2005).

[16] B. Zhang, T. Egawa, H. Ishikawa, Y. Liu, and T. Jimbo, Jpn. J. Appl. Phys. **42**, L226 (2003).

[17] A. Dadgar, Jpn. J. Appl. Phys. **39**, L1183 (2000).

[18] T. Riemann, T. Hempel, J. Christen, P. Veit, R. Clos, A. Dadgar, A. Krost, U. Haboeck, and A. Hoffman, J. Appl. Phys. **99**, 123518 (2006).

[19] E. Feltin, B. Beumont, P. Vennéguès, M. Vaille, p. Gibart, T.Riemann, J. Christen, L. Dobos, and B. Pécz, J. Appl. Phys. 93, 182 (2003).

[20] T. Gehrke, K. J. Linthicum, E. Preble, P. Rajagopal, C. Ronning, C. Zorman, M. Mehregany, and R. F. Davis, J. Electron. Mater. **29**, 306 (2002).

[21] A. Watanable, T. Takeuchi, and K. Hirosawa, J. Cryst. Growth **128**, 391 (1993).

[21] A. Watanable, T. Takeuchi, and K. Hirosawa, J. Cryst. Growth **128**, 391 (1993).

[22] A. Ohtani, K. S. Stevens, and R. Beresford, Appl. Phys. Lett. **65**, 61 (1994).

[23] P. Kung, A. Saxler, X. Zhang, D. Walker, T. C. Wang, I. Ferguson, and M. Razeghi, Appl. Phys. Lett. **66**, 2958 (1995).

[24] M. Godlewski, J. P. Bergmann, B. Monemar, U. Rossner, and A. Barski, Appl. Phys. Lett. **69**, 2089 (1996).

[25] J. M. Redwing, J. S. Flynn, M. A. Tischler, W. Mitzchel, and A. Saxler, Mater. Res. Soc. Symp. Proc. **395**, 201 (1996).

[26] F. Widmann, B. Daudin, G. Feuillet, Y. Samson, M. Arlery, and J. L. Rouviere, MRS Internet J. Nitride Semicond. Res. **2**, 20 (1997).

[27] H. P. D. Schenk, E. Feltin, M. Laugt, O. Tottereau, P. Vennegues, and E. Dogheche, Appl. Phys. Lett. **83**, 5139 (2003).

[28] K. Hirosawa, K. Hiramatsu, N. Sawaki, and I. Akasaki, Jpn. J. Appl. Phys. **32**, L1039 (1993).

[29] T. Soga, S. Hattori, S. Sakai, M. Takeyasu, and M. Umeno, J. Appl. Phys. **57**, 4578 (1985).

[30] A. Georgakilas, and A. Christou, J. Appl. Phys. **76**, 7332 (1994).

Chapter 3

Characterization for GaN-based Materials and Light Emitting Diodes

3.1 Introduction

Thin epitaxial film characterization and device evaluation are important to understand the phsical mechanism of materials, such as lattice defects, photonic transitions in the band-gap, and so on. In addition, the proper measurement and discussion are also necessary, especially, in terms of comprehension in the nano-scale crystalline level, it allows easily control of parasitic property, then, it will result in optimization of growth parameters to improve GaN-based epitaxial quality.

3.2 Lattice Defect

Most of GaN-based optoelectronics and electronic devices are hetero-epitaxially grown on three kinds of substrate such as Si, sapphire, and SiC. However, lattice mismatch and thermal expansion coefficient difference between GaN and substrate often lead to large quantity of lattice defects in the GaN crystalline. The lattice defect modifies active layer growth pattern, varies optical property, and deteriorates device performance. Therefore, understanding the characteristics of lattice Defect is essential to control or remove the defects.

In a conventional high quality GaN grown on c-face sapphire or SiC substrate using AlN or GaN buffer layer by MOCVD [1-2], the first several tens nanometer thickness after the hetero-epitaxial interface between GaN and substrate exhibits large

number of stacking faults and c-face defects to relax the strain in the layers. It is well known that, after the initial buffer layer, all other types of lattice imperfections disappear, leaving only threading dislocations (TDs) with a magnitude of 10^8-10^{10} cm^{-2} [3-5].

Lattice defects can be classified into point-defect, line-defect, and face defect. In GaN film, the normal type of lattice defect observed is line defect, that is called to dislocation, which extremely influences device characeristics, including its lifetime reliability.

Line defect can be devided to three kinds of type, they screw-disloction, edge-dislocation, and mixed-dislocation [6]. Figure 3.1 illustrates the mechanism of screw- and edge-dislocation in the c-plane GaN. In screw-disloction, the dislocation line and Burgers vetor are in parallel direction, while in edge-disloction, disloction lline and Burgers vector are in perpendicular direction. For screw-disloction, it occurs due to partial atomic step, with Burgers vector b=<0001>. On the other hand, edge-disloction occurs due to excess lattice penetration on (11-20) face, with Burgers vector in b=1/3<11-20> direction. Mixed-disloction is a mix of screw- and edge-dislocation, with Burgers vector b=1/3<11-23>. The line-defect described in this section is for hexagonal crystalline strucutre, which occurs when epitaxial growth is performed on c-face. GaN crystal structure exists in cubic zincblende and hexagonal wurzite structure. However, the later one is the meta-stable structure for GaN.

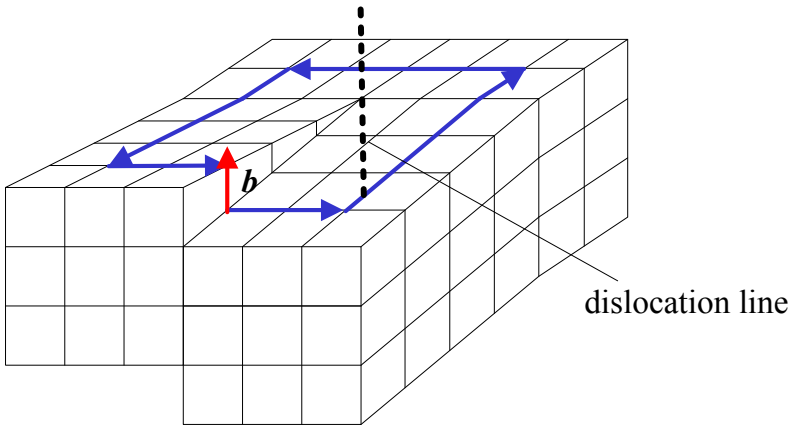

***b*=<0001>**

(a) screw dislocation

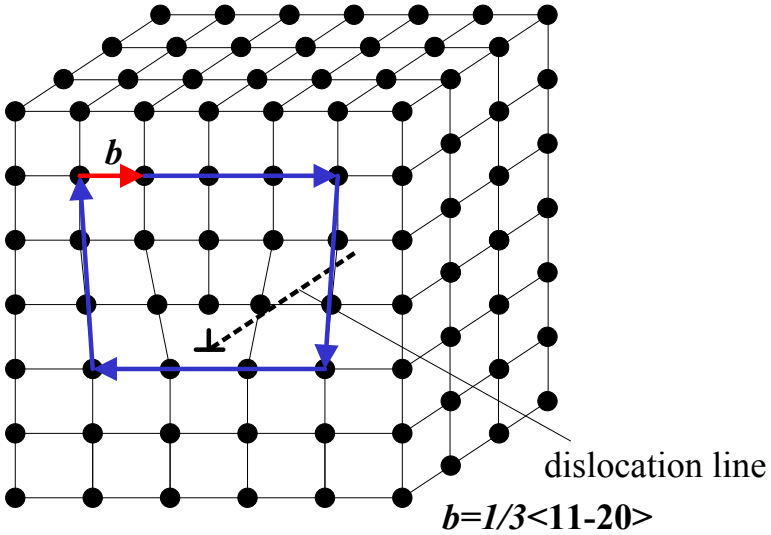

***b*=*1/3*<11-20>**

(b) edge dislocation

Fig. 3.1. Mechanism of dislocation (a) screw dislocation, (b) edge dislocation.

3.2.1 X-Ray Diffraction (XRD)

X-ray diffraction (XRD) ω-scan method is conventionally used to characterize structural qulity of GaN crystalline, because density of line defect influence the ω-scan full-width at half maximum (FWHM) line width. Increase of screw and mixed

component of the disloction increases tilt component in c-plane GaN, and thus increases FWHN line width of symmetric reflection in (0002) and (0004) diffraction peak. While, increase of edge and mixed component of the dislocation density increases twist component of c-plane GaN, and therefore increases FWHM line width of asymmetric reflection. The wavelength of the common x-ray resource is shown in Table III.I. In the XRD measurement of this research, the Cu-$K\alpha_2$ has been used.

Table III.I The wavelength of the common x-ray resource.

X-ray resource	wavelength (Å)		
	$K\alpha_1$	$K\alpha_2$	$K\beta$
Cr	2.2935	2.2896	2.0848
Fe	1.9399	1.9360	1.7565
Co	1.7927	1.7989	1.6208
Cu	1.5443	1.5405	1.3922
Mo	0.7235	0.7093	0.6323
Ag	0.5638	0.5594	0.7970
W	0.2188	0.2090	0.1844

As well known, Bragg diffraction occurs when electromagnetic radiation or subatomic particle waves with wavelength comparable to atomic spacings are incident upon a crystalline sample, are scattered in a specular fashion by the atoms in the system, and undergo constructive interference in accordance to Bragg's law. The Bragg diffraction is shown in Fig. 3. 2. For a crystalline solid, the waves are scattered from

lattice planes separated by the interplanar distance. Where the scattered waves interfere constructively, they remain in phase since the path length of each wave is equal to an integer multiple of the wavelength. The path difference between two waves undergoing constructive interference is given by 2dsinθ, where θ is the scattering angle. This leads to Bragg's law, which describes the condition for constructive interference from successive crystallographic planes (h, k, and l, as given in Miller Notation) [7] of the crystalline lattice:

$$2d\sin\theta = n\lambda \tag{3.1}$$

Where n is an integer, λ is the wavelength of incident wave, d is the spacing between the planes in the atomic lattice, and θ is the angle between the incident ray and the scattering planes.

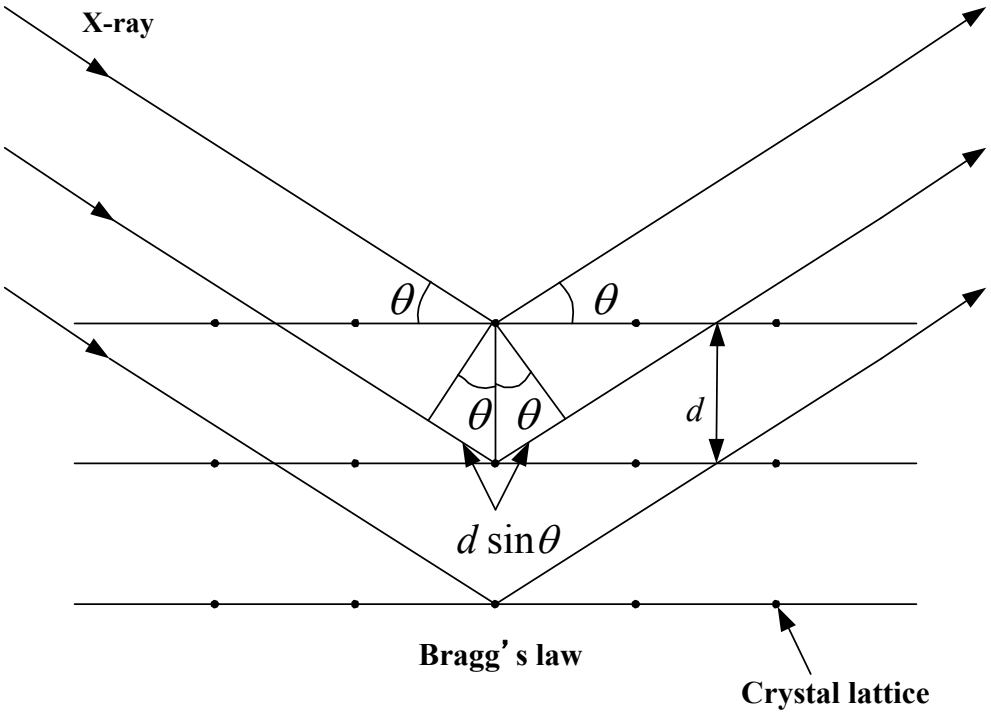

Fig. 3.2. The schematics of Bragg diffraction machanism.

While, the used system of XRD in this research is shown in Fig. 3.3. It should be noted that the resolution of XRD is high.

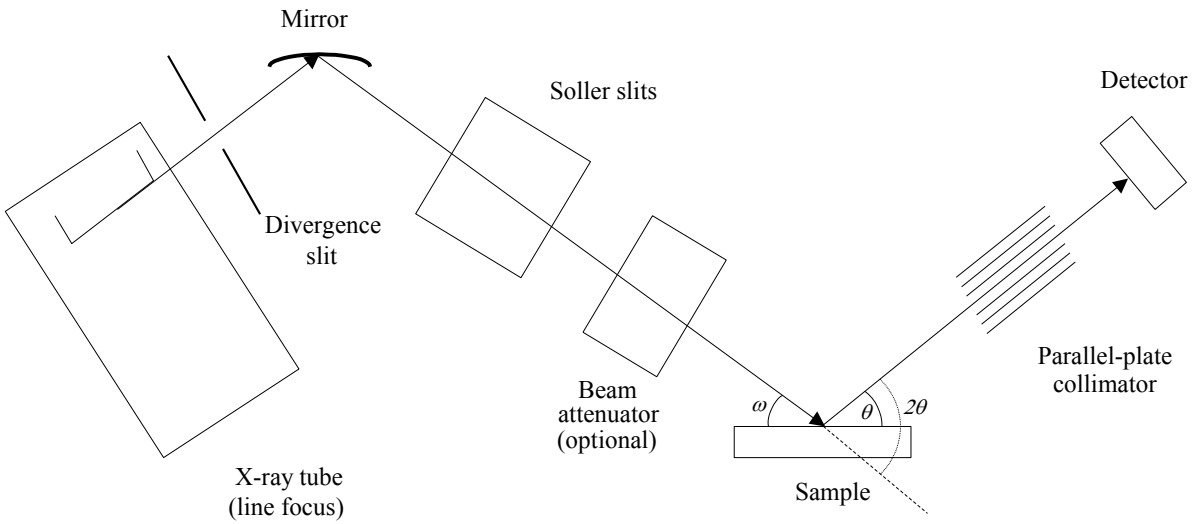

Fig. 3.3. The schematics of high-resolution XRD system.

3.2.2 Transmission Electron Microscope (TEM)

Characteristics of line defects can be analyzed by transmission electron microscopy (TEM). However, a proper measurment and enough time are necessary for sample preparation, prior to actual cross-sectional TEM observation. In cross-sectional TEM observation, when inversed lattice vector is g, and Burgers vector for line defects is b, line defects can be classified using $g \times b=0$ invisibility criterion. In particular, when g=<11-20>, Burgers vector b=<0001> that is perpendicular to this direction will eliminate visibility of screw dislocation component, showing only edge and mixed dislocation components. In g=<0002> direction, Burgers vectors b=1/3<11-20> at perpendiculare direction will eliminate visibility of edge dislocation component, indicating only screw and mixed dislocation components, Screw dislocation density is normally lower relative to that of edge dislocation density.

3.3 Luminescence Characteristics

Semiconductor materials are divided into two categories: direct-bandgap semiconductors and indirect-bandgap semiconductors, depending on the position of conduction band minimum point and valence band maximum point in k space of each material.

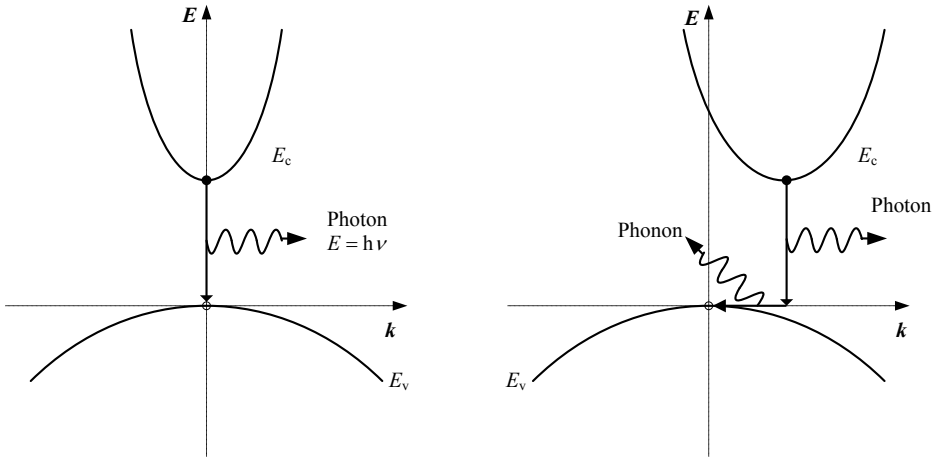

(a) Direct-Bandgap Semiconductor (b) Indirect-Bandgap Semiconductor

Fig. 3.4. Energy band structures of (a) direct-bandgap semiconductor and (b) indirect-bandgap semiconductor.

Materials such as GaN and gallium arsenide (GaAs) are called direct-bandgap semiconductors due to the fact that minima in the conduction-band and maxima in the valence-band occur at the same point in k space, as shown in Fig. 3.4 (a). On the other hand, materials such as silicon (Si) and germanium (Ge) are called indirect-bandgap semiconductors since the conduction-band minima and the valence-band maxima occur at different points in k space, as shown in Fig. 3.4 (b). For efficient emission of photon, energy and momentum must be conserved during electron transition from the conduction band minima to the valence band maxima. In a direct-bandgap semiconductor, electrons in the conduction band can fall to an empty state in the

valence band with only energy change, giving off the energy difference Eg as a photon of light. In indirect-bandgap semiconductors, electrons in the conduction band minimum cannot directly fall to the valence band maximum but must undergo a momentum change as well as changing its energy, which causes phonon emission (lattice vibration) rather than as an photon emission. This difference between direct and indirect band structures is very important in deciding which semiconductor materials can be used in devices requiring light output such as LEDs and LDs.

On the other hand, interaction between a photon and an electron in a solid involves three basic processes: absorption, spontaneous emission and stimulated emission. To demonstrate the processes, two energy levels E_1 and E_2 of an atom can be considered, where E_1 corresponds to the ground state and E_2 corresponds to the excited state, as shown in Fig. 3.5. Any transition between these states involves the emission or absorption of photon with frequency ν_{12} given by

$$h\nu_{12} = E_2 - E_1 \tag{3.2}$$

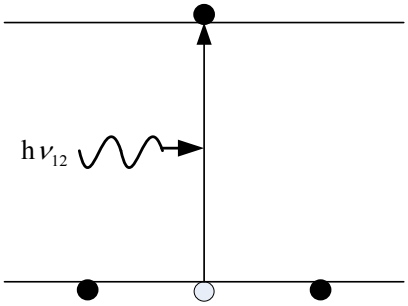

(a) Absorption

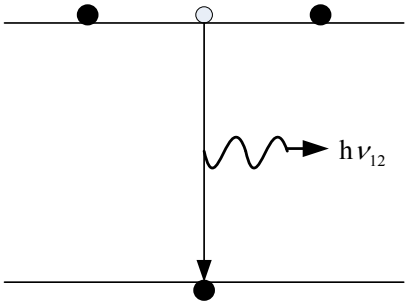

(b) Spontaneous Emission

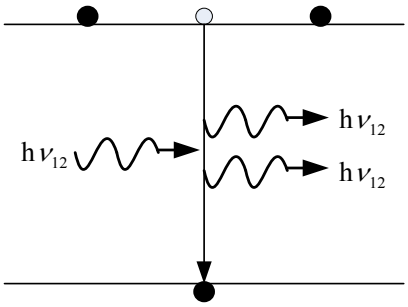

(c) Stimulated Emission

Fig. 3.5. Three basic transition processes between two energy levels. Clear dot indicates the state of an electron before transition, while black dot indicates the state of an electron after transition.

At room temperature, most of the atoms in a solid are at the ground state. This situation is disturbed when a photon of energy exactly equal to $h\nu_{12}$ impinges on the system. An atom in state E_1 absorbs the photon and thereby goes to the excited state E_2. The change in the energy state is absorption process, shown in Fig. 3.5(a). The excited state of the atom is unstable, so after a short time, without any external stimulus, the excited electron makes a transition to the ground state, giving off a photon of energy $h\nu_{12}$. This process is called spontaneous emission, shown in Fig. 3.5(b). When a photon of energy $h\nu_{12}$ impinges on an atom in the excited state (Fig. 3.5(c)), the atom can be stimulated to make a transition to the ground state and gives off a photon of energy $h\nu_{12}$, which is in phase with the incident radiation. This process is called stimulated emission. The radiation from stimulated emission is monochromatic because each photon has precisely an energy $h\nu_{12}$ and is coherent because all photons emitted are in phase.

Typical rediative recombination processes occurring in semiconductor are schematically illustrated in Fig. 3. 6. In general, luminescence spectra of high purity, high quality semiconconductors are dominated by free exciton (FE) emission at low temperature. The FE emission from wurtzite GaN at low temperature has been observed in the early 1970s by Pankove et al. [8] and Dingle et al. [9]. There are various forms of exciton complex that are composed of excitons and other particles [10]. Neutral donar has an outer electron, which turns around the donor ion with larger orbit diameter. It binds a free hole at the position where the static dipole between the hole and the neutral donor balances, and then charge neutrality of the complex is satisfied. This complex is

an exciton bound to a neutral donor (I_2) and is in general called a bound exciton (BE). Neutral acceptor also produces the bound exciton (I_1). Similarly, ionized donor and acceptor can produce excitons bound to them. The transition energy of BEs associated with neutral impurities is lower than that of Fes by their localization energy, $E_{loc,}$ which is nearly on tenth of the impurity ionization energy, E_a [11]. The relation between E_a and E_{loc} changes depend on material [12]. As E_{loc} is very small, BE recombination is dominant at very low temperatures and FE emission dominates the emssion spectrum at intermediate temperatures between 20 and 100 K, in general depending on the stability of excitons in the matrix. Another process involving excitons at low temperature is a formation of exciton-polariton, which is a complex between the electromagnetic (photons) and excitons (or oscillators) that have the same resonance frequency as the photons at finite value of very small wave vector, *k* [13-15]. The contribution of exciton-polariton in optical spectra of wurtzite GaN has been reported by Gil et al. [10,11] and Stepniewski et al. [12]. Excitons couple with several kind of phonons. A remarkable feature of the PL spectrum of GaN at low temperature is the appearance of longitudinal optical (LO) phonon replicas of FE and BE lines [9]. In impurity doped semiconductors, emission due to recombination of free carriers (electrons or holes) and the imputity levels (acceptors or donors) are dominant at intermediate temperature or RT depending on E_a of the impurity. They are referred to as free-to-bound (FB) or bound-to-free (BF) emissions. The simultaneous existence of donor and acceptor impurities introduce a pair type emission between them, and is called donar-acceptor pair (DAP) recombination. The band-to-band (BB) emission occurs in direct band-gap semiconductor with relatively high temperature, high carrier density, small exction binding energy, E_b, or high number of active phonons which procuce free carriers.

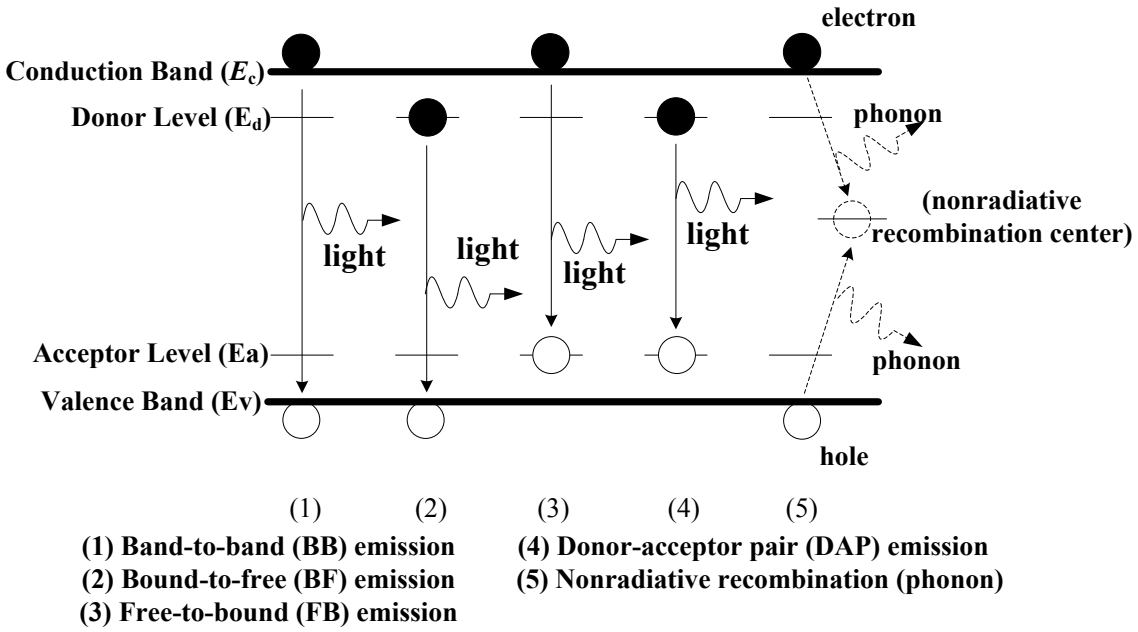

Fig. 3.6. Schematic drawing of radiative and nonradiative recombination process in semiconductor preferably at low temperature where the impurity-related emission occurs.

On the other hand, the quantum-well (QW) LEDs have similar structure to the double-heterostructure (DH) LEDs except the thickness of the active layer in a QW LEDs is very small, lower than 5 nm. Figure 3.7(a) shows the band diagram of a single-quantum-well (SQW) LEDs where the central $In_{0.2}Ga_{0.8}N$ well (L_y=2.5 nm) is sandwiched between two larger bandgap $In_{0.05}Ga_{0.95}N$ barrier layers. The length L_y is comparable to the de Broglie wavelength (λ=h/p, where h is the Planck constant and p is the momentum of the charge carrier), and the carriers are confined in a finite potential well in the y-direction.

The energy of the charge particle can be separated into a confinement component in the y-direction and two unconfined components in the x- and z-direction of the QW layer.

$$E\left(n,k_{\mathrm{x}},k_{\mathrm{z}}\right)=E_{\mathrm{n}}+\frac{\hbar^{2}}{2m^{*}}\left(\kappa_{\mathrm{x}}{}^{2}+k_{\mathrm{z}}{}^{2}\right) \tag{3.3}$$

where E_n is the n th eigenvalue of the confined particle, m* is the effective mass, and K_x and K_z are the wave number in the x- and z-direction, respectively. Figure 3.7(b) shows the energy levels in the quantum well. The values of E_n are shown as E_1, E_2, $E_3$for electrons, E_{hh1}, E_{hh2}, $E_{hh3}$for heavy holes, and E_{th1}, $E_{th2}$for light holes. The usual parabolic forms for the conduction and valence band density of states have been replaced by a "staircase" representation of discrete levels as shown in Fig. 3.7(c), each corresponding to a constant density of states per unit area given by

$$\frac{dN}{dE}=\frac{m^{*}}{\pi\hbar^{2}} \tag{3.4}$$

Since the density of states is constant, rather than gradually increasing from zero, as in a conventional laser, there is a group of electrons of nearly the same energy available to recombine with a group of holes of nearly the same energy, for example, the level E_1 in the conduction with the level E_{hh1} in the valence band.

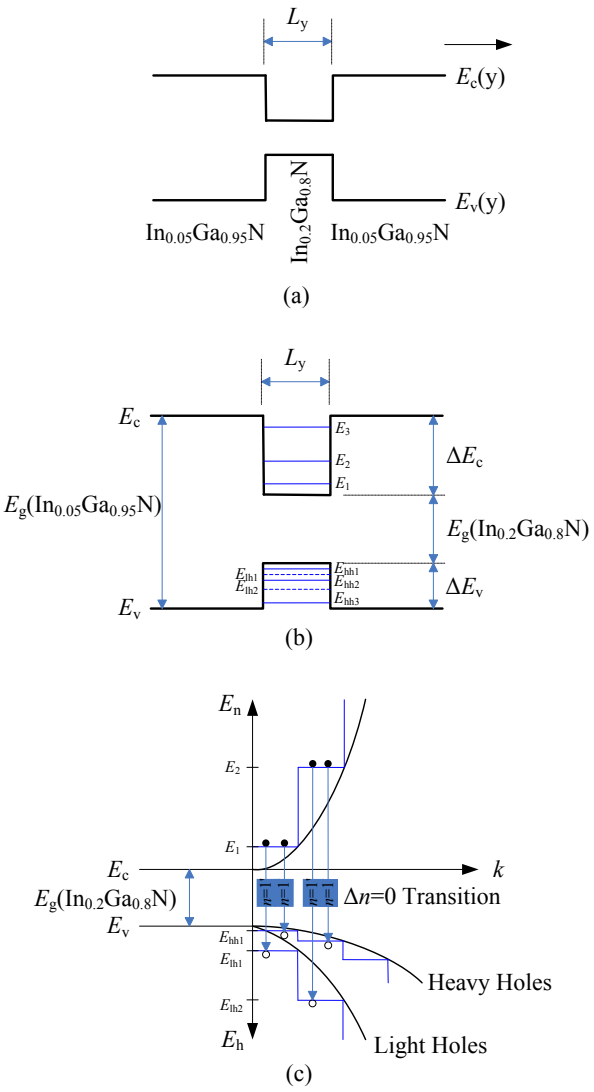

Fig. 3.7. The quantum-well (QW) laser. (a) InGaN Single Quantum Well, (b) Discrete energy levels within the well, (c) Density of states for electrons and holes within the well.

3.4 Light Emitting Diodes Evaluation

After the LEDs processing, the device performance should be evaluated, and some parameters such as operating voltage and light output power will be obtained. The

LEDs characteristics include electrical and opitical property. Which are characterized by measurements of current-voltage (*I-V*) , electroluminescence (EL), and current-light output power (*I-L*). Figure 3.7 shows the *I-V* measurement system and the LED pattern. EL and *I-L* characterization system is shown in Fig 3.8. The system is MCPD-7000 of the Otsuka Electronics Co., Ltd. Moreover, the ambience of measurement is also shown in Fig3.9. In addition, the experiment condition is under the room temperature (R.T.) and direct injection current (DC).

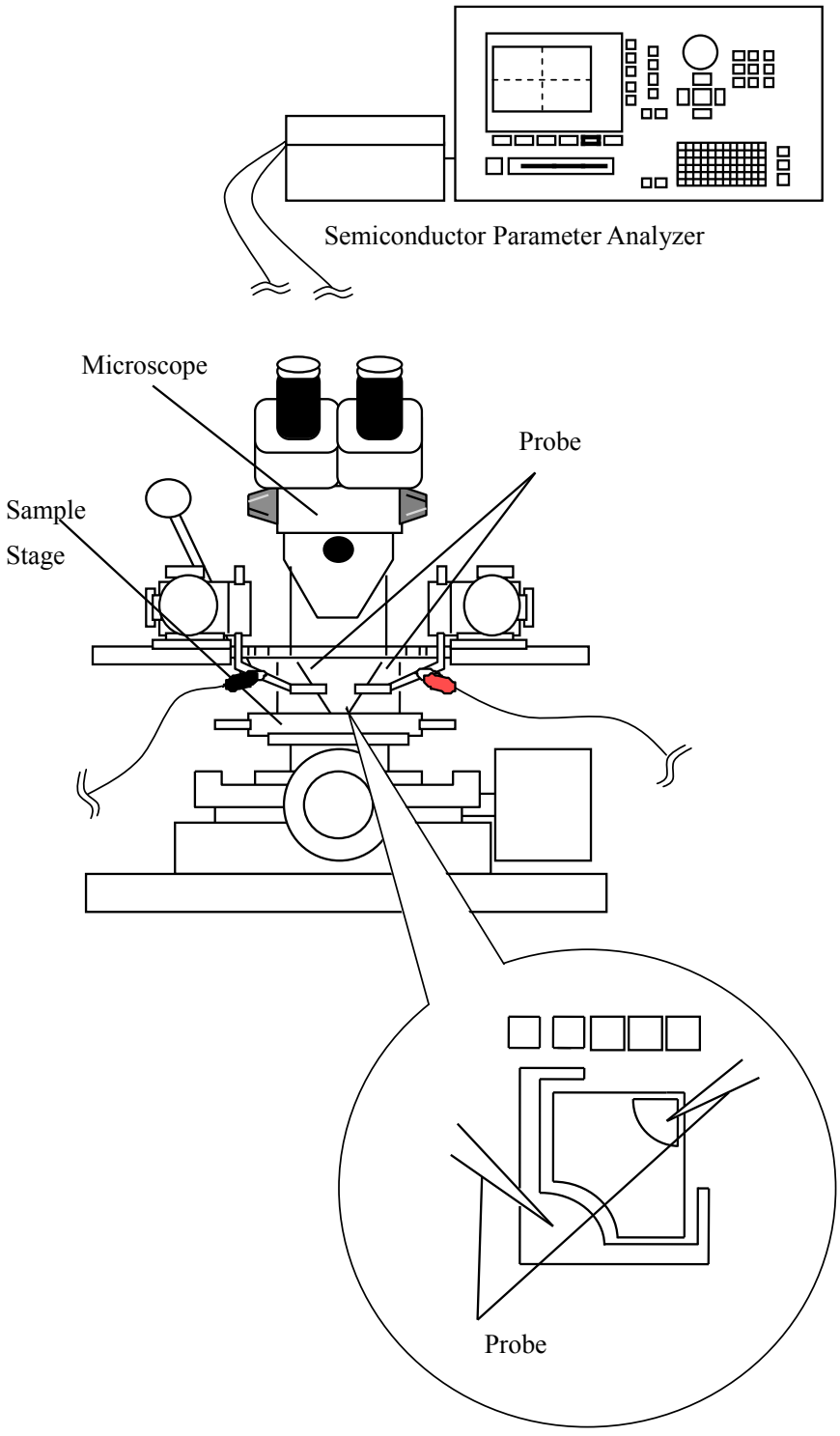

Fig. 3.7. Schematic of the *I-V* measurement system and the LED pattern.

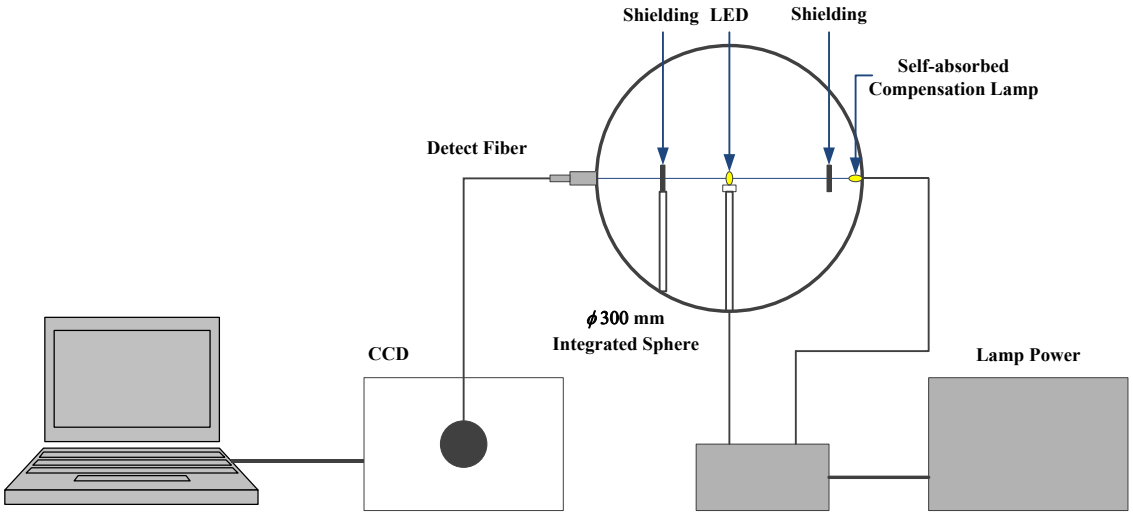

Fig. 3.8. Schematic of the EL and *I-L* characterization system.

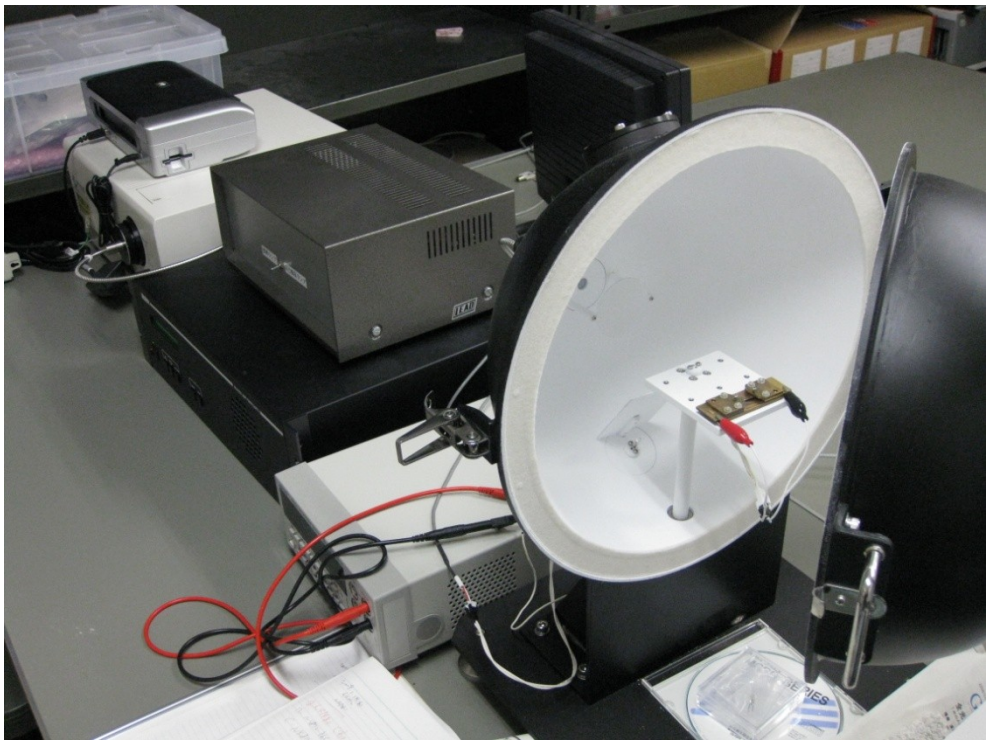

Fig. 3.9. The ambience of EL and *I-L* measurement (MPCD-7000).

3.5 Internal, Extraction, External and Power Efficiency

In a semiconductor crystalline, several mechanisms for nonradiative recombination exist, including Shockley-Read, Auger, and surface recombination [16]. Even though nonradiative recombination can be reduced, it can never be totally eliminated. Any semiconductor crystal has some native defects. Although the concentration of these native defects can be low, it is never zero. Thermodynamic considerations predict that if an energy E_a is needed to create a specific point defect in a crystal lattice, the probability that such a defect does indeed form at a specific lattice site, is given by the Boltzmann factor, i.e. $\exp(-E_a/kT)$. The product of the concentration of lattice sites and the Boltzmann factor gives the concentration of defects. A native point defect or extended defect may form a deep state in the bandgap, and thus be a nonradiative recombination center.

If rediative lifetime in a semiconductor crystal is nenoted as τ_r and nonradiative lifetime is denoted as τ_{nr}, the total probability of recombination is given by the sum of the radiative and nonradiative probabilities,

$$\tau^{-1} = \tau_r^{-1} + \tau_{nr}^{-1} \tag{3.5}$$

The relative probabiltity of radiative recombination is given by the radiative probability over the the total probability of recombination. Thus, the probability of radiative recombination or **internal quantum efficiency** (η_{IQE}) is give by,

$$\eta_{IQE} = \tau_r^{-1} / (\tau_r^{-1} + \tau_{nr}^{-1}) \tag{3.6}$$

The η_{IQE} gives the ratio of the number of light quanta emitted inside the semiconductor to the number of charge quanta undergoing recombination.

In device evaluation viewpoint, active region of an ideal LED emits one photon for every injected electron. Each charge quantum particle, that is, electron produces one

light quantum particle, which is called to photon. Therefore, the ideal active region of an LED has a quantum efficiency of unity. The η_{IQE} is defined as,

$$\eta_{IQE} = \frac{\text{Number of photons emitted from active region per second}}{\text{Number of electrons injected into LED per second}}$$

$$= \frac{\boldsymbol{P_{int}}/_{(\boldsymbol{hv})}}{\boldsymbol{I}/_{\boldsymbol{e}}} \tag{3.7}$$

Where P_{int} is the optical power emitted from the active region and I is the injected current.

In an ideal LED, all photons emitted by the active region are also emitted into free space. Such an LED has unity extraction efficiency. However, in real LED, only partial of the optical power is emitted into free space. Some photons may never leave the semiconductor die, due to several possible loss mechanisms. For example, light emitted by the active region can be reabsorbed in the substrate of the LED, assuming that the substrate is absorbing at the emission wavelength. This problem is crucial for wide bandgap InGaN-based LED grown in narrower bandgap Si substrate. Emitted light may be incident on a metallic contact surface and be absorbed by the meal. In addition, the phenomenon of total internal reflection, also referred as trapped light phenonmenon, reduces the abilty of the light to escape from the semiconductor. Light **extraction efficicency** (η_{ext}) is defined as,

$$\eta_{ext} = \frac{\text{Number of photons emitted into free space per second}}{\text{Number of photons emitted from active region per second}}$$

$$= \frac{\boldsymbol{P}/_{(\boldsymbol{hv})}}{\boldsymbol{P_{int}}/_{(\boldsymbol{hv})}} \tag{3.8}$$

Where P is the optical power emitted into free space.

The η_{ext} can be a severe limitation for high performance LEDs. It is quite difficult to increase the η_{ext} beyond 50% without resorting to highly sophisticated and costly device processes.

The **external quantum efficiency** (η_{EQE}) is defined as,

$$\eta_{EQE} = \frac{\text{Number of photons emitted into free space per second}}{\text{Number of electrons injected into LED per second}}$$

$$= \frac{P/(h\nu)}{I/e} = \eta_{IQE} \bullet \eta_{ext} \tag{3.9}$$

The η_{EQE} gives the ration of the number of useful light particles to the number of injected charge particles.

The **power efficiency** (η_{power}) is defined as,

$$\eta_{power} = \frac{P}{IV} \tag{3.10}$$

Where IV is the electrical power provided to the LED. The power efficiency (η_{power}) is also called wall plug efficiency.

3.6 Conclusions

This chapter describes the fundamental characterization measuments for GaN-based epitaxy. Lattice defects mechanism in GaN is briefly explained, including the characterization methods using the XRD and TEM, which are the common way to evaluate GaN epitaxial layer quality. Luminescence characteristics from semiconductor, including single quantum well, is also discussed. This is important to characterize GaN quality and device performance.. The four parameters of the efficiency, that are internal, extraction, external, and power efficiency are important factor to evaluate light emission of the LEDs and LDs.

References

[1] H. Amano, N. Sawaki, I. Akasaki, and T. Toyoda, Appl. Phys. Lett. **48**, 353 (1986).

[2] S. Nakamura, Jpn. J. Appl. Phys. **30**, L1705 (1991).

[3] S. D. Lester, F. A. Ponce, M. G. Craford and D. A. Steigerwald, Appl. Phys. Lett. 66, 1245 (1995).

[4] W. Qian, M. Skowronski, M. D. Graef, K. Doverspike, L. B. Rowland and D. K. Gaskill, Appl. Phys. Lett. **66**, 1252 (1995).

[5] X. H. Wu, L. M. Brown, D. Kapolnek, S. Keller, B. Keller, S. P. Denbarrs and J. S Speck, J. Appl. Phys. **80**, 3238 (1996).

[6] T. Hino, S. Tomiya, T. Miyajima, K. Yanashima, S. Hashimoto and M. Ikeda, Appl. Phys. Lett. **76**, 3421 (2000).

[7] H. P. Myers, *Introductory Solid State Physics.* Taylor & Francis (2002)

[8] J. I. Pankove, J. E. Berkeyheiser, H. P. Maruska and J. Wittke, Solid State Commun. **8**, 1051 (1970).

[9] R. Dingle, D. D. Sell, S. E. Stokowski and M. Ilegems, phys. Rev. B **4**, 1211 (1971).

[10] M. A. Lampert, Phys. Rev. Lett. **1**, 450 (1958).

[11] J. R. Haynes, Phys. Rev. Lett. **4**, 361 (1960).

[12] H. B. Bebb and E. Williams, *Semiconductor and Semimetals,* eds. R.K. Willardson and A. C. Beer, Academic, New York, USA, **8**, 182-392 (1972).

[13] Y. Toyozawa, prog. Theor. Phys. Suppl. **12**, 111 (1959).

[14] J. J. Hopfield, *II-VI Semiconducting Compounds,* W. A. Benjamin, New York, USA, P.**786** (1967).

[15] W. C. Tait, D. A. Cambell, J. R. Packard and R. L. Weiher, *II-VI Semiconducting Compounds,* W. A. Benjamin, New York, USA, P.**370** (1967).

[16] E. F. Schubert, *Light-Emitting Diodes,* Cambridge University Press, New York, USA, P.**44** (2003).

Chapter 4

Demonstration on GaN-based Light Emitting Diodes Grown on 3C-SiC/Si(111)

This chapter demonstrates the GaN-based light-emitting diodes (LEDs) grown on template of 3C-SiC/Si(111). The structural properties have been investigated systematically by means of atomic force microscopy, X-ray diffraction, and transmission electron microscopy. It is found that the intermediate layer (IL) of 3C-SiC leads to not only a significant improvement in the crystalline quality of GaN, but also better interfaces between the buffer layer and initial layers of strained-layer superlattice. The device properties were also evaluated using the measurements of current-voltage, electroluminescence, and light output power-current. Comparing to the conventional LEDs that do not contain 3C-SiC IL, the device with IL exhibits the enhanced output power by more than 200% at an injection current of 20 mA, and the operating voltage is slightly increased from 3.7 to 3.9 V. These results indicate that using 3C-SiC as IL is one of the promising approaches to improve the performance of LEDs on silicon.

4.1 Introduction

GaN based optoelectronic devices, including light-emitting diodes (LEDs), grown on Silicon (Si) substrates have been attractive since the last century because of several benefits, such as low manufacturing cost, large size, good thermal conductivity, and integration potential. However, there are some issues regarding the quality of GaN

epilayers grown on Si. For instance, there is a large mismatch in the lattice constants up to 17% and as much as 116% difference in the thermal expansion coefficients between the GaN epilayer and Si substrate. In the past, many methods have been suggested to improve the crystalline quality and light output power by applying novel growth techniques, such as using low-temperature AlN and Si_xN_y interlayer [1], or growth on patterned Si substrate [2]. Meanwhile, some researchers have focused on enhancing the light extraction efficiency by using distributed Bragg reflector [3], or micro-roughening of p-GaN surface [4]. Recently, Cuong et al. [5] have reported that the fabrication of micro-pit LEDs constructed on wet-etched patterned sapphire substrate (PPS), has simultaneously improved both the epitaxial layer quality and light extraction efficiency. Previously, it was also proved that, using 3C-SiC as an intermediate layer (IL) could improve the quality of the GaN grown on Si [6-8]. Consequently, GaN based high electron mobility transistors [9] and Schottky diodes [10] were realized by using IL of 3C-SiC. However, until now, the demonstration of GaN based LEDs grown on Si using 3C-SiC IL has not been reported.

In this work, the effect of 3C-SiC IL on the structural property and device performance in GaN-based LEDs grown on Si by MOCVD has been reported. The quality of the epitaxial layers was found to be improved by using 3C-SiC IL, which thereby leads to more than two times enhancement in the light output power when comparing to those devices without 3C-SiC IL.

4.2 Experiment

Prior to the device growth by MOCVD, the Si substrate was carbonized through annealing in an atmosphere of propane at 1100 ^{o}C, which resulted in the

formation of a thin (<50 nm) crystalline 3C-SiC that serves as a template for the 3C-SiC growth [11]. Subsequently, a thicker layer of 3C-SiC IL was obtained on the Si (111) substrate using silane (SiH_4) and propane (C_3H_8) as the precursors at the same temperature in low pressure (10^4 Pa) [12]. The 3C-SiC crystal polarity was Si polarity [13], and the total thickness was approximately 700 nm. Over the template of 3C-SiC/Si(111), InGaN-based multiple-quantum wells (MQWs) LED structure was grown by MOCVD using a Taiyo Nippon Sanso SR2000 system. Trimethylgallium (TMG), trimethylindium (TMIn) and ammonia (NH_3) were used as sources for gallium, indium and nitrogen, respectively. Monosilane (SiH_4) diluted in hydrogen was used as n-type dopant, and the p-type dopant was bis-cyclopentadienyl magnesium (Cp_2Mg). Before the growth of LED structure, a buffer layer (BL) consisting of an AlN layer and an n-AlGaN layer was grown at 1000 ^oC [14]. Then, 20 pair AlN/GaN (5/20 nm) strained-layer superlattice (SLS) layers and a 200 nm thick n-GaN layer were grown at 1080 ^oC. Finally, an undoped 15 period MQWs consisting of 1.5 nm thick $In_{0.16}Ga_{0.84}N$ wells and 10 nm thick $In_{0.01}Ga_{0.99}N$ barriers, a 20 nm thick p-AlGaN layer at 780 ^oC, and a 200 nm thick p-GaN cap layer at 1080 ^oC were grown successively. For comparison, a sample was grown directly on Si substrate without 3C-SiC IL by the identical growth conditions. For the convenience of following discussion, the two samples are denoted as sample A (without 3C-SiC IL) and sample B (with 3C-SiC IL).

The surface morphology was analyzed using atomic force microscopy (AFM). In order to confirm the crystalline quality of epitaxial layers, high-resolution x-ray diffraction (HR-XRD) (Philips X'Pert Epitaxy), and transmission electron microscopy (TEM) (JEM-2010F) measurements were performed. The top-emitting LEDs with a chip size of 500×500 μm^2 were fabricated using a standard process. In the fabrication

procedure of LEDs, firstly, the Mg acceptors were activated by furnace annealing in nitrogen atmosphere at 800 ^{o}C for 25 min. Then, the thin Ni/Au (6/12 nm) transparent metals were formed on p-GaN layer by the electron-beam evaporation and annealed in air ambient at 600 ^{o}C for 3 min. Subsequently, the Ni/Au (5/60 nm) p-type contact electrode was deposited and annealed in air ambient at 450 ^{o}C for 90 s. Finally, the n-type ohmic contact was made on the backside of Si substrate from the AuSb/Au (20/ 100 nm) and annealed in nitrogen atmosphere at 320 ^{o}C for 30 s. Figure 4. 1 shows the schematic structure of the LEDs used in this study. The LEDs were characterized using an on-wafer configuration. Current-voltage (*I-V*) measurements were carried out using a semiconductor parameter analyzer (Agilent 4155C). Electroluminescence (EL) spectra and light output power-current (*L-I*) were measured at room temperature using an integrated sphere detector (Otsuka Electronics MPCD-7000).

4.3 Results and Discussion

The two samples in this study are crack-free, with mirror-like surface. AFM images of p-GaN surface for sample A and B are shown in Fig. 4. 2. Some small pits can be observed in both samples. The formation of pit is common in the planar growth of InGaN/GaN MQWs due to the large lattice mismatch [15]. It can be found that the pit density of sample B is lower than that of sample A. In addition, when the scan areas are 3×3 and 1×1 μm^2, the root-mean square roughness of sample A are 0.67 and 0.25 nm, and those of sample B are 0.43 and 0.12 nm, respectively.

Figure 4. 3(a) shows GaN (0002) ω-2θ scans of sample A and B. The strongest peak in each spectrum arises from GaN epitaxial layer. Several distinct satellite peaks from AlN/GaN SLS can be observed on both sides of GaN-peak, and the high-order

fringes indicate the superior crystalline quality of SLS structure with sharp interfaces. Based on the positions of fringe peaks, the calculated average thicknesses of SLS period are 23.6 and 25.3 nm for sample A and B, respectively, close to the designed value (25 nm). In addition, it is found that the diffraction peak at 17.83° (0.2579 nm lattice constant) in sample B is stronger than that of sample A. It is believed that this peak originates from the 3C-SiC (111) IL. The position at 41.36° (0.2181 nm lattice constant) corresponds to the peak of 3C-SiC (002) 2θ-ω scan of sample B is also shown in the inset of Fig. 4. 3(a). Figure 4. 3(b) shows GaN (0002) and $(10\bar{1}2)$ rocking curves of the two samples. The full width at half-maximum of (0002) are 1310 and 991 arcsec, and those of $(10\bar{1}2)$ are 1836 and 1464 arcsec for sample A and B, respectively.

During the MOCVD growth, strain can be relieved by the 3C-SiC IL because of the less lattice mismatch (3%) between (0001) GaN and (111) 3C-SiC [15]. It is reasonable that the tensile stress in GaN films with 3C-SiC IL can be reduced to half of that of GaN films without 3C-SiC IL [6,16], resulted from the reduction of thermal expansion coefficient from 116% (between GaN and Si) to 24% (between GaN and 3C-SiC). Consequently, a higher crystalline quality GaN epitaxial layer was realized by utilizing 3C-SiC as IL [6,15]. Figure 4. 4 shows cross-sectional TEM bright-filed images of the two samples. Threading dislocations (TDs) in the buffer and the SLS layers of sample A can be observed, while the corresponding TDs in sample B were somewhat suppressed. Moreover, as can be seen in the other layers, including n-GaN, MQWs and p-GaN, the threading dislocation density (TTD) of sample B is lower than that of sample A. In particular, the average TTD in n-GaN of sample A and B are calculated to be approximately 9.7×10^{9} and 2.5×10^{9} cm^{-2}, respectively. These results are consistent with aforementioned data of XRD. In addition, as shown in Fig. 4. 5, a

number of V-groove defects exist in the region close to the interfaces between the BL and the initial SLS layers in sample A, while the corresponding interfaces are very smooth in sample B. Therefore, it is believed that a significant improvement in the crystalline quality of the epitaxial layers can be realized by using the 3C-SiC IL.

The forward *I-V* curves of the two samples are shown in Fig. 4. 6. The operating voltage of 3.7 and 3.9 V were obtained at the injection current of 20 mA for sample A and B, respectively. From the *I-V* slope, the series resistances of sample A and B are derived to be 34 and 47 Ω, respectively. It should be noted that using 3C-SiC as IL resulted in a slight higher operation voltage and a higher series resistance due to the 3C-SiC IL. Room temperature EL spectra of the two samples under a drive current of 20 mA are shown in the inset of Fig. 4. 6. The EL peaks are at 480 and 467 nm for sample A and B, respectively.

Figure 4. 7 shows the *L-I* characteristics of the two samples. At an injunction current of 20 mA, the output power of sample A and B is approximately 50 and 120 μW, respectively. The result indicates that more than 200% enhancement in the output power has been achieved by using 3C-SiC as IL. The enhanced light output power is attributed to the lower pit density on the sample surface, the flat interfaces of SLS, and the higher crystalline quality of GaN epitaxial layers, as mentioned above. It is well known that various compressive strain-relief defects, such as pits, V-groove defects and TDs might be generated during the growth [17]. These defects act as nonradiative recombination centers and/or paths for current leakage, which will deteriorate the device performance [18]. The inset of Fig. 4. 7 is the image of emission from sample B at 5 mA under normal room light condition, which reveals crack-free and uniform emission.

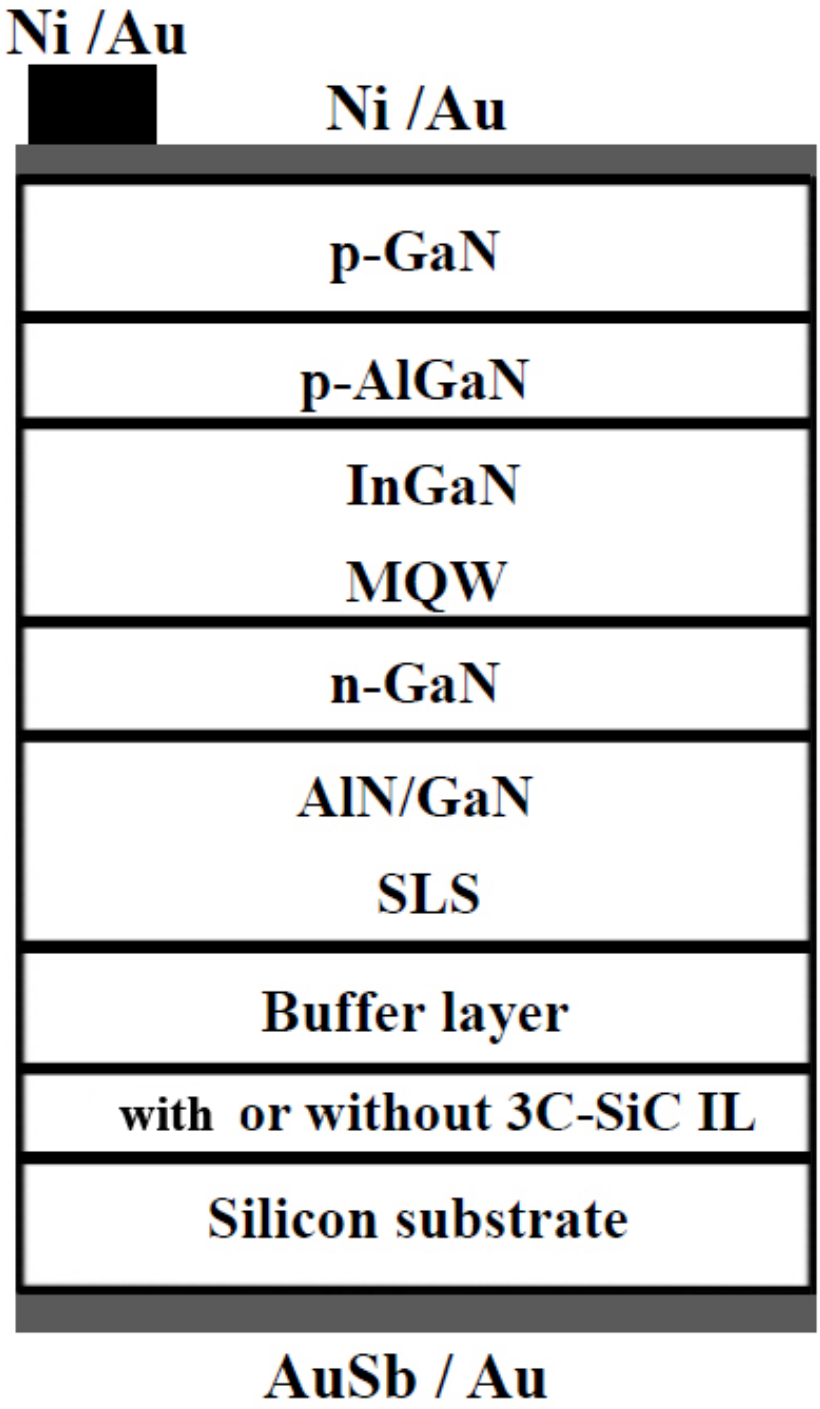

Fig. 4.1. Schematic structure of GaN-based LEDs on Si substrate with or without 3C-SiC IL.

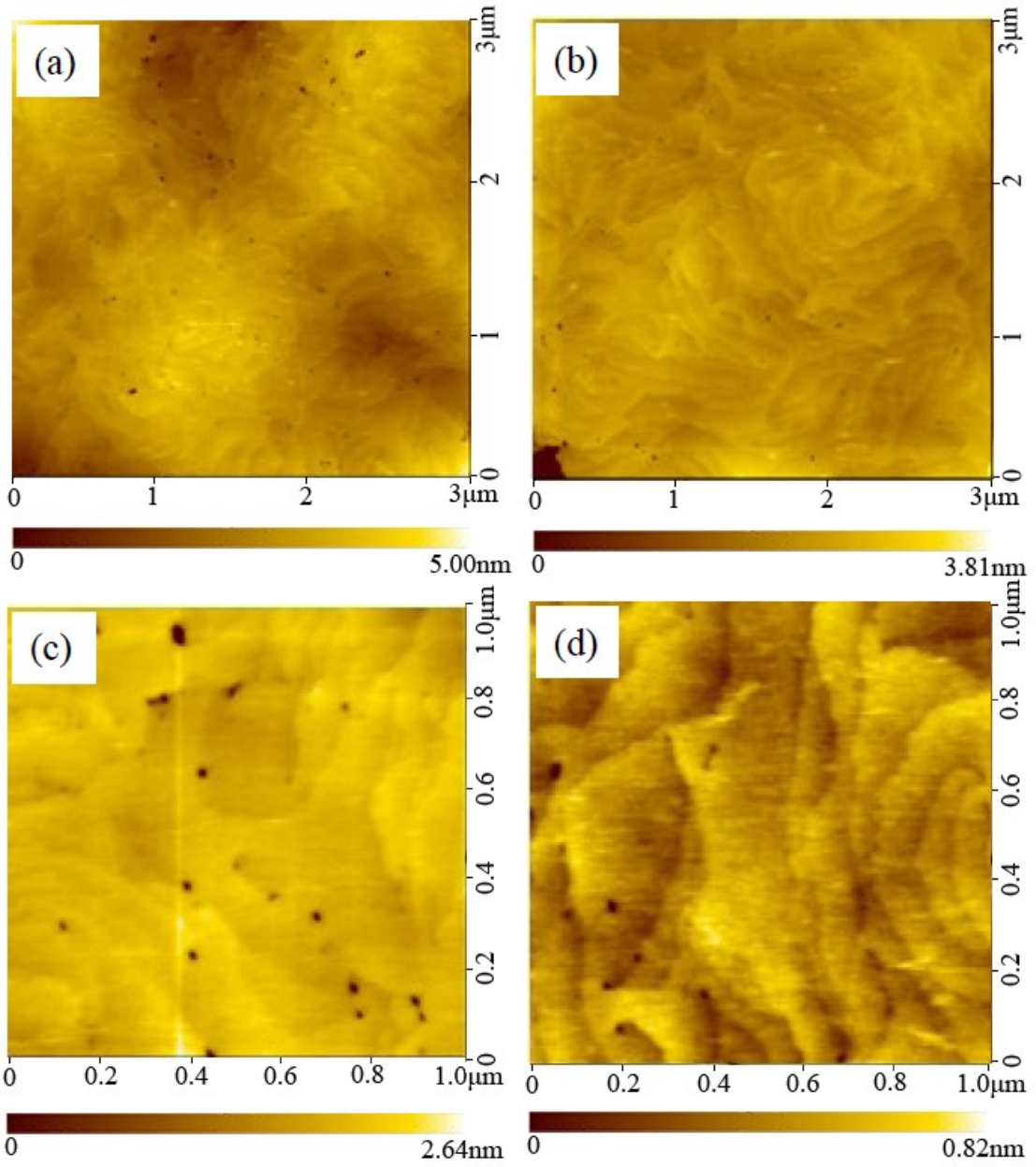

Fig. 4. 2. AFM images of p-GaN surface for sample A ((a) and (c)) and sample B ((b) and (d)). The scan area of (a) and (b) is 3×3 μm^2. For (c) and (d), the scan area is 1×1 μm^2.

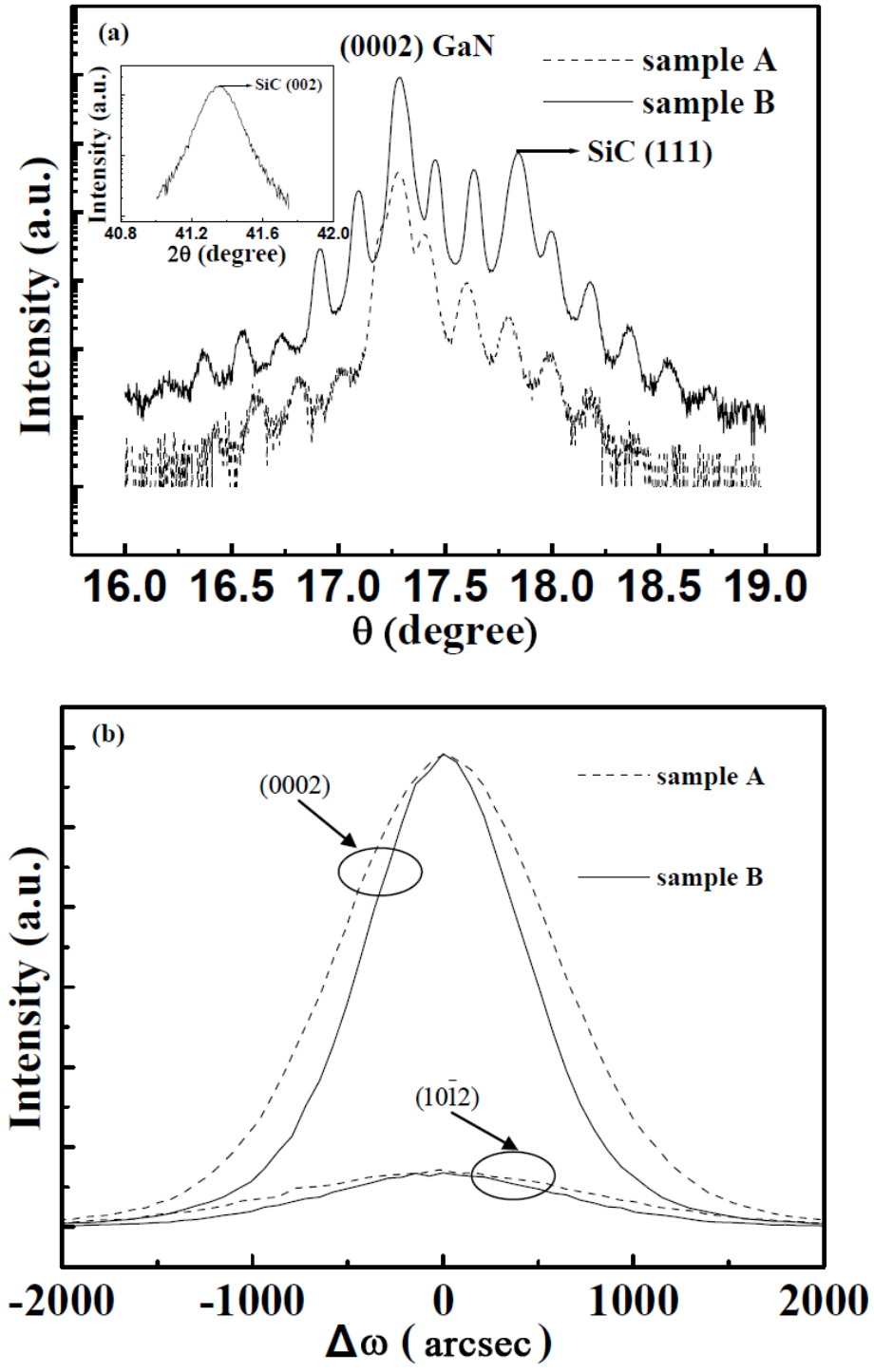

Fig. 4. 3. (a) HR-XRD of ω-2θ scans of GaN (0002) for sample A and B. The inset shows the 2θ-ω scan of SiC (002). (b) HR-XRD of ω-scans of GaN (0002) and (10$\bar{1}$2) for sample A and B.

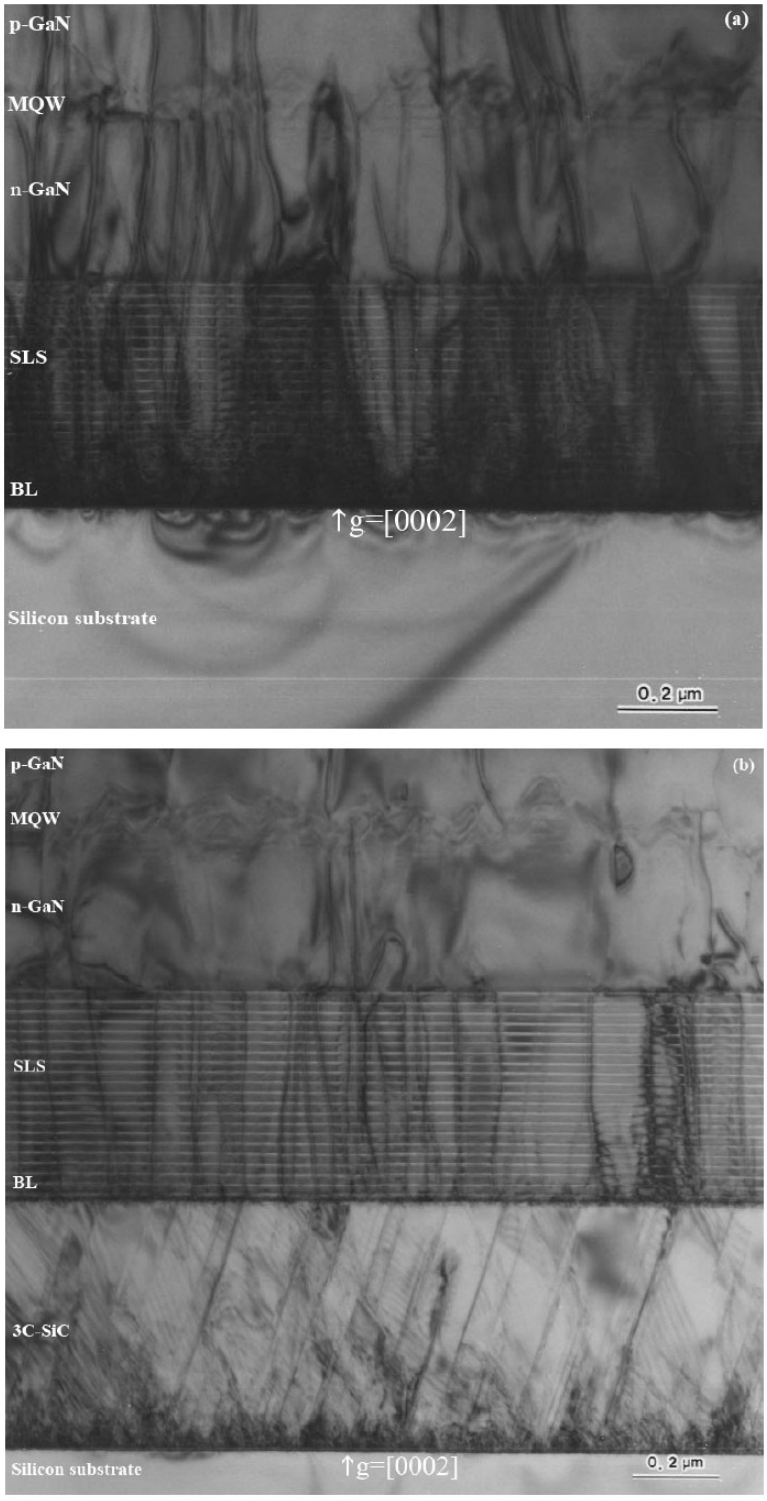

Fig. 4.4. Cross-sectional TEM bright-field images of epitaxial structure for sample A (a) and B (b).

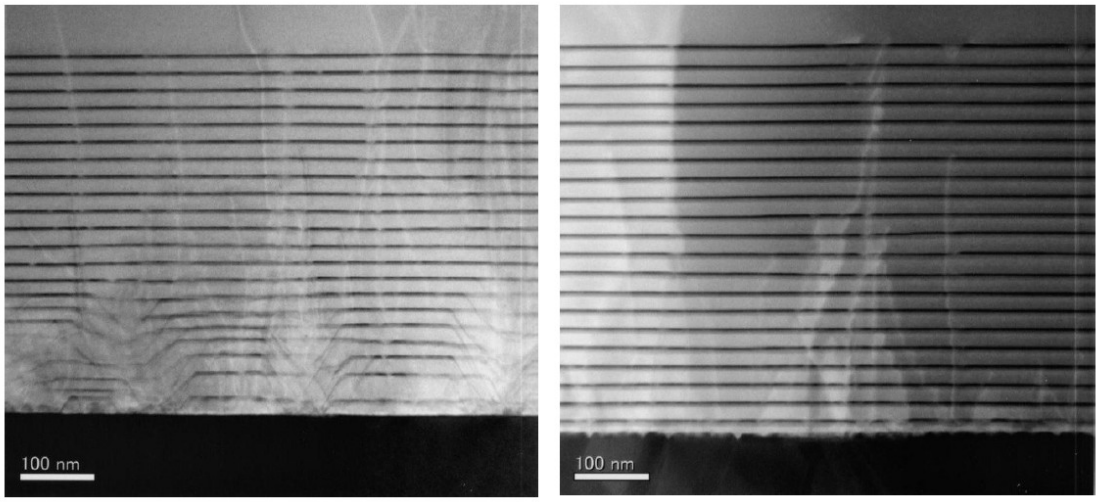

Fig. 4.5. Cross-sectional STEM images of the AlN/GaN SLS layers for sample A (left) and B (right).

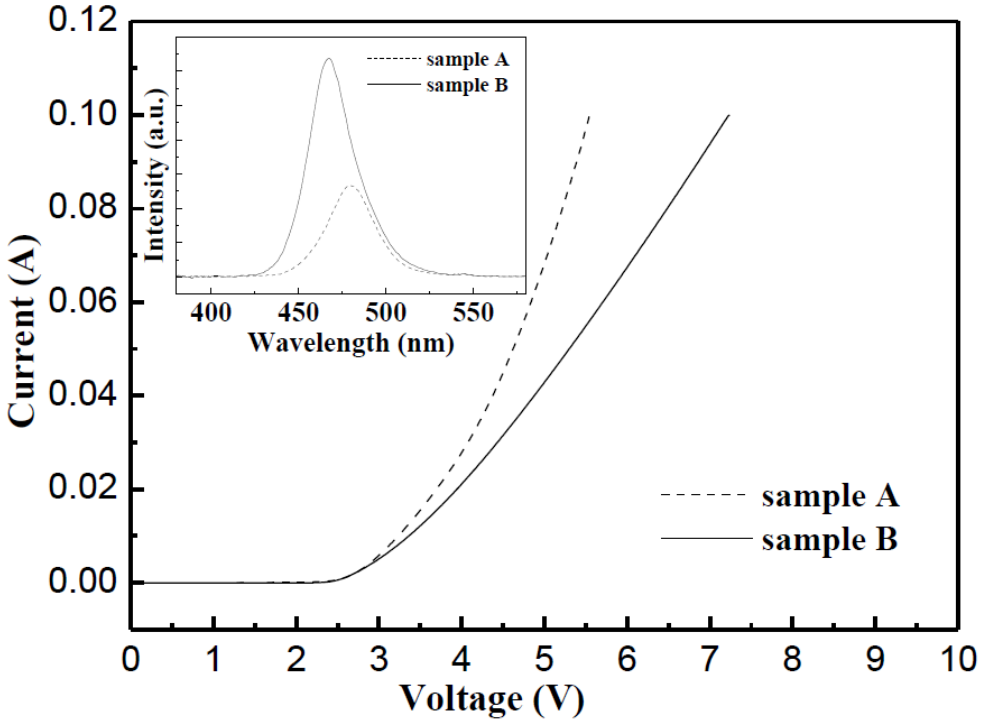

Fig. 4.6. Forward *I-V* characteristics of LEDs for sample A and B. The inset shows EL spectra of LEDs at an injection current of 20 mA for sample A and B.

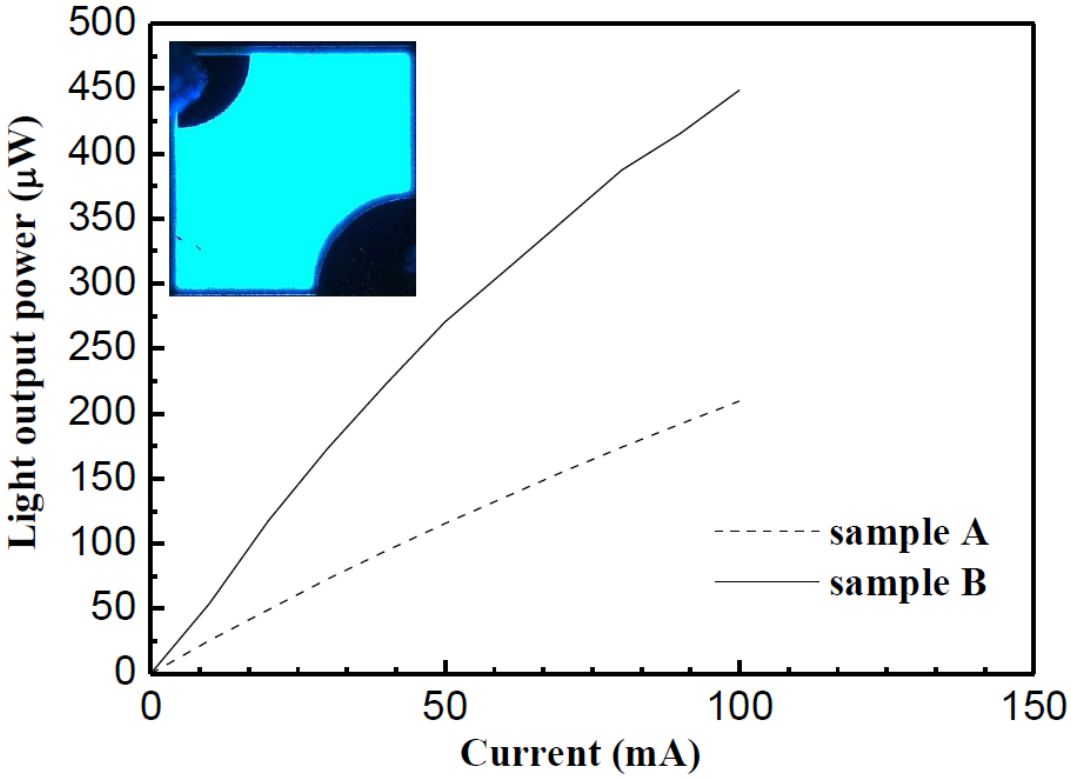

Fig. 4.7. *L-I* characteristics of LEDs for sample A and B. The inset shows the image from sample B which was operated at an injection current of 5 mA.

4.4 Conclusions

In summary, the GaN-based LEDs on Si substrate by using 3C-SiC as IL has been demonstrated. The effect of 3C-SiC IL on the characteristics of LED has been investigated. The addition of 3C-SiC IL has resulted in the improved GaN crystalline quality, the better interfaces between the buffer and initial SLS layers, and the smoother morphology of the sample surface. As a consequence, the device with 3C- SiC IL showed an enhanced light output power by a factor of 2.4 at a drive current of 20 mA. The superior device performance was attributed to the improvement in the structural properties, which were clarified by the AFM, XRD, and TEM measurements. This work implies that using 3C-SiC as IL is one of the effective methods for enhancing the light output power of LEDs grown on Si substrate. It will also be of interest for a further study of GaN-based optoelectronic device grown on Si.

References

[1] A. Dadgar, M. Poschenrieder, J. Bläsing, O. Contreras, F. Bertram, T. Riemann, A. Reiher, M. Kunze, I. Daumiller, A. Krtschil, A. Diez, A. Kaluza, A. Modlich, M.Kamp, J. Christen, F. A.Ponce, E. Kohn, and A. Krost, J. Cryst. Growth **248**, 556 (2003).

[2] B. S. Zhang, H. Liang, Y. Wang, Z. H. Feng, K. W. Ng, and K. M. Lau, J. Cryst.Growth **298**, 725 (2007).

[3] H. Ishikawa, K. Asano. B. Zhang, T. Egawa, and T. Jimbo, Phys. stat.sol. (a) **201**, 2653 (2004).

[4] C. Huh, K. S. Lee, E. J. Kang, and S. J. Park, J.Appl. Phys. **93**, 9383 (2003).

[5] T. V. Cuong, H. S. Cheong, H. G. Kim, H. Y. Kim, C. H. Hong, E. K. Suh, H. K. Cho, and B. H. Kong, Appl. Phys. Lett. **90**, 131107 (2007).

[6] J. Komiyama, Y. Abe, S. Suzuki, and H. Nakanishi, J.Appl. Phys. **100**, 033519 (2006).

[7] A. Yamamoto, T. Yamauchi, T. Tanikawa, M. Sasase, B. K. Ghosh, A. Hashimoto, and Y. Ito. J. Cryst. Growth **261**, 266 (2004).

[8] H. M. Liaw, R. Venugopal, J. Wan, and M. R. Melloch, Solid-State Electron. **45**, 1173 (2001).

[9] Y. Cordier, M. Portail, S. Chenot, O. Tottereau, M. Zielinski, and T. Chassagne, J. Cryst. Growth **310**, 4417 (2008).

[10] J. Komiyama, Y. Abe, S. Suzuki, T. Kita, and H. Nakanishi, J. Cryst. Growth **275**, e1001 (2005).

[11] S. Nishino, J. A. Powell, and H. A. Will, Appl. Phys. Lett. **42**, 460 (1983).

[12] J. Komiyama, Y. Abe, S. Suzuki, and H. Nakanishi, J.Appl. Phys. **100**, 033519 (2006).

[13] T. Egawa, B. Zhang, and H. Ishikawa, IEEE Electron Device Lett. **26**, 169 (2005).

[14] F. Lin, N. Xiang, P. Chen, S. Y. Chow, and S. J. Chua, J.Appl. Phys. **103**, 043508 (2008).

[15] J. Komiyama, Y. Abe, S. Suzuli, and H. Nakanishi, Appl. Phys. Lett. **88**, 091901 (2006).

[16] T. Kozawa, T. Kachi, H. Kano, H. Nagase, N. Koide, and k. Manabe, J. Appl. Phys.**77**, 4389 (1995).

[17] H. K. Cho, J. Y. Lee, G. M. Wang, and C. S. Kim, Appl. Phys. Lett. **79**, 215 (2001).

[18] C. Netzel, H. Bremers, L. Hoffmann, D. Fuhrmann. U. Rossow, and A. Hangleiter, Phys. Rev.B **76**, 155322 (2007).

Chapter 5

Improvement of GaN-based Light Emitting Diodes by Altering n-GaN Thickness

This chapter reports enhanced external quantum efficiency (η_{EQE}) inGaN-based multi-quantum well (MQWs) light emitting diodes (LEDs) grown on 4-inch (in.) Si(111) substrate by altering n-GaN thickness. While, some corresponding structure and device characterization have also been presented.

In section 5.1, GaN-based light emitting diodes (LEDs) with a total thickness of 4.8 μm have been grown by metal-organic chemical vapor deposition (MOCVD) on 4-in. Si(111) substrate. The structural property has been revealed by the measurements of high-resolution X-ray diffraction, scanning electron microscopy and transmission electron microscopy. It can be clarified that the LEDs in sample have the good interfaces and layer periodicities for the strained-layer superlattices and multiple quantum wells. In addition, the optical property in the light output power has been evaluated. As a result, LEDs with a maximum output power of 3.3 mW and a high saturation operating current of 400 mA have exhibited the good device performance.

In section 5.2, the GaN-based LEDs grown by MOCVD on 4-in. Si(111) substrates have been demonstrated. The structural property has been revealed by the measurement of X-ray diffraction. One of the full widths at half maximum of ω-scans of the GaN (0002) reflection is around 630 aresec. Also, it can be found that the GaN epitaxial quality can be improved by increasing the thickness of n-GaN. The device properties have been evaluated through current-voltage, electroluminescence, and light

output power-current measurements. As the n-GaN thickness increases from 1 to 2 μm, the light output powers of the LEDs have enhanced approximately two times under the injection current of 20 mA. Moreover, the maximum values of respective external quantum efficiency are achieved as 0.3 and 0.6%, respectively.

5.1 Characterization of GaN-Based Light Emitting Diodes Grown on 4-in. Si(111) Substrate

5.1.1 Introduction

GaN and its related alloys have been investigated extensively in optoelectronic and microelectronic devices since the last century [1-2]. Nowadays GaN-based in the range of ultraviolet to visible light emitting diodes (LEDs) are commercially available. Those device structures almost have been grown on sapphire or SiC substrates. However, in the case of a larger scale fabrication, employing those substrates will be hindered because of their size and high costs. For solving this issue, as one of the effective methods, the growth of LEDs on highly conducting 4- to l2-in. silicon (Si) substrates has been proposed. Moreover, choosing Si as substrate can offer lots of advantages, such as good thermal conductivity, the simplicity of process, and the possibility of integration of Si electronics on the same chip [3]. On the other hand, regarding the GaN epitaxial growth on Si, it is still a challenging issue to modulate tensile stress, resulting from the large mismatches in the lattice constants and thermal expansion coefficients between the GaN layer and Si substrate. Therefore, it always results in the occurrence of cracks and high density threading dislocations [4]. Nevertheless, including our group, many demonstrations of LEDs grown on Si have been reported [2,5-9]. At the same time, it can be found that, with respect to the structure characterization, such as cross-section scanning electron microscopy (SEM) and transmission electron microscopy (TEM), only some few related results have been presented in those reports until now. Actually, in order to improve the device

performance, it is significantly necessary to get some important information through some corresponding accurate measurements.

In this study, the GaN-based LEDs grown on 4-in. Si(111) substrate by MOCVD have been successfully fabricated. The structural property of the sample has been investigated by high-resolution X-ray diffraction (HR-XRD), SEM, and TEM measurements. Based on these results, some consistent correlations have been discussed. In addition, the device performance in the light output power has been characterized. The maximum output power of 3.3 mW and a saturation operating current of 400 mA imply the good performance of LED grown on 4-in. Si(111) substrate.

5.1.2 Experiment

A commercial MOCVD reactor system (Nippon Sanso SR-4000) was used for the epitaxial growth of InGaN-based multiple-quantum wells (MQWs) LEDs structure. Prior to the growth of LEDs structure, a buffer layer consisting of a 5 nm n-AlN layer and a 20 nm n-AlGaN layer was grown. Then, 100 pair n-AlN/GaN (5/20 nm) strained-layer superlattice (SLs) layers and n-GaN layer were grown. Finally, an undoped 10 period MQWs consisting of 4 nm $In_xGa_{1-x}N$ wells and 8 nm $In_yGa_{1-y}N$ barriers, a 20 nm p-AlGaN layer and a 100 nm p^+-GaN cap layer were grown successively. The detailed growth conditions can be also found in our previous report [10]. Here, it should be noted that, in this sample during the epitaxial growth of 2 μm n-GaN, there are no any interruption layers, such as AlN or SiN layer. In order to confirm the crystalline quality of epitaxial layers, the measurements of HR-XRD (Philips X'Pert Epitaxy), cross-section SEM (Hitachi SU-70), and TEM (JEM-2010F, 200 kV) were performed.

The top-emitting LEDs with a chip size of 500×500 μm^2 were fabricated using a standard process. In the main LEDs processing, there are multiple-mask photo-lithography, reactive ion etching, metal evaporation and annealing. The details and the schematic structure of the LEDs can be referred to our previous report [11]. No roughening or LED die shaping was used in this study to enhance the extraction efficiency. The LEDs were characterized using an on-wafer configuration. Light output power was measured under the conditions of room temperature and various direct current (DC) using an integrated sphere detector (Otsuka Electronics MPCD-7000).

5.1.3 Results and Discussion

The sample in this study is crack-free, and shows mirror-like surface for the whole wafer. Figure 5. 1 shows GaN(0002) XRD 2θ-ω scan of the sample. The strongest peak arises from the GaN layer. Also, it is interesting that two kinds of fringe peaks simultaneously appear on the both sides of the major GaN peak, which indicates the good interface and layer periodicity. It should be noted that a position of an average Indium composition of the InGaN layers in the MQWs is indicated by the 0th peak of MQWs. Using the equation $D=n\lambda/2(\sin_{nth}-\sin_{0th})$ [12], the period thickness can be determined. For example, the average period thickness of MQWs can be calculated to be 13.5 nm, and which is close to the designed value (12 nm). At the same time, the thickness of one period SLs has been calculated to be 19.5 nm. Therefore, it can be concluded that one kind of well-defined satellite diffraction peaks to high orders (until ±6) originate from the SLs, and another one as marked by arrow, which arise from MQWs. Zhang et al. have reported the similar results [13]. Comparing with those date, however, the SLs and MQWs relative intensity of our sample have become much

stronger, which are mainly attributed to the more SLs pairs and higher crystalline quality of MQWs.

Figure 5. 2 shows the cross-section images for the SLs layers of the sample under the magnifications of 35 and 100 K. The considerably smooth interfaces can be clearly observed in the area of SLs. This result is consistent with the aforementioned date of HR-XRD. Also, the pairs have been confirmed to be 100, it is in good agreement with the designed value. Moreover, the thickness of one period SLs from SEM images is 22.2 nm. However, the discrepancy seems a little large when comparing with the corresponding value (19.5 nm) of XRD, and we suppose that it might result from in-plane distribution of the growth rate, especially for using the larger 4-inch substrate. On the other hand, the cross-section TEM images for the MQWs layers of the sample are shown in Fig. 5. 3. It can be confirmed that 10 period MQWs with one period thickness of 14 nm, the significantly good interfaces as well have been grown. It also coincides with the above result of HR-XRD. Based on these structure characterizations, it can be concluded that, the epitaxial layers of both the SLs and MQWs with the high crystalline quality in this sample have been successfully grown. Therefore, its aforementioned characterizations suggest that the growth of GaN-based LEDs grown on Si should lead to good performance device.

The light output power versus various injection current (*L-I*) characteristics of the sample are shown in Fig. 5. 4. It can be clearly seen that the output power of LED increases linearly with the injection current up to 100 mA. And, it still continues to increase steadily. However, the output power starts to saturate and finally reaches at a maximum value of 3.3 mW. Then, it decreases slightly as the injection current is further increased, which is attributed to the thermal dissipation at high injection currents [14].

While the saturation operating current of the sample is 400 mA. In the LEDs structure of this study, the total thickness beneath MQWs is 4.5 μm. It should be noted that only in the SLs layers, the total thickness of the AlN layers reaches to 0.5 μm, these factors including Si substrate have been contributed to the good thermal dissipation. It will further influent on the saturation operating current. Actually, the LED performance in this study is close enough to those in other group (6.3 mW at the saturation current of 500 mA) [15], which has been reported to be also comparable to those in the sapphire substrate case. It is worth noting that, some thermal dissipation technologies, such as bonding on a metal head (as shown in ref. 15), have not been employed in our device. Therefore, it can be supposed that this device with good performance is mainly attributed to the high quality of epitaxial layer and good thermal conductivity of Si substrate. The inset of Fig. 4 indicates the emission image of the sample under an injection current of 20 mA. It implies bright and uniform light, resulting from active layers of InGaN-based MQWs. From these results, it can be concluded that the LED in this study has exhibited the good optical characteristics. The other device properties, including current-voltage and electroluminescence, can be found in our previous report [10].

As well known, comparing to the LEDs grown on sapphire, the LEDs on Si show the relative lower light output power. It often results from several typical factors, such as, the light absorption of Si substrate, the crystalline quality of epitaxial layers, and the device structure. In particular, due to absorption in the Si substrate, the light extraction efficiency for device on Si (3.74%) is even lower than on sapphire (5.4%) [15]. This indicates the need for substrate removal methods should be implemented in device processing. Zhang et al. have used wafer bonding and selective lift-off technique

to eliminate not only substrate absorption but also the large band offset between the AlN buffer layer and the Si substrate [16]. In that report, the optical power has been revealed an enhancement of 47% compared to the LED before substrate removal. Although those influence issues exist, it can be also expected that the performance of LEDs grown on Si will be further improved by means of some new effective approaches in the future.

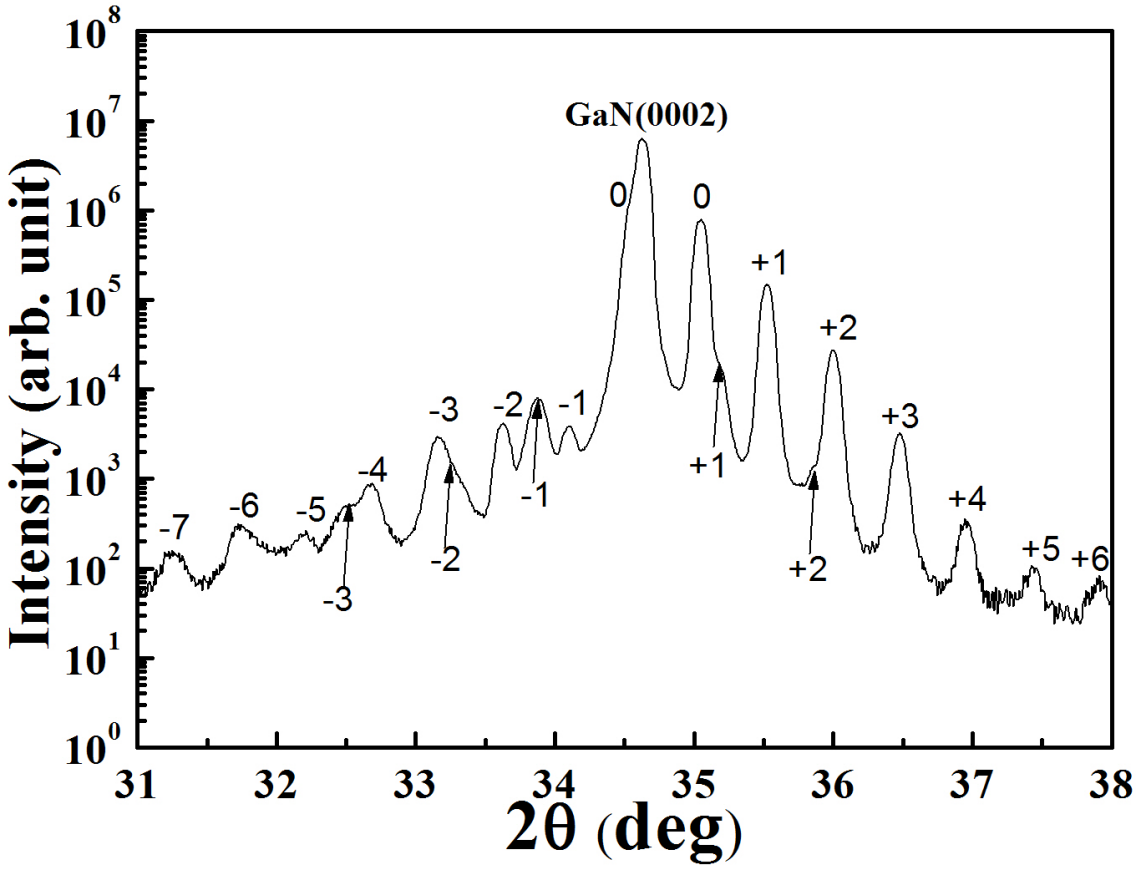

Fig. 5. 1. HR-XRD in GaN(0002) ω-2θ scan of sample. In this figure, the fringe peaks indicated by the number from -7 to +6 originate from the SLs layers. And the fringe peaks indicated by the arrow with the number from -3 to +2 arise from the MQWs layers. The 0th peak (left side to the GaN peak) of MQWs typically indicates a position of an average In composition in the MQWs. And, the 0th peak (right side to the GaN peak) of SLs typically indicates a position of an average Al composition in the SLs.

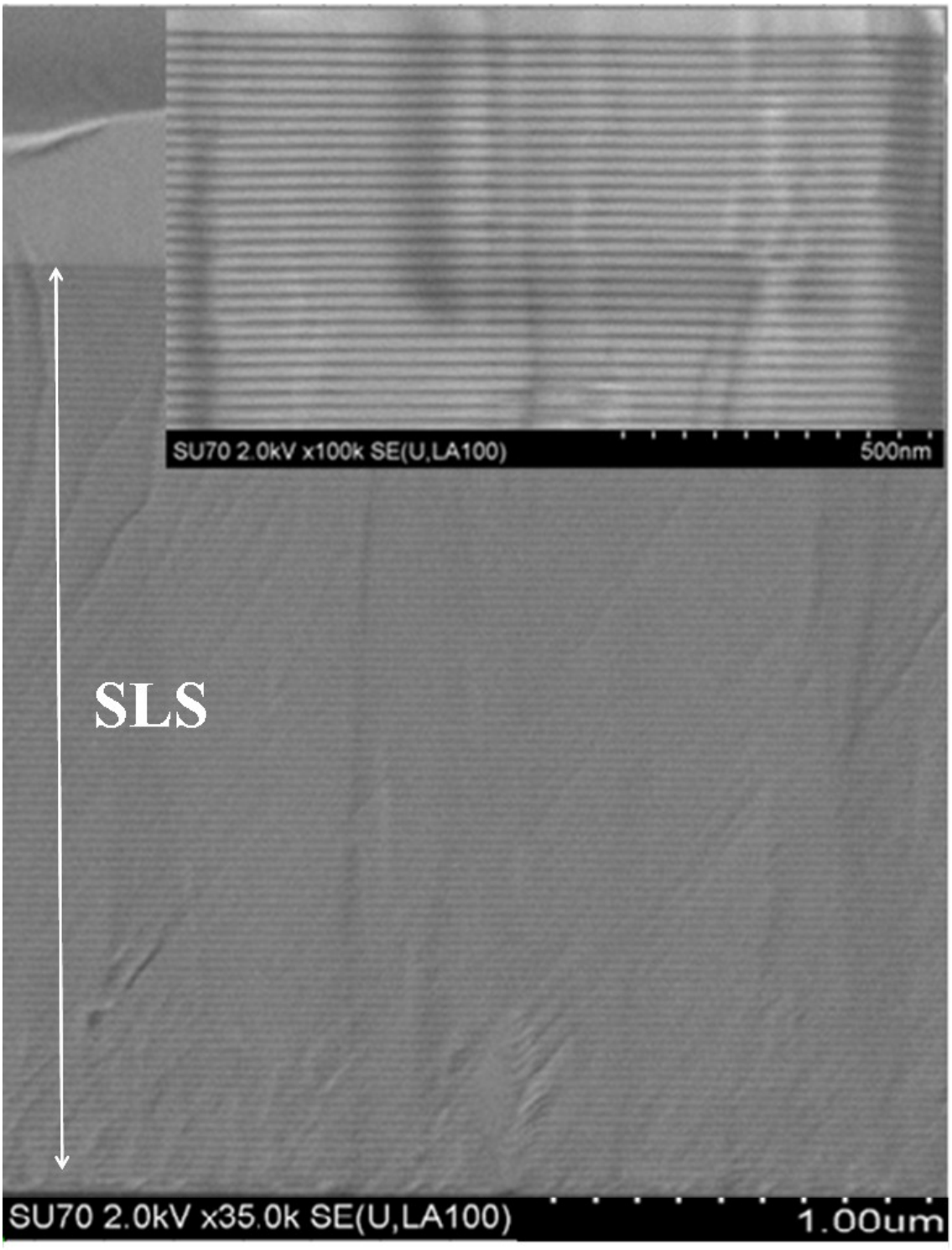

Fig. 5. 2. Cross-section SEM images for the SLs layers of sample under the two magnifications of 35 and 100 K.

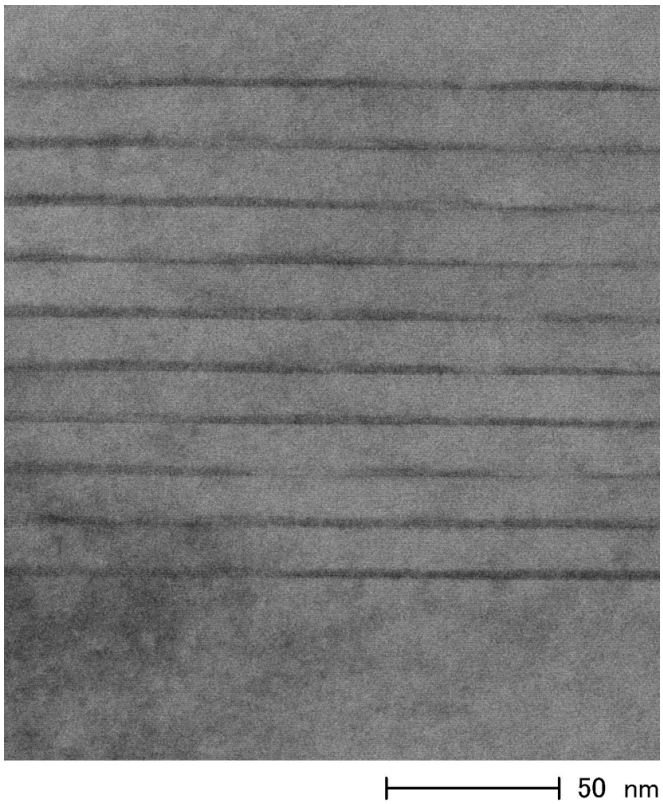

Fig. 5. 3. Cross-section TEM image for the MQWs layers of sample.

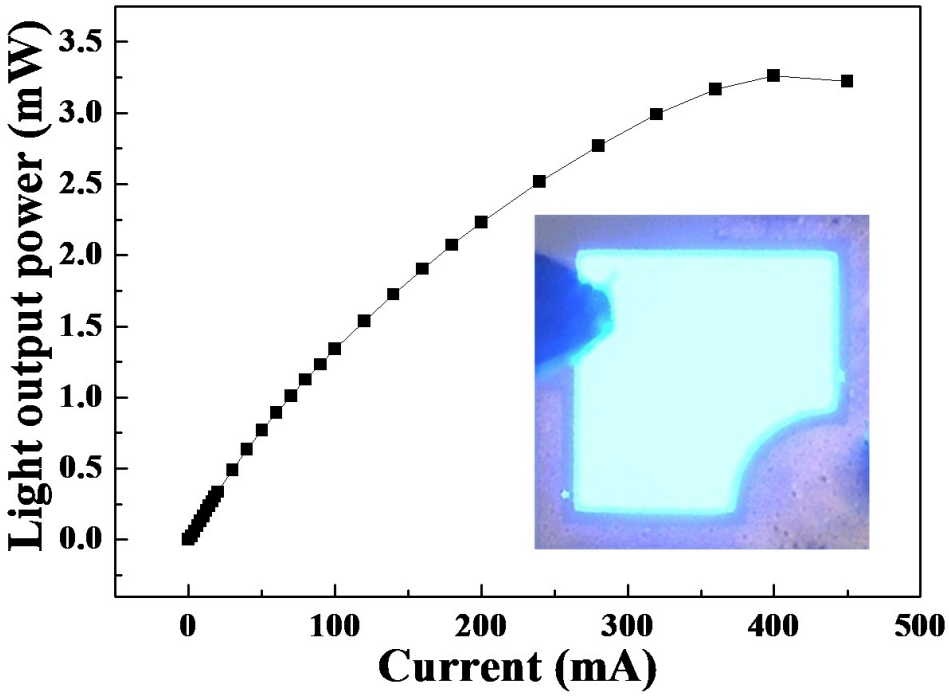

Fig. 5. 4. Light output power of sample as a function of injection DC current. The inset shows the emission image (@ 20 mA).

5.2 High Performance of GaN-based Light Emitting Diodes Grown on 4-in. Si(111) substrate

5.2.1 Introduction

GaN and related alloys are one of the promising materials for applications in optoelectronic and microelectronic devices [1-2]. Nowadays GaN-based blue-green and white light emitting diodes (LEDs) are commercially available almost on sapphire and SiC substrates. For a larger scale fabrication, however, those substrates are limited because of their size and higher costs. In order to solve this issue, one of the effective approaches is to grow LEDs on highly conducting 4- to l2-in. silicon (Si) substrates. Moreover, choosing Si as substrate can offer a great deal of advantages, such as the good thermal conductivity, the simplicity of process, and the possibility of integration of Si electronics on the same chip [3]. On the other hand, in terms of the GaN epitaxial growth on Si, it is well known that the most challenging issues are to relieve tensile stress due to the large thermal expansion coefficient and lattice constant mismatches between GaN layer and Si substrate, which always result in the occurrence of cracks and high density threading dislocations [4]. Nevertheless, the demonstrations of LEDs grown on Si have been reported by some groups [2,5-9]. Several approaches have been previously attempted to control the strain and minimize the cracks, such as using AlN/GaN multilayers with a thin AlN/AlGaN buffer layer [2-3], the insertion of AlGaN/GaN superlattice structure [17], employing low-temperature AlN and Si_xN_y interlayer[5,18] , and so on [7-8,11]. In those previous demonstrations, LEDs structures have been grown almost on 2-in. Si substrates until now [2,5,8,17], except some few

groups have used 6-in. Si substrates [6]. Because the growth of thick GaN will be more difficulty with increasing the size of Si substrate due to the larger strain, which further leads to a bigger value of curvature and induces some cracks. In addition, with respect to the external quantum efficiency (EQE), some few data have been reported. Fenwick et al. have presented it with a low value of 0.1% [19]. So far of our knowledge, although the GaN-based hetero-junction field effect transistors and high electron mobility transistors have been demonstrated on 4-in. Si substrate [20-21] , there have been no previous demonstrations of the LEDs grown on the same diameter Si substrate.

In this work, we have successfully fabricated the GaN-based LEDs grown on 4-in. Si(111) substrate by metal-organic chemical vapor deposition (MOCVD) for the first time. The properties of samples have been investigated in detail by high-resolution X-ray diffraction (HR-XRD), current-voltage (*I-V*), electroluminescence (EL), and light output power-current (*L-I*) measurements. It is found that the light output power of the LEDs has been enhanced by two times with increasing n-GaN layer thickness. Regarding the enhancement of the optical power, some mechanisms have also been discussed between the structural and device property.

5.2.2 Experiment

A commercial MOCVD reactor system (Nippon Sanso SR-4000) was used for the epitaxial growth of InGaN-based multiple-quantum wells (MQWs) LEDs structure. Trimethylgallium (TMG), trimethylindium (TMIn), and ammonia (NH_3) were used as sources for gallium, indium and nitrogen, respectively. Monosilane (SiH_4) diluted in hydrogen was used as n-type dopant, and the p-type dopant was biscyclopentadienyl magnesium (Cp_2Mg). Prior to the growth of LEDs structure, a buffer layer (BL)

consisting of a 5 nm n-AlN layer and a 20 nm n-AlGaN layer was grown at 1030 ^{o}C. Then, 100 pair n-AlN/GaN (5/20 nm) strained-layer superlattice (SLS) layers and n-GaN layer were grown at 1130 ^{o}C. Finally, an undoped 10 period MQWs consisting of 4 nm $In_xGa_{1-x}N$ wells and 8 nm $In_yGa_{1-y}N$ barriers at 800 ^{o}C, a 20 nm p-AlGaN layer and a 100 nm p^+-GaN cap layer at 1030 ^{o}C were grown successively. For comparison, two samples were prepared, in which only n-GaN thicknesses were different. The thicknesses of n-GaN were 2 and 1 μm in sample A and B, respectively. In order to confirm the crystalline quality of epitaxial layers, HR-XRD (Philips X'Pert Epitaxy) measurement was performed.

The top-emitting LEDs with a chip size of 500×500 μm^2 were fabricated using a standard process. Main fabrication procedure of the LEDs included multiple-mask photo-lithography, reactive ion etching, metal evaporation and annealing. The details can be referred to our previous report [11]. Figure 5. 5 shows the schematic structure of the LEDs used in this study. The LEDs were characterized using an on-wafer configuration. *I-V* measurement was carried out using a semiconductor parameter analyzer (Agilent 4155C). EL spectra and light output power were measured under the conditions of room temperature and various direct current using an integrated sphere detector (Otsuka Electronics MPCD-7000).

5.2.3 Results and Discussion

Two samples in this study are crack-free, and show mirror-like surface for the whole wafer. Figure 5. 6 shows GaN(0002) and (10-12) XRD ω-scans rocking curves of samples A and B. The full width at half maximum (FWHM) of (0002) are 626 and 916 arcsec, and those of (10-12) are 1464 and 1604 arcsec for samples A and B, respectively.

This indicates that there is a significant improvement of GaN epitaxial quality when increasing the thickness of n-GaN. For sample A, the density of screw component threading dislocation (TDs) is calculated to be $7.9\times10^{8}/cm^{2}$ from the extracted tilt value [22], which is lower by one order of magnitude comparing with our previous results [11]. Therefore, it can be expected that the LEDs with high performance grown on Si will be realized.

The typical *I-V* characteristics of the two samples are shown in Fig. 5. 7. At an injection current of 20 mA, the operating voltage of sample A and B is 6.1 and 8.0 V, respectively. For the study of vertical-LED on Si, the electrons injection is carried out from Si substrate into the active layer through the BL and SLS layers. Consequently, the electrons will encounter some large barriers during the injection. And it will also lead to the high turn-on and operating voltages [23]. In addition, the epitaxial quality also influences the electrical property, that is, some TDs are related with the voltage. It should be noted that the results of *I-V* are in good agreement with the results of XRD. On the other hand, room temperature EL spectra of sample A under various currents are shown in Fig. 5. 8. The EL peak is centered at 487 nm at the injection current of 20 mA, which corresponds to near band edge luminescence from the optically active region. In addition, it is interesting to note that a few blue-shifts have occurred with increasing the current. This is attributed to the free-carrier-screening and band-filling effects[24].

Figure 5. 9. shows the typical light output power and EQE versus injection current (*L-EQE-I*) characteristics of samples A and B. It can be seen clearly that the output power of LEDs increases linearly with injection current initially. At the injection current of 20 mA, the output power of sample A and B is 298.3 and 152.4 μW, respectively. This indicates that the increment of sample A has reached near to 200%

with comparing to sample B. However, the output power starts to saturate and finally reaches at maximum value, then decreases slightly as the injection current is further increased. It can be observed that the maximum output power of sample A and B is 1.71 and 0.68 mW, respectively. While the saturation operating current of sample A and B is 280 and 170 mA, respectively. From those results, it can be confirmed that the optical power of sample A has been improved by increasing the thickness of n-GaN. The aforementioned data are consistent with the results of XRD and *I-V*.

Recently, Li et al. have reported that the saturation current of GaN-based LEDs grown on Si was about 170 mA [6]. Comparing with this result, it is worth noting that the corresponding date of sample A is higher by a factor of 1.75. Therefore, it can be speculated that the device with high performance are mainly attributed to the high quality of epitaxial layer and good thermal conductivity of Si substrate. In addition, as shown in Fig. 5. 9, we can find that the maximum EQE of sample A and B is about 0.6 and 0.3%, respectively. These results are well consistent with aforementioned ones. On the other hand, it can be also found that the efficiency droop is remarkable, resulting from several factors, such as carrier leakage from the active region, Joule heating from the series and parasitic resistances, high polarization and so on [25].

As well known, concerning the LEDs grown on Si, lower light output power comparing to that on sapphire results from several factors, such as, the light absorption by the Si substrate, the quality of GaN, the structural design and growth parameters [8]. Actually, in our study, if the n-GaN thickness is over 2 μm, some cracks will emerge on the device surface. It can be expected to be solved by strain modulation of the optimized SLS. In addition, one of hard issues is distribution controlling in the whole wafer, in particular, for the big size of 4- to 12- in. Si substrate. In this demonstration, the

standard deviation of peak position is approximately 12% for the two samples. It can be contributed to the indium fluctuation in the MQWs, which might due to different InGaN-phase segregation. It is well known that bowing values will be larger with increasing the size of Si substrate, and it results from the variation of strain. Moreover, it will result in the distribution of growth temperature of epitaxial layers. Consequently, the indium corporations will not be same in the whole wafer. Despite those above influence issues, it can be believed that the performance of LEDs grown on Si will be improved further by means of some new effective approaches in the near future.

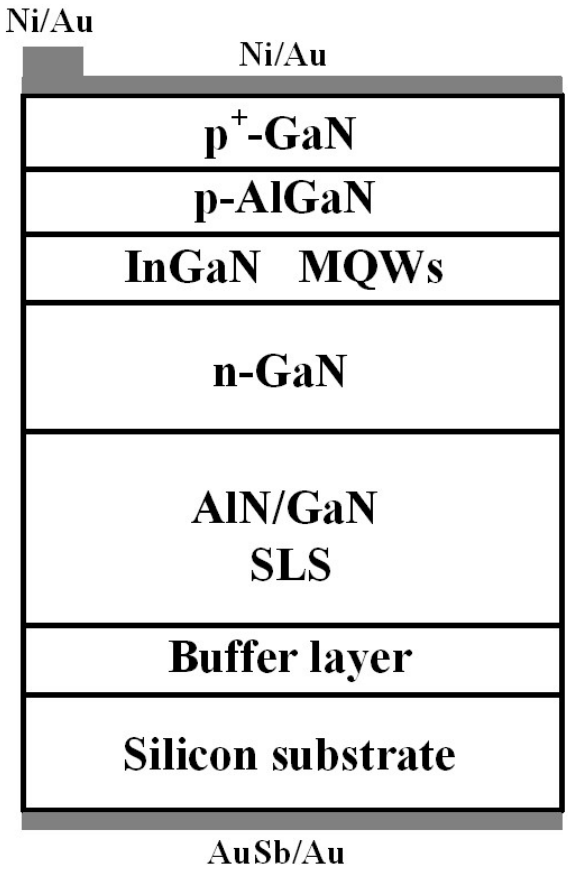

Fig. 5. 5. Schematic structure of GaN-based LEDs.

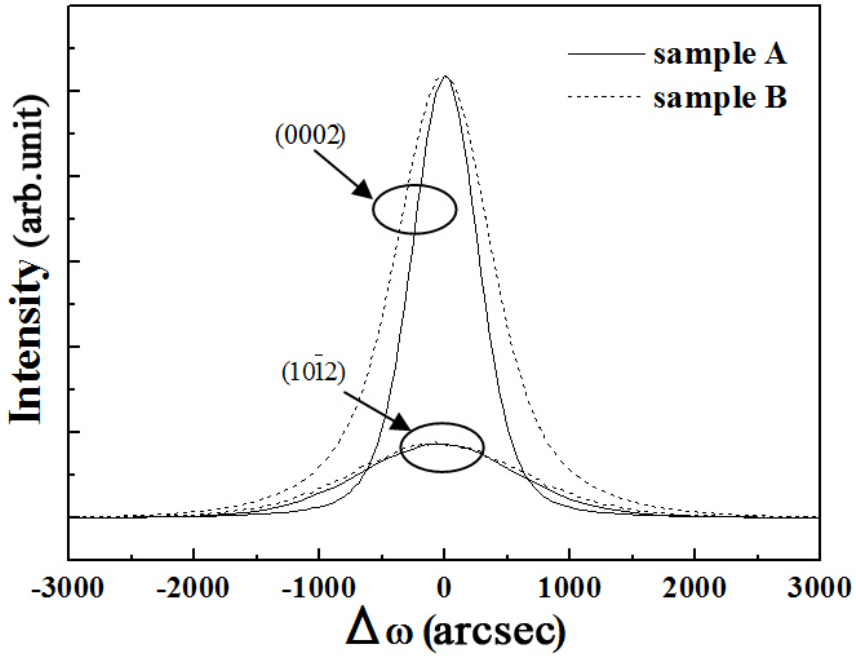

Fig. 5. 6. XRD rocking curves in GaN (0002) and (10-12) ω-scans of sample A and B.

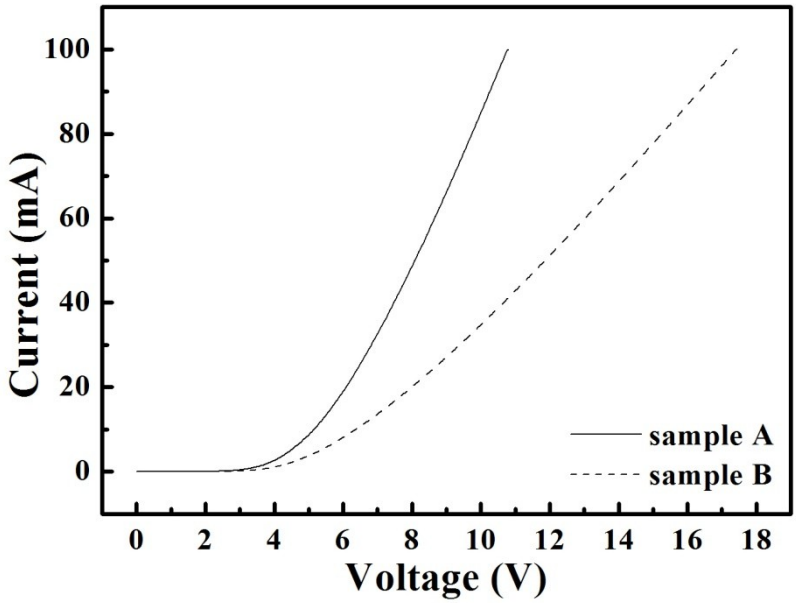

Fig. 5. 7. *I-V* characteristics of sample A and B.

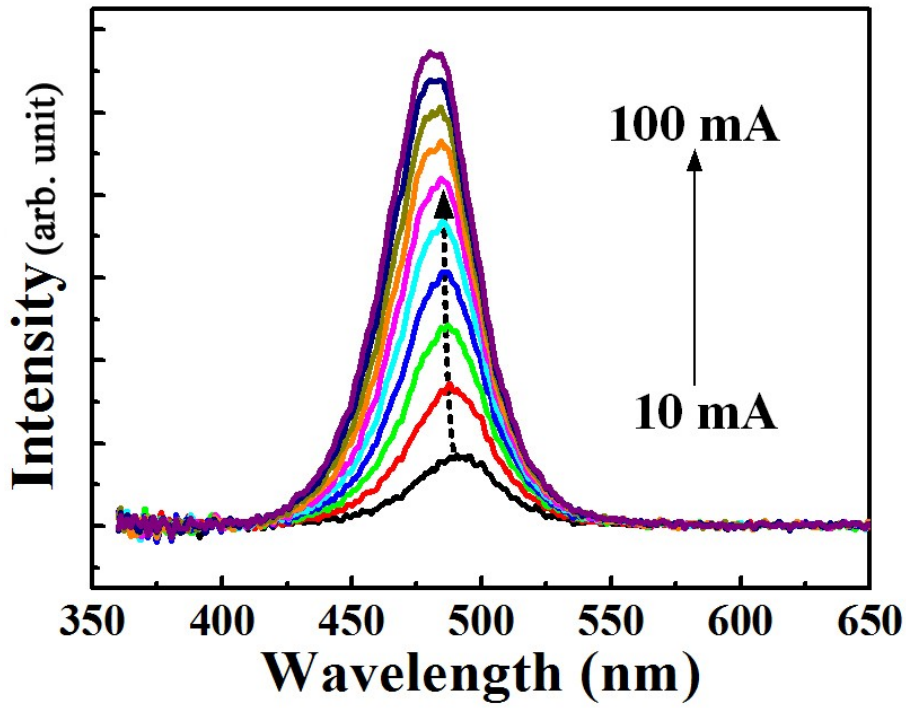

Fig. 5. 8. EL spectra of sample A as a function of injection current, and the blue-shifts of emission peak are indicated by dot line arrow.

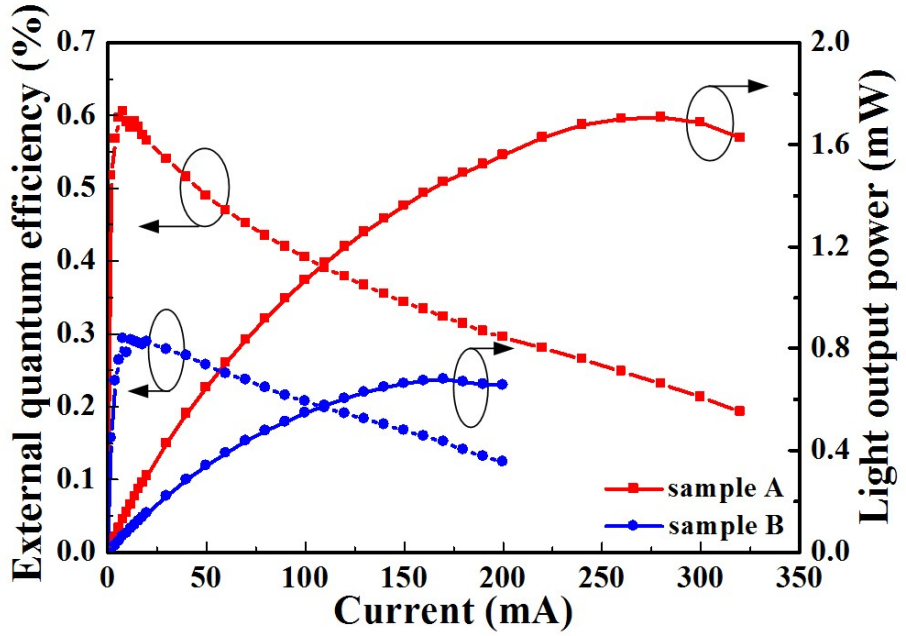

Fig. 5. 9. *L-EQE-I* characteristics of sample A and B as a function of injection current.

5.3 Conclusions

In conclusion, in the section 5.1, the high quality GaN-based LEDs with a 2 μm n-GaN grown on 4-in. Si(111) substrate by MOCVD have been characterized. The sample structural property with the smooth interfaces has been confirmed by XRD, SEM, and TEM measurements. Moreover, the LED with a maximum light output power of 3.3 mW and a high saturation operating current of 400 mA has been realized. Nevertheless, the characterizations have revealed some important results, which would boost the researchers to further improve the performance of LEDs grown on Si substrate.

On the other hand, in the section 5.2, the feasibility for growing high quality GaN-based LEDs by MOCVD on 4-in. Si(111) substrate have been demonstrated. The structural, electrical, and optical properties of the samples have been systematically clarified. It is demonstrated that the performance of GaN-based LEDs can be improved by increasing the thickness of n-GaN. As a consequent, 1.7 mW output power of LEDs with a high saturation operating current of 280 mA have been fabricated. Therefore, the demonstration revealed some important results, which would promote the device researchers to further improve the performance of LEDs grown on Si substrate.

References

[1] S. Nakamura, G. Fasol, and S.J. Pearton: *The Blue Laser Diode: The Complete Story* (Springer, New York, 2000), 2nd ed., and references therein.

[2] T. Egawa, B. Zhang, and H. Ishikawa: IEEE Electron Device Lett. **26**,169 (2005).

[3] T. Egawa, T. Moku, H. Ishikawa, K. Ohtsuka, and T. Jimbo: Jpn. J. Appl. Phys. **41**, L663 (2002).

[4] H. Ishikawa, G. Y. Zhao, N. Nakada, T. Egawa, T. Jimbo, and M. Umeno: Jpn. J. Appl. Phys. **38**, L492 (1999).

[5] A. Dadgar, M. Poschenrieder, J. Bläsing, K. Fehse, A. Diez, and A. Krost: Appl. Phys. Lett. **80**, 3670 (2002).

[6] J. Li, J. Y. Lin, and H. X. Jiang: Appl. Phys. Lett. **88**, 171909 (2006).

[7] S. Tripathy, V. K. X. Lin, S. L. Teo, A. Dadgar, A. Diez, J. Bläsing, and A. Krost: Appl. Phys. Lett. **91**, 231109 (2007).

[8] B. Zhang, H. Liang, Y. Wang, Z. Feng, K. W. Ng, and K. M. Lau: J. Cryst. Growth **298**, 725 (2007).

[9] C. Mo, W. Fang, Y. Pu, H. Liu, and F. Jiang: J. Cryst. Growth **285**, 312 (2005).

[10] Y. Zhu, A. Watanabe, L. Lu, Z. Chen and T. Egawa: Jpn. J. Appl. Phys. **50**, 04DG08 (2011).

[11] Y. H. Zhu, J. C. Zhang, Z. T. Chen and T. Egawa: J. Appl. Phys. **106**, 124506 (2009).

[12] I. H. Kim, H. S. Park, Y. I. Park, and T. Kim: Appl. Phys. Lett. **73**, 1634 (1998).

[13] B. Zhang, T. Egawa, H. Ishkawa, Y. Liu, and T. jimbo: Jpn. J. Appl. Phys. **42**, L226 (2003).

[14] D. S. Wuu, W. K. Wang, K. S. Wen, S. C. Huang, S. H. Lin, S. Y. Huang, C. F.

Lin, and R. H. Horng: Appl. Phys. Lett. **89**, 161105 (2006).

[15] D. Zhu, C. McAleese, M. Häberlen, C. Salcianu, T. Thrush, M. Kappers, A. Phillips, P. Lane, M. Kane, D. Wallis, T. Martin, M. Astles, N. Hylton, P. Dawson, and C. Humphreys: J. Appl. Phys. **109**, 014502 (2011).

[16] B. J. Zhang, T. Egawa, H. Ishkawa, Y. Liu, and T. jimbo: Appl. Phys. Lett. **86**, 071113 (2005).

[17] S. Raghvan and J. M. Redwing: J. Appl. Phys. **98**, 023514 (2005).

[18] A. Dadgar, M. poschenrieder, O. Contreras, J. Christen, K. Fehse, J. Bläsing, A. Diez, F. Schlze, T. Riemann, F. A. Ponce, and A. Krost: Phys. Status Solidi (A) **192**, 308 (2002).

[19] W. E. Fenwick, A. Melton, T. Xu, N. Li, C. Summers, M. Jamil, and L. T. Ferguson: Appl. Phys. Lett. **94**, 222105 (2009).

[20] J. D. Brown, R. Borges, E. Piner, A. Vescan, S. Singhal, and R. Therrien: Solid-State Electron. **46**, 1535 (2002).

[21] J . Selvaraj, S. L. Selvaraj, and T. Egawa: Jpn. J. Appl. Phys. **48**, 121002 (2009).

[22] Z. T. Chen, K. Xu, L. P. Guo, H. Zhang, and G. Y. Zhang: J. Cryst. Growth **294**, 156 (2006).

[23] T. Egawa, B. Zhang, N. Nishikawa, H. Ishikawa, and M. Umeno: J. Appl. Phys. **91**, 528 (2002).

[24] T. Kuroda and A. Tackeuchi: J. Appl. Phys. **92**, 3071 (2002).

[25] M. H. Kim, M. F. Schubert, Q. Dai, J. K. Kim, E. F. Schubert, J. Piprek, and Y. Park: Appl. Phys. Lett. **95**, 241109 (2009).

Chapter 6

Strain Evolution in GaN-based Light Emitting Diodes with Different n-GaN Thickness

This chapter presents strain evolution in GaN-based light emitting diodes (LEDs) with different n-GaN thickness. GaN-based LEDs with various thickness of n-GaN have been grown on 4-inch Si(111) substrate by metal-organic chemical vapor deposition. The crystalline quality of GaN epilayer has been evaluated by X-ray diffraction (XRD) and transmission electron microscopy. It is found that a significant improvement of epilayer quality can be achieved by increasing n-GaN thickness. As a consequence, the sample with total thickness of approximately 4.8 μm and a comparatively low screw component threading dislocation density of 8.0×10^{8} cm^{-2} was found to have the best property. The influence of n-GaN thickness on the strain state has been directly investigated by means of micro-Raman scattering. It was observed that the compressive strain changed to tensile one with increasing n-GaN thickness from 0.5 to 2.0 μm. As a result, in a sample with a 2 μm n-GaN thickness, the tensile stress of GaN epilayer was calculated to be 0.44 GPa. In addition, the strain states of GaN epilayer have been revealed from the variations of its a- and c-lattice constants using XRD. The emission peak shift of GaN epilayer has also been confirmed by cathodoluminescence measurement. Finally, some other consistent correlations have been interpreted in this study.

6.1 Introduction

GaN and its related alloys have always been considered as one of the promising materials for applications in optoelectronic and microelectronic devices [1-2]. It is also well known that GaN-based light emitting diodes (LEDs) in a wide range of wavelengths from UV to green have already been commercially available. Those LEDs are commonly grown on sapphire and SiC substrates by metal-organic chemical vapor deposition (MOCVD). However, in large scale fabrication, those substrates are limited due to their smaller size and high cost. In order to overcome this limitation, growing LEDs on highly conducting 4- to l2-inch silicon (Si) substrates has been suggested as one of the most effective approaches since last century. In addition, the potential cost reduction by successful growth of GaN-based LEDs on the larger Si substrates is thought to give solid state lighting a boost towards replacing incandescent light [3]. Moreover, choosing Si substrate can offer a great deal of advantages, such as the good thermal conductivity, simplicity in processing, and possibility of the integration of Si electronics on the same chip [4].

However, the biggest challenging in terms of GaN epitaxial growth on Si is to relieve the tensile strain, caused by the large mismatch in lattice constants (17%) and difference in the thermal expansion coefficients (116%) between GaN layer and Si substrates [2]. The tensile strain usually leads to emergence of cracks and a high threading dislocations (TDs) density by a magnitude of 10^{9}-10^{11} cm^{-2} at layer thicknesses exceeding 1 μm [5-6]. Nevertheless, our group and others have demonstrated growth of LEDs on Si [2-10]. LEDs with normal structures have been grown almost entirely on the 2-inch Si substrates until now [4-6,8-13], except for few groups who have employed 6-inch Si substrates [3,7]. The growth of thick epitaxial

GaN layers will be more difficult with increasing size of Si substrate due to the resulting larger strain, which further results in a bigger value of curvature, and induces some cracks at the same time.

Fortunately, the induced strain during growth can be controlled by the careful tuning of using some novel growth technologies. Nowadays, several approaches have been attempted to modify the strain and minimize the cracks, such as using AlN/GaN multilayers with a thin AlN/AlGaN buffer layer [2,4], the insertion of AlGaN/GaN superlattice structure [11], employing low-temperature AlN and Si_xN_y interlayer [6,12], and others [8-9,13-14]. Therein, it should be noted that the main purpose of the above methods is to improve the GaN epilayer quality, which directly determines the LEDs performance. Therefore, understanding the quality and strain evolution of GaN epilayers is significantly important for designing the device structure. Until now, in numerous relative reports, the investigations of strain have been carried out almost in the bulk GaN structure [15-23]. Moreover, lots of literatures have been focused on the GaN epilayers grown on sapphire [18-22]. In two cases of using the sapphire and Si substrates, the introduced strain form into the GaN films is just opposite upon cooling from a high growth temperature to room temperature. Consequently, it is necessary to simultaneously analyze the quality and strain of GaN epitaxial layers in the LEDs grown on Si substrate as demonstrated in very few recent reports [14,23].

In this study, GaN-based LEDs have been successfully grown on 4-inch Si (111) substrate by MOCVD with different n-GaN thickness. Influence of n-GaN thickness on crystalline quality and strain of GaN epilayers have been comprehensively investigated by high-resolution X-ray diffraction (HR-XRD), cross-sectional transmission electron microscopy (TEM), micro-Raman scattering, and

cathodoluminescence (CL) measurements. In addition, regarding the quality and strain of GaN epilayer, some consistent relations derived from those characterizations have also been discussed.

6.2 Experiment

A commercial MOCVD reactor system (Nippon Sanso SR-4000) was used for the epitaxial growth of InGaN-based multiple-quantum wells (MQWs) LEDs structure. Trimethylgallium (TMG), trimethylaluminum (TMA), trimethylindium (TMIn), and ammonia (NH_3) were used as sources for gallium, aluminum, indium, and nitrogen, respectively. Monosilane (SiH_4) diluted in hydrogen was used as n-type dopant, and the p-type dopant was biscyclopentadienyl magnesium (Cp_2Mg). Prior to the growth of LEDs structure, a buffer layer (BL) consisting of a 5 nm n-AlN layer and a 20 nm n-AlGaN layer was grown at 1030 ^{o}C. Then, 100-pair n-AlN/GaN (5/20 nm) strained-layer superlattice (SLS) layers and an n-GaN layer were grown at 1130 ^{o}C. Finally, an undoped 10-period MQWs consisted of 4 nm $In_xGa_{1-x}N$ wells and 8 nm $In_yGa_{1-y}N$ barriers at 800 ^{o}C, a 20 nm p-AlGaN layer and a 100 nm p^{+}-GaN cap layer at 1030 ^{o}C were grown successively. In total three samples were prepared in this study. And, for comparison, sample A, B, and C represent the sample with an n-GaN thickness of 0.5, 1.0, and 2.0 μm, respectively. The other growth conditions were identical for all samples. The sample schematic structure is shown in Fig. 6. 1.

Sample surface morphology was characterized by Nomarski optical microscopy. Both symmetric (0002) and asymmetric ($10\bar{1}2$) ω-scan rocking curves were performed to characterize the tilt and twist factors in the structural imperfection of epitaxial layers. Moreover, in order to observe TDs variation, the microstructure was

also investigated by cross-sectional TEM (JEM-2010F, 200 kV). On the other hand, to confirm the strain states in those samples, micro-Raman scattering (JASCO, NRS-3300) experiments were carried out in a backscattering geometry with a combination of instruments of monochromator, equipped with 2400 lines/mm grating, microscope, and a charger couple device detector cooled by liquid nitrogen. At room temperature, Raman scattering experiments using coherent green laser (λ=532 nm) as the excitation light, a 100× objective lens was used in the confocal microscope to focus and collect the laser light before and after scattering. Then, the a- and c-axis GaN epilayer lattice constants of samples were determined by HR-XRD (Philips X'Pert MRD) tripe axis $2\theta-\omega$ scans. Finally, CL (Gatan MonoCL4 system) measurements were conducted to analyze the emission property of GaN epilayer using an electron-beam acceleration voltage of 10 kV at room temperature.

6.3 Results and Discussion

All three samples in this study are crack-free, and show mirror-like surface for the whole wafer. Figure 6. 2 shows the optical Nomarski surface image of sample C. This indicates that strain controlling in the device structure has been successful. It should be noted that no interlayer such as SiN or AlN has been inserted during the growth of the n-GaN.

Figure 6. 3 shows GaN (0002) and $(10\bar{1}2)$ XRD ω-scan rocking curves of those samples. The full width at half maximum (FWHM) of (0002) are 1153.2, 904.7, and 631.5 arcsec, while those of (10-12) are 1766.7, 1690.7, and 1604 arcsec for samples A, B and C, respectively. For sample C, the screw component TDs density is calculated to be $8.0\times10^{8}/cm^{2}$ from the above corresponding FWHM value [24], which is lower by

one order of magnitude than our previous results [13], and the same order as compared with the other groups [25-26]. It can be concluded that there is a significant improvement of GaN epilayer quality when increasing the thickness of n-GaN.

TEM is an effective technique for investigating dislocation characteristics in GaN related material system. In principle, TEM can reveal and identify each individual dislocation directly through its strain field. Figure 6. 4 shows the cross-sectional TEM images of samples B and C (sample A not shown here), which were taken in weak beam diffraction conditions with $\boldsymbol{g}$= [0002] and $\boldsymbol{g}$= $[11\bar{2}0]$, respectively. As shown in Fig. 6. 4. a1 and b1, it is obvious that the number of TDs in n-GaN epilayer remarkably decreases as the n-GaN thickness increases. Also, in same area, the TDs number of Fig. 6. 4. b2 is somewhat less than that of Fig. 6. 4. a2. All these results are consistent with the aforementioned XRD results. In addition, it can be also found that the interfaces of the SLS are extremely smooth.

It is well known that Raman scattering spectroscopy is a sensitive, local and nondestructive tool, which has been widely employed to measure strain or stress in semiconductor heterostructures [27]. Figure 6. 5 shows the room temperature Raman spectra of the three samples. The strongest peak (around 520 cm^{-1}) results from Si substrate as confirmed by Tripathy et al. [28]. On the other hand, as illustrated by red dashed line in the inset of Fig. 6. 5, the distinct GaN E_2-High peaks can be observed around the position of 568 cm^{-1}. This is consistent with previous literature reports [14, 28-29]. It is also found that its positions are shifting, implying the different stress states in those samples. It was reported that the Raman wavenumber of E_2-High in stress-free bulk GaN layer is 568 cm^{-1} [29]. For GaN, the E_2-High mode shifts linearly with a stress coefficient of 4.3 cm^{-1}/GPa [30]. The calculated stress in sample C is 0.44 GPa, which is

smaller comparing with another group [15]. All the stress values are listed in Table I. It is of interesting that a compressive form of strain is found in sample A, while it is tensile in sample C. Moreover, the E_2-high FWHM of sample C is the narrowest comparing with the samples A and B. It indicates that the sample C has the best GaN epilayer quality compared to the samples A and B. This again confirms the aforementioned GaN epilayer quality results of XRD and TEM.

Considering the above experimental results, it is important to further evaluate the variation of lattice constants in the GaN epilayer of these samples. With respect to the GaN layer, the a- and c-axis lattice constants and stress values in the epilayer can be calculated from triple axis HR-XRD measurements. Figure 6. 6(a) and 6(b) show GaN (0002) and ($10\bar{1}2$) XRD 2θ-ω scan results of three samples. The strongest peak in each spectrum arises from GaN epilayer. Several satellite peaks from AlN/GaN SLS can be clearly observed on both sides of the GaN peak. Its high-order fringes indicate the high quality of SLS structure with perfect interfaces. It is in good agreement with TEM result. This is also similar with our previous report [13]. however, as compared to our previous report, the intensity ratio of GaN to low-order (+1 to +3) satellite peaks is bigger in this study. This can be attributed to much more SLS pairs. In addition, based on the GaN diffraction peak positions, the lattice spacing of the d_{0001} and $d_{10\bar{1}2}$ can be calculated using the equations of Bragg diffraction [31]. In fact, d_{0001} is equal to the lattice constant c, and the lattice constant a can be obtained from the following formula [17] .

$$\frac{1}{3a^2}+\frac{1}{c^2}=\frac{1}{4d_{10\bar{1}2}{}^2} \tag{6-1}$$

While, the stain ε_{zz} in the z direction and ε_{xx} or ε_{yy} in the perpendicular plane are expressed by the below equations [32].

$$\varepsilon_{zz} = \varepsilon_{\perp} = \frac{c_s - c_0}{c_0} \quad (6\text{-}2)$$

$$\varepsilon_{xx} = \varepsilon_{yy} = \varepsilon_{\parallel} = \frac{a_s - a_0}{a_0} \quad (6\text{-}3)$$

where c_s (a_s) and c_0 (a_0) are the lattice constants for strained and strain-free GaN layers, respectively, in the z direction and the in-plane direction. Here, for unstrained bulk single crystals, the value of c_0 and a_0 is 5.1850 and 3.1892Å, respectively [16].

Finally, the in-plane biaxial stress σ_{xx} GaN epilayer can be derived as follows:

$$\sigma_{xx} = \left(C_{11} + C_{12} - 2\frac{C_{13}^2}{C_{33}}\right)\varepsilon_{xx} \quad (6\text{-}4)$$

where C_{11}, C_{12}, C_{13}, and C_{33} are independent components of the elastic stiffness tensor of the form C_{ij}. These values can be obtained from literature [33].

Using the above equations, all the corresponding calculated results are also listed in Table IV-I. The calculated stress in sample C is 0.44 GPa. The stress trend and values derived from HR-XRD have good coincidence with the Raman results. It is worth to noting here that the Si substrate size is 4-inch and the n-GaN epilayer growth is sequence in this study.

The room temperature a- and c-axis lattice constants with the n-GaN thickness have also been plotted in Fig. 6. 7. Early experimental results showed that c decreases with the increase of a, that is, the tensile stress increases with the decrease of c [34-35]. The three samples follow this trend. However, for sample A, the reason that the lattice constant of c-axis cannot surpass c_o although that of a-axis is lower than a_o is still unclear. It might be due to triclinic lattice distortions, instead of conventional tetragonal deformations, caused by the large lattice mismatch existing at some stage during the growth [36]. Further investigations are being carried out to confirm it.

It is known that the energy band gap of a semiconductor is affected by the residual stress in the film. A tensile stress will result in a decrease of energy band gap while a compressive strain causes an increase of the band gap [15]. In other words, differences in the strain shift the luminescence line position, that is, a compressive strain blue-shifts the emission peaks resulting from a larger band gap, on the contrary, a tensile strain red- shifts the emission peaks originating from reduction of the band gap [32]. Figure 6. 8 shows the CL spectra of the samples A, B, and C. The GaN emission peaks are centered below the 360 nm (3.44 eV). It indicates that there is a slight blue-shift as compared the PL result (3.40 eV) [15], which can be contributed to the different mechanisms of the two characterization techniques and different condition of strain states in the samples. On the other hand, comparing the sample C to the samples A and B, as indicated by red dashed line, the red-shift of GaN emission peak position occurs, while the FWHM of CL spectrum decreases. The red shift and FWHM reduction indicate that the sample C has a largest tensile strain with the best GaN epilayer quality. Therefore, it can be concluded that there are no discrepancies among all the results and discussions.

Table VI-I Parameters, including c-, a-axis lattice constant, and strain stress, deduced from Raman and XRD data for the samples grown with various thickness of n-GaN layers. σ_{xx} presents in-plane biaxial stress.

Sample	c-axis lattice constant (Å)	a-axis lattice constant (Å)	σ_{xx} stress Raman (GPa)	σ_{xx} stress XRD (GPa)
A	5.1840	3.1874	-0.23	-0.27
B	5.1823	3.1909	0.21	0.25
C	5.1818	3.1922	0.44	0.44

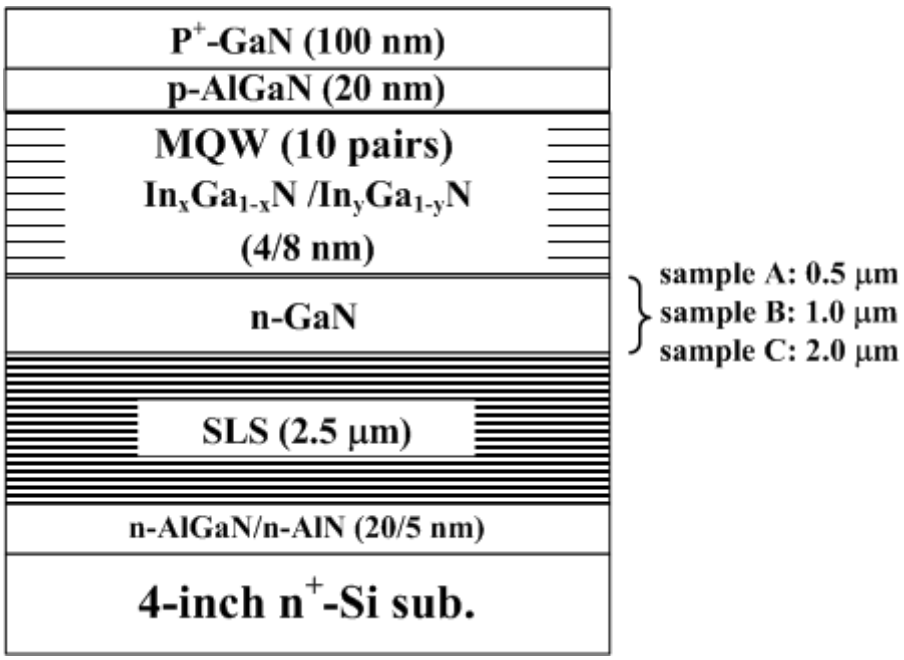

Fig. 6. 1. Schematic structure of the three samples with different n-GaN thickness.

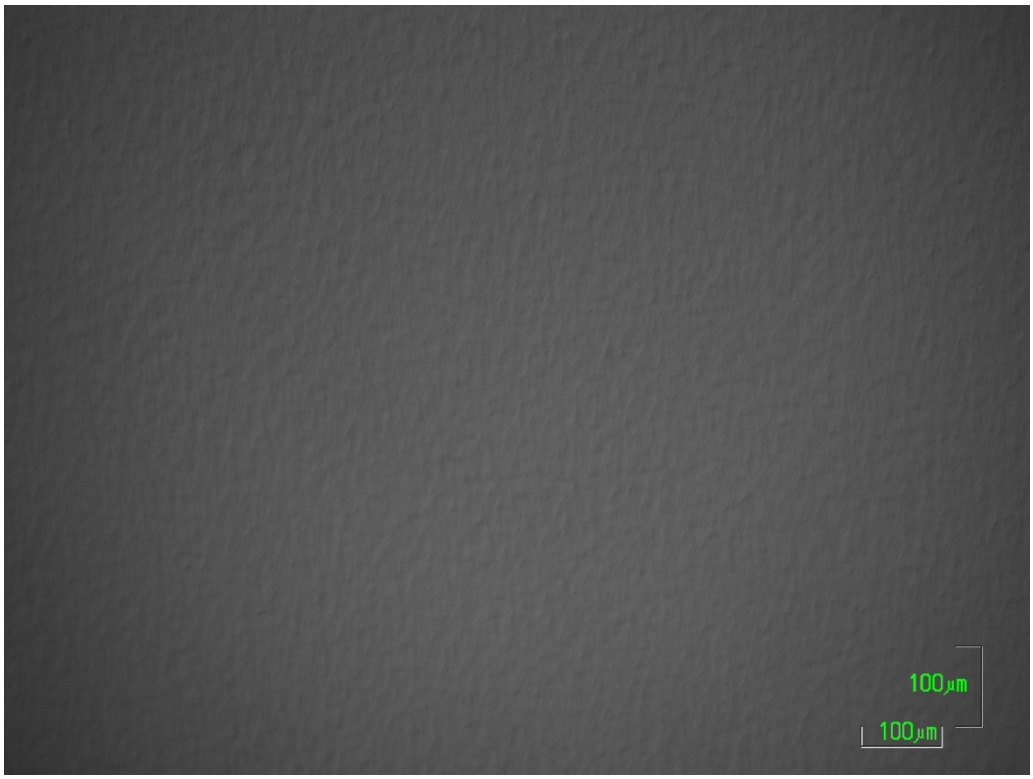

Fig. 6. 2. Optical Nomarski surface image of sample C with a 2 μm GaN epilayer.

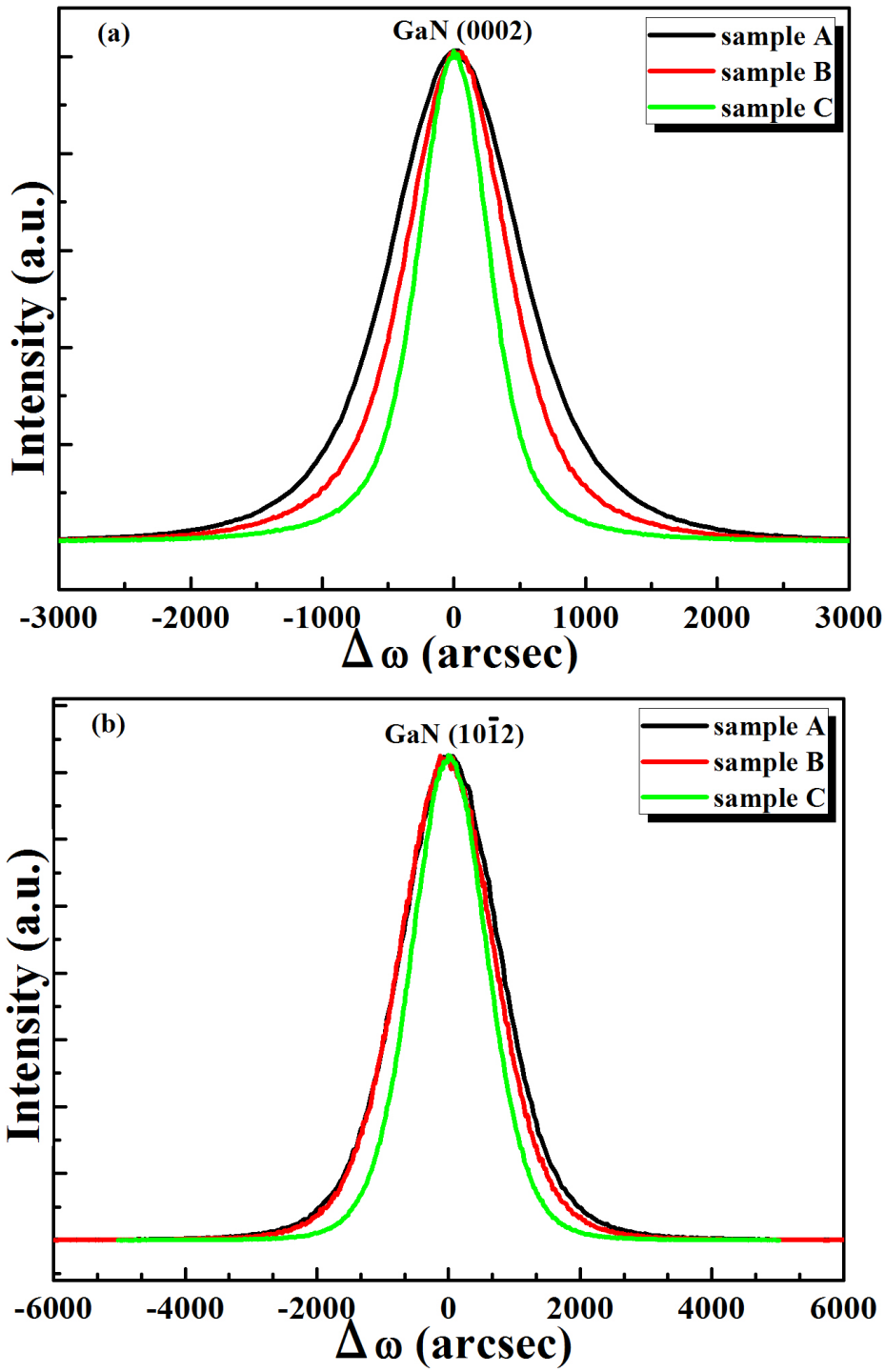

Fig. 6. 3. (a) HR-XRD rocking curves in GaN (0002) ω-scan of the three samples. (b) HR-XRD rocking curves in GaN ($10\bar{1}2$) ω-scan of the three samples.

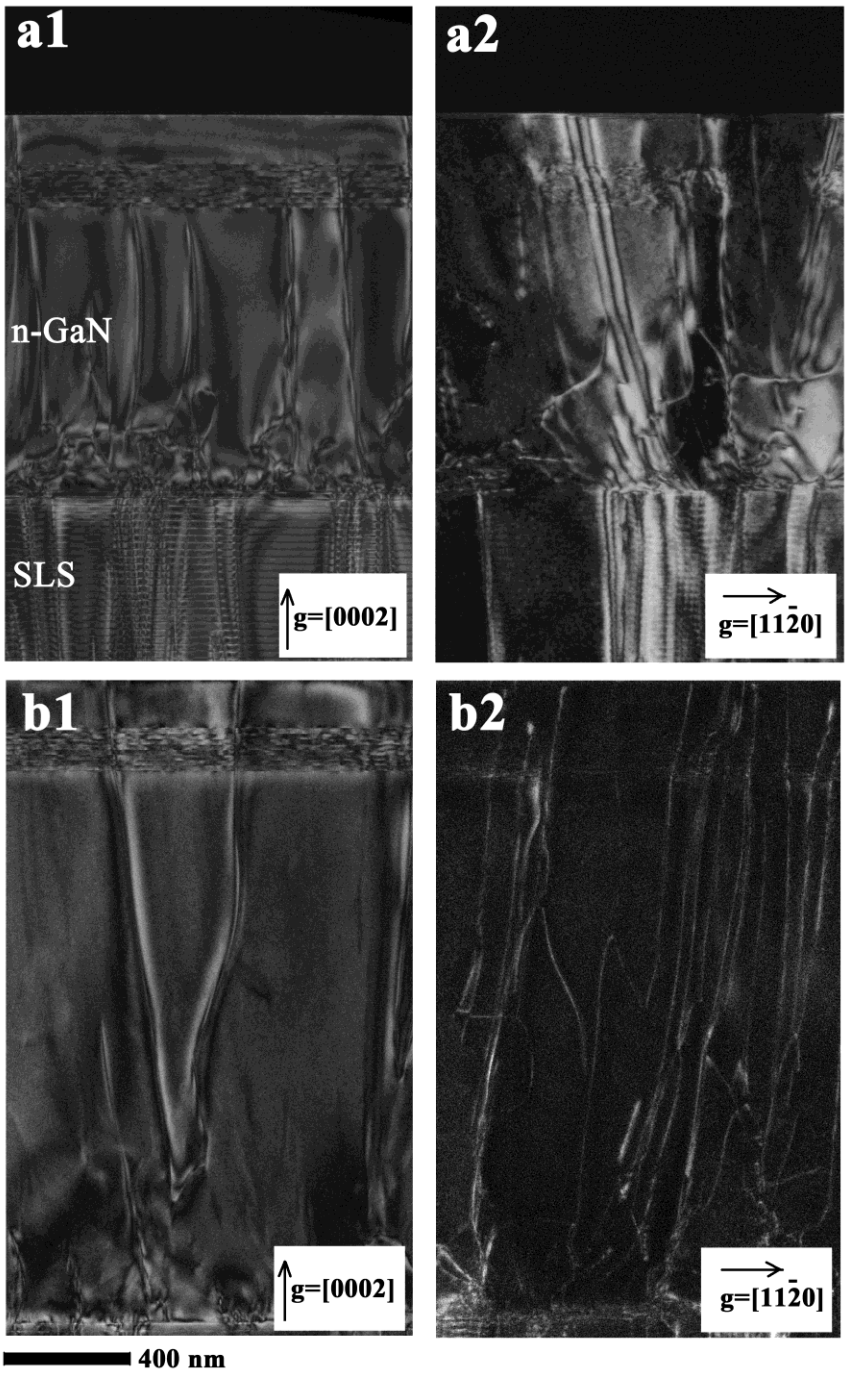

Fig. 6. 4. Cross-section dark-field TEM images of the representative samples B and C, that were taken under weak-beam diffracting condition with ***g***= [0002] (left) and ***g***= [$1\bar{1}\bar{2}0$] (right), respectively. Fig. a1and a2 for sample B, Fig. b1 and b2 for sample C (sample A not shown here).

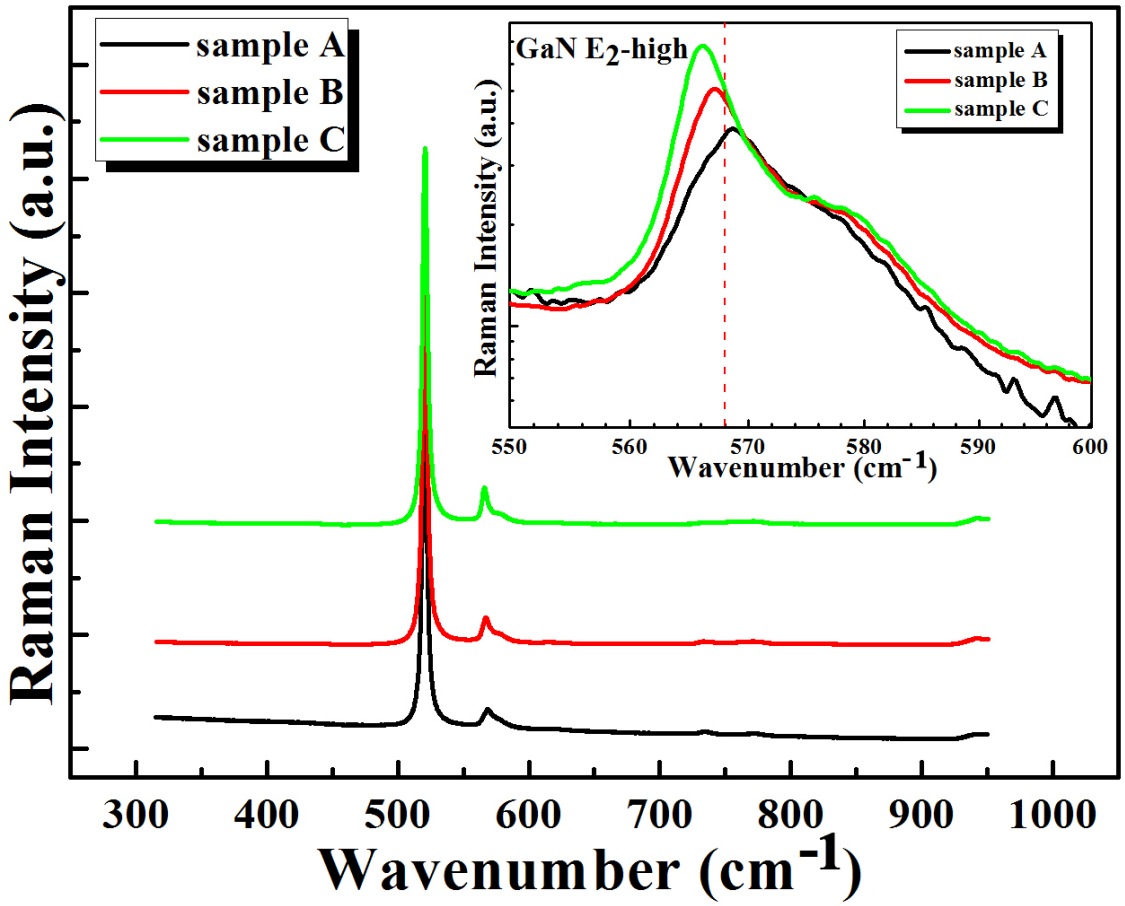

Fig. 6. 5. Raman spectra of the three samples. The inset shows GaN peaks for the three samples with a logarithm vertical axis. The red dashed line represents the Raman wavenumber position (568 cm^{-1}) of the stress-free bulk GaN epilayer.

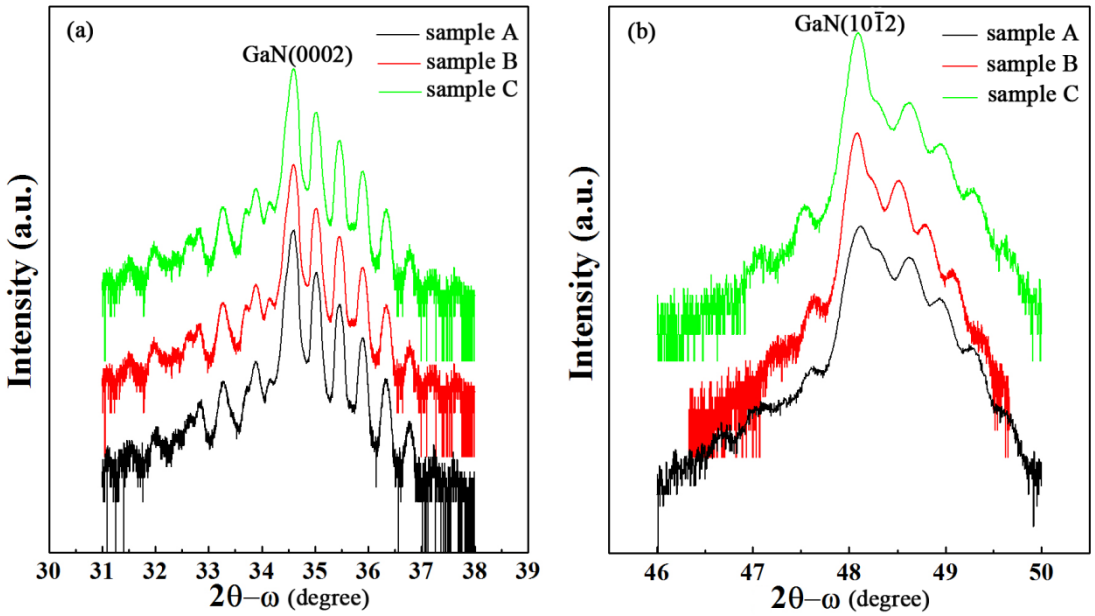

Fig. 6. 6. (a) HR-XRD of 2θ-ω scan of GaN(0002) for the three samples. (b) HR-XRD of 2θ-ω scan of GaN(10$\bar{1}$2) for the three samples. The intensity is shown by a logarithm vertical axis in the two figures.

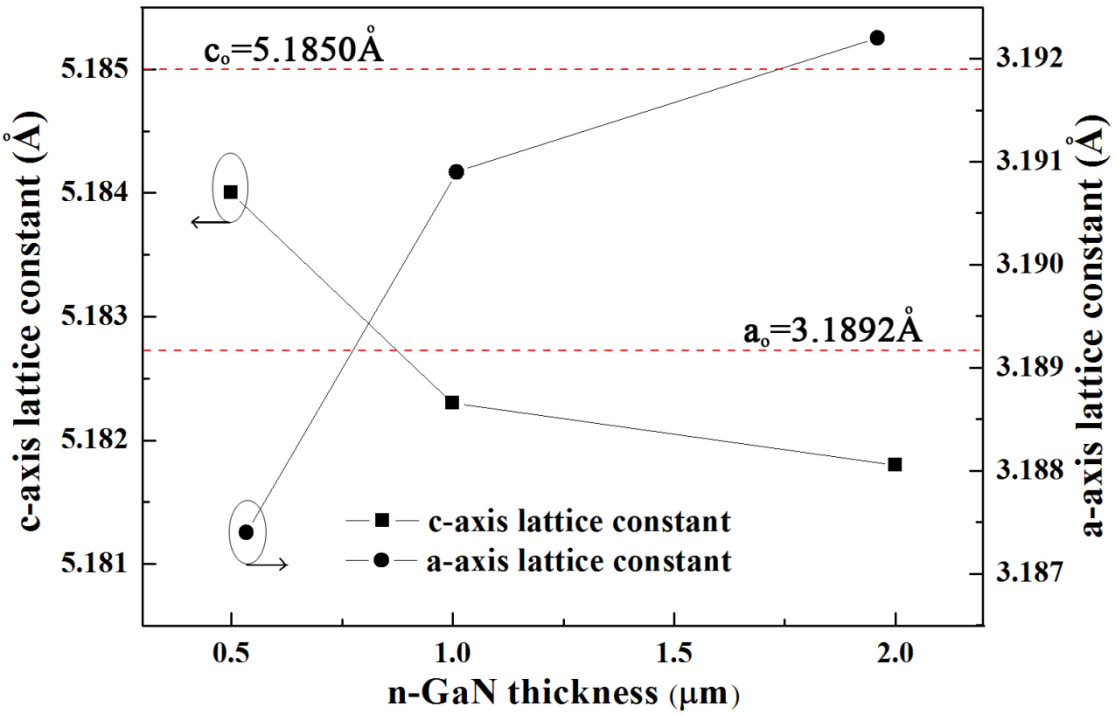

Fig. 6. 7. The a- and c-axis lattice constants as a function of the thickness of n-GaN. The two red dashed lines represent the value positions of c_o and a_o for full relaxed GaN epilayer.

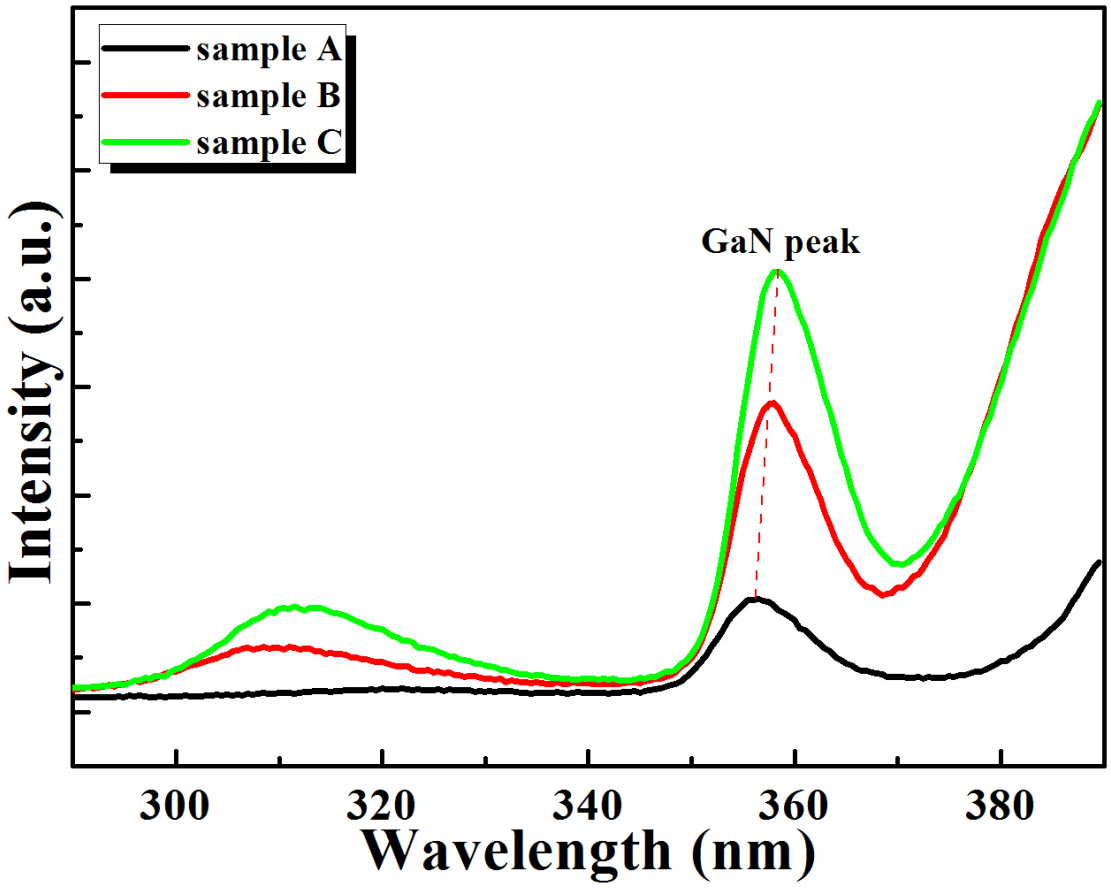

Fig. 6. 8. CL spectra of the three samples. The red dashed line represents the shifts of the GaN peak position.

6.4 Conclusions

Crack free and mirror-like GaN-based LEDs have been successfully grown on 4-inch Si(111) substrate by MOCVD with a respective n-GaN thickness of 0.5, 1.0 and 2.0 μm. Influence of n-GaN thickness on both the epilayer quality and strain in GaN epilayer have been investigated in detail by a combination of HR-XRD, cross-sectional TEM, micro-Raman, and CL measurements. It is found that when n-GaN thickness increases, the quality of GaN epilayer is considerably improved with a transition from compressive to tensile strain. In this study, some consistent relations regarding the quality and strain of GaN epilayer derived from those measurements have also been discussed. For example, the stress values of the GaN epilayer from Raman results are in agreement with XRD data. In addition, the red-shift of GaN emission peak has also been confirmed by CL. All the demonstrations have revealed several important results, which would inspire some device researchers to further improve the performance of LEDs grown on Si substrate. At the same time, these results again clearly imply that, especially for the structure of GaN-based LEDs grown on Si, both the improvement of GaN epilayer quality and modulation of its strain are imperative.

References

[1] S. Nakamura, G. Fasol, and S.J. Pearton, *The Blue Laser Diode: The Complete Stor*y (Springer, New York, 2000), 2nd ed., and references therein.

[2] T. Egawa, B. Zhang, and H. Ishikawa, IEEE Electron Device Lett. **26**, 169(2005).

[3] D. Zhu, C. McAleese, K. K. McLaughlin, M. Häberlen, C. O. Salcianu, E. J. Thrush, M. J. Kappers, W. A. Phillips, P. Lane, D. J. Wallis, T.Martin, M. Astles, S. Thomas, A. Pakes, M. Heuken, and C. J. Humphreys, Proc. SPIE **7231**, 723118 (2009).

[4] T. Egawa, T. Moku, H. Ishikawa, K. Ohtsuka, and T. Jimbo, Jpn. J. Appl. Phys. **41,** L663 (2002).

[5] H. Ishikawa, G. Y. Zhao, N. Nakada, T. Egawa, T. Jimbo, and M. Umeno, Jpn. J. Appl. Phys. **38,** L492 (1999).

[6] A. Dadgar, M. Poschenrieder, J. Bläsing, K. Fehse, A. Diez, and A. Krost, Appl. Phys. Lett. **80**, 3670 (2002).

[7] J. Li, J. Y. Lin, and H. X. Jiang, Appl. Phys. Lett. **88**,171909 (2006).

[8] S. Tripathy, V. K. X. Lin, S. L. Teo, A. Dadgar, A. Diez, J. Bläsing, and A. Krost, Appl. Phys. Lett. **91,** 231109 (2007).

[9] B. Zhang, H. Liang, Y. Wang, Z. Feng, K. W. Ng, and K. M. Lau, J. Cryst. Growth **298,** 725 (2007).

[10] C. Mo, W. Fang, Y. Pu, H. Liu, and F. Jiang, J. Cryst. Growth **285**, 312 (2005).

[11] S. Raghvan and J. M. Redwing, J. Appl. Phys. **98,** 023514 (2005).

[12] A. Dadgar, M. poschenrieder, O. Contreras, J. Christen, K. Fehse, J. Bläsing, A. Diez, F. Schlze, T. Riemann, F. A. Ponce, and A. Krost, Phys. Status Solidi (A) **192,** 308 (2002).

[13] Y. H. Zhu, J. C. Zhang, Z. T. Chen and T. Egawa, J. Appl. Phys. **106,**124506

(2009).

[14] D. Deng, N. Yu, Y. Wang, X. Zou, H. Kuo, P. Chen, and K.M. Lau, Appl. Phys. Lett. **96**, 201106 (2010).

[15] D. G. Zhao, S. J. Xu, M. H. Xie, S. Y. Tong, and H. Yang, Appl. Phys. Lett. **83**, 677 (2003).

[16] Y. Lu, X. Liu, D. Lu, H. Yuan, G. Hu, X. Wang, Z. Wang, and X. Duan, J. Cryst. Growth **247**, 91 (2003).

[17] B. S. Zhang, M. Wu, J. P. Liu, J. J. Zhu, X. M. Shen, G. Feng, D. G. Zhao, Y. T. Wang, H. Yang, and A. R. Boyd, J. Cryst. Growth **270**, 316 (2004).

[18] K. Hiramatsu, T. detchprohm, and I. Akasaki, Jpn. J. Appl. Phys., Part 1 **32**, 1528 (1993).

[19] C. Kisielowski, J. Krüger, S. Ruvimov, T. Suski, T. W. Ager, III, E. Jones, Z. Liliental-Weber, M. Rubin, E. R. Weber, M. D. Bremser, and R. F. Davis, Phys. Rev. B **54**, 17745 (1996).

[20] S. Ruvimov, Z. Liliental-Weber, T. Suski, J. W. Ager, J. Washburn, J. Krueger, C. Kisielowski, E. Weber, H. Amano, and I. Akaski, Appl. Phys. Lett. **69**, 990 (1996).

[21] L. Lee, I. Choi, C. Lee, E. Shim, D. Kim, D. Kim, S. K. Noh, S. Son, K. Lim, and H. J. Lee, J. Appl. Phys. **83**, 5787 (1998).

[22]L. T. Romano, C. G. Van de Walle, J. W. Ager III, W. GÖtz, and R. S. Kern, J. Appl. Phys. **87**, 7745 (2000).

[23] A. krost, A. Dadgar, G. Strassburger, and R. Clos, Phys. Status. Solidi A **200**, 26 (2003).

[24] J. C. Zhang, D. G. Zhao, J. F. Wang, Y. T. Wang, J. Chen, J. P. Liu, and H. Yang, J. Cryst. Growth **268**, 24 (2004).

[25] K. Cheng, M. Leys, S. Degroote, M. Germain, and G. Borghs, Appl. Phys. Lett. **92**, 192111 (2008).

[26] D. Zhu, C. McAleese, K. K. McLaughlin, M. Häberlen, C. Salcianu, T. Thrush, M. Kappers, A. Phillips, P. Lane, D. Wallis, T. Martin, M. Astles, N. Hylton, P. Dawson, and C. Humphreys, J. Appl. Phys. **109**, 014502 (2011).

[27] See, for example, in *Raman Scattering in Materials Science*, edited by W, H. Weber and R. Merlin (Springer, Berlin, 2000).

[28] S, Tripathy, S, J. Chua, P, Chen, and M. L. Miao, J. Appl. Phys. **92**, 3503 (2002).

[29] See, for example, a recent review article and references therein, H.Harima, J. phys.: Condens. Matter **14,** R967 (2002).

[30] B. H. Bairamov, O. Gürdal. A. Botchkarev, H. MorkoÇ, G. Irner, and J. Monecke, Phys. Rev. B **60**, 16741 (1999).

[31] X. H. Zheng, Y. T. Wang, Z. H. Feng, H. Yang, H. Chen, J. M. Zhou, and J. W. Liang, J. Cryst. Growth **250**, 345 (2003).

[32] L. Zhang, K. Cheng, S. Degroote, M. Leys, M. Germain, and G. Borghs, J. Appl. Phys. **108**, 073522 (2010).

[33] A. Polian, M. Grimsdich, and I. Grzegory, J. Appl. Phys. **79**, 3343 (1996).

[34] H. K. Cho, J. Y. Lee, K. S. Kim, G. M. Yang, J. H. Song, and P. W. Pu, J. Appl. Phys. **85 (5)**, 2617 (2001).

[35] T. Detchprohm, K. Hiramatsu, K. Itoh, and I.Akasaki, Jpn. J. Appl. Phys., **31**, L1454 (1992).

[36] C. Gianini, L. D. Caro, and L. Tapfer, Solid State commun **91**, 635 (1994)

Chapter 7

Summary and Future Work

This dissertation describes the study on the material characterization, fabrication, and evaluation for GaN-based light emitting diodes (LEDs) grown on silicon (111) substrate. In the chapter 1 to 3, the research background, epitaxial growth of MOCVD, and characterization for the material and LED, including some basic theories for the optical semiconductor device have been presented, respectively. It is known that the high quality GaN grown on Si is difficult to be achieved, which can be contributed to the large tensile stress induced by the lattice mismatch of 17% different thermal expansion coefficients of 116% and between GaN and Si substrate. In particular, during the cooling to room temperature, it often results in the cracks on the surface and the high threading dislocation density (TDD) in the layers, these are useless for device applications. Especially, these problems are the major obstacle to realize high performance GaN-based LEDs grown on Si(111) substrate. For example, the high TDD quickly degrades the LEDs lifetime, which is critical for application in commercial products. On the other hand, large substrate bowing is also the origin of cracks in the epitaxial layer. In order to obtain crack free layer, which has limited the n-GaN layer thickness with the maximum value of 2 μm in the LEDs structure of this study.

Prior to the growth of layers for GaN-based LEDs, a thin n-AlN nucleation layer and n-AlN/GaN strained-layer superlattice (SLS) has been utilized. In normal growth design of LED, n-type GaN layer, multiple quantum wells (MQWs), and p-type GaN are followed after the aforementioned SLS layers. However, in this conventional design, a part of light emitted from MQWs in the active layer is absorbed

by the underlying Si(111) substrate. In these approaches of improving the material, electrical, and optical characteristics of GaN-based LEDs grown on Si(111) substrate, the templet of 3C-SiC/Si(111) has been employed. In addition, based on increasing the pair of SLS to 100, the n-GaN thickness has been varied. Herein, it should be noted that the size of Si substrate in the latter one is 4-inch.

In the chapter 4, the GaN-based LEDs on Si substrate by using 3C-SiC as an intermediate layer (IL) have been demonstrated. The effect of 3C-SiC IL on the characteristics of LED has been investigated. The addition of 3C-SiC IL has resulted in the improved GaN crystalline quality, the better interfaces between the buffer and the initial SLS layers, and the smoother morphology of sample surface. As a consequence, the device with 3C- SiC IL showed an enhanced light output power by a factor of 2.4 at a drive current of 20 mA. The superior device performance was attributed to the improvement in the structural properties, which were clarified by AFM, XRD, and TEM measurements. This study implies that using 3C-SiC as IL is one of the effective approaches for enhancing the light output power of LEDs grown on Si substrate. It will also be of interest for a further study of GaN-based optoelectronic device grown on Si.

While, there are two sections in the chapter 5. In the section 5.1, GaN-based LEDs with a total thickness of 4.8 μm have been grown by metal-organic chemical vapor deposition on 4-in. Si(111) substrate. The structural property has been revealed by the measurements of high-resolution X-ray diffraction, scanning electron microscopy and transmission electron microscopy. It can be clarified that the LEDs in sample have the good interfaces and layer periodicities for the strained-layer superlattices and multiple quantum wells. In addition, the optical property in the light output power has been evaluated. As a result, LEDs with a maximum output power of 3.3 mW and a high

Saturation operating current of 400 mA have exhibited the good device performance. And , in section 5.2, the GaN-based LEDs grown by metal-organic chemical vapor deposition on 4-in. Si(111) substrates have been demonstrated. The structural property has been revealed by the measurement of X-ray diffraction. One of the full widths at half maximum of ω-scans of the GaN (0002) reflection is around 630 arcsec. Also, it can be found that the GaN epitaxial quality can be improved by increasing the thickness of n-GaN. The device properties have been evaluated through current-voltage, electroluminescence, and light output power-current measurements. As the n-GaN thickness increases from 1 to 2 μm, the light output powers of the LEDs have enhanced approximately two times under the injection current of 20 mA. Moreover, the maximum values of respective external quantum efficiency are achieved as 0.3 and 0.6%, respectively. Therefore, it can be believed that the high performance of GaN-based LEDs have been realized through this effective approach.

In order to understand the strain and lattice constant evolution in GaN-based LEDs with different n-GaN thickness, lots of characterization measurements have been performed, such as Raman, XRD, and so on. These descriptions have been shown in the chapter 6. Crack free and mirror-like GaN-based LEDs have been successfully grown on 4-inch Si(111) substrate by MOCVD with a respective n-GaN thickness of 0.5, 1.0 and 2.0 μm. Influence of n-GaN thickness on both the epilayer quality and strain in GaN epilayer have been investigated in detail by a combination of HR-XRD, cross-sectional TEM, micro-Raman, and CL measurements. It is found that when n-GaN thickness increases, the quality of GaN epilayer is considerably improved with a transition from compressive to tensile strain. In this study, some consistent relations regarding the quality and strain of GaN epilayer derived from those measurements have also been

discussed. For example, the stress values of the GaN epilayer from Raman results are in agreement with XRD data. In addition, the red-shift of GaN emission peak has also been confirmed by CL. All the demonstrations have revealed several important results, which would inspire some device researchers to further improve the performance of LEDs grown on Si substrate. At the same time, these results again clearly imply that, especially for the structure of GaN-based LEDs grown on Si, both the improvement of GaN epilayer quality and modulation of its strain are imperative.

Finally, some points should be taken into account in the future work. Actually, in this thesis, it is also agin proved that the material quality and LEDs performance improvement are limited to GaN epitaxy grown on Si (111). Even though the two approaches have been tried to improve the overall material quality, electrial and opitical property in the investigation of epitaxial structure and LEDs performance, there are lots of possible ways for further quality and performance improvement by some combinations with the other methods, such as Si_xN_{1-x} interlayer, etc, Also, there are the other advance approaches for epitaxial quality improvements, for instance, i) epitaxial lateral overgrowth (ELO), ii) pendeo epitaxial overgrowth (PEO), and iii) lateral epitaxial on a patterned substrate (LEPS), etc., which are not yet widely investgated for III-V nitride growth on Si substrate. The above methods are considered to significantly reduce TDD in the epitaxial layers, resulting in a high performance and reliable device lifetime. It can be expected that the advance growth techniques such as ELO/PEO/LEPS, and the new approaches, are necessary. While, it must be performed to achieve a commercial-grade high performance GaN-based high brightness LEDs and LD on Si substrate. The author believes that day will be coming by some achievable challenges of lots of reseachers, including our group.

Acknowledgements

I would like to express my sincere gratitude and deep indebtedness to my research supervisor, Professor Takashi Egawa from Research Center for Nano-Device and System, Nagoya Institute of Technology, for giving me tremendous opportunities to have a really excellent research in GaN-based wide-bandgap compoud semiconductor field. If there were not his significant guidance, support, and encouragement throughout the master and doctor course of my study, I could not accomplish my research and obtain my Ph.D. degree.

Also, I am grateful to Professor Shigeo Ohara from Department of Engineering Physics, Electronics and mechanics, Nagoya Institute of Technology, for his sincere guidance and valuable comments during the critical part of my study. And, I am grateful to Professor Tetsuo Soga from Department of Frontier Materials, Nagoya Insititute of Technology, for his papatience in reviewing this dissertation. I am especially grateful to associate professor Akio Wakejima and assitant professor Toshiharu Kubo from Department of Engineering Physics, Electronics and Mechanics, Nagoya Institute of Technology, for their sincere guidance and valuable comments throughout this research. In additon, thanks are to special professor Kazuhisa Fujita and Osamu Oda of our research center for their constant encouragement and advice during this research.

I also wish to appreciate all members and colleagues including previous ones from Research Center for Nano-Device and System, Nagoya Institute of Technology, in particular, to Professor Gang Wang, Yang Liu, Baijun Zhang, Hao Jiang (all members currently at Sun Yan-sen University (SYSU), China), Dr. Jicai Zhang (currently at

Suzhou Institute of Nano-Tech and Nano-Bionics (SINANO), Chinese Academy of Sciences), Dr. Bin Abu Bakar AHMAD SHUHAIMI (currently at at University of Malaya (UM), Kuala Lumpur, Malaysia), Dr. Zhitao Chen, and Dr. Lin Lu for their honest and fruitful discussions during the entire study.

I am also grateful to the award of doctoral fellowship from the Ministry of Education, Culture, Sports, Science and Technology of Japan (MEXT), for financial support to accomplish my study at Nogoya Institute of Technology.

Finally, I wish to thank my family members, my relatives and friends, especially to my parents, wife, and ten-year-old son for their constant hearty supports and encouragements. In particular, I owe much to my wife Meiyu Wang, who has always inspired me to try my best and to realize my full potential. Moreover, I hope they would be proud of my Ph.D. study accomplishments.

Publications and Conferences List:

Publications:

1. J. C. Zhang, **Y. H. Zhu**, and T. Egawa, S. Sumiya, M. Miyoshi, and M. Tanaka, "Quantum-well and localized state emissions in AlInGaN deep ultraviolet light-emitting diodes" Appl. Phys. Lett. **91**, 221906 (2007).
2. J. C. Zhang, **Y. H. Zhu**, and T. Egawa, S. Sumiya, M. Miyoshi, and M. Tanaka, "Influence of pulse width on electroluminescence and junction temperature of AlInGaN deep ultraviolet light-emitting diodes" Appl. Phys. Lett. **92**, 191917 (2008).
3. J. C. Zhang, **Y. H. Zhu**, and T. Egawa, S. Sumiya, M. Miyoshi, and M. Tanaka, "Suppression of the subband parasitic peak by 1 nm *i*-AlN interlayer in AlGaN deep ultraviolet light-emitting diodes" Appl. Phys. Lett. **93**,131117 (2008).
4. Shigeaki SUMIYA, **Youhua ZHU**, Jicai ZHANG, Kei KOSAKA, Makoto MIYOSHI, Tomohiko SHIBATA, Mitsuhiro TANAKA, and Takashi EGAWA, "AlGaN-Based Deep Ultraviolet Light-Emitting Diodes Grown on Epitaxial AlN/Sapphire Templates", Jpn. J. Appl. Phys. **47**, 43 (2008).
5. **Y.H. Zhu**, S. Sumiya, J.C. Zhang, M. Miyoshi, T. Shibata, K. Kosaka, M. Tanaka and T. Egawa,"Improved performance of 264 nm emission AlGaN-based deep ultraviolet light-emitting diodes", Electron. Lett. **44**, 493 (2008).
6. **Y. H. Zhu**, J. C. Zhang, Z. T. Chen, and T. Egawa, "Demonstration on GaN-based light-emitting diodes grown on 3C-SiC/Si(111)", J. Appl. Phys. **106**, 124506 (2009).

7. Yusuke Sakai, **Youhua Zhu**, Shigeaki Sumiya, Makoto Miyoshi, Mitsuhiro Tanaka, and Takashi Egawa, "Demonstration of AlGaN-Based Deep-Ultraviolet Light-Emitting Diodes on High-Quality AlN Templates", Jpn. J. Appl. Phys. **49**, 022102 (2010).
8. **Youhua Zhu**, Arata Watanabe, Lin Lu, Zhitao Chen, and Takashi Egawa, "High Performance of GaN-Based Light Emitting Diodes Grown on 4-in. Si(111) Substrate", Jpn. J. Appl. Phys. **50**, 04DG08 (2011).
9. L. Lu, **Y. H. Zhu**, Z. T. Chen, and T. Egawa, "Effect of n-GaN thickness on internal quantum efficiency in $In_xGa_{1-x}N$ multiple-quantum-well light emitting diodes grown on Si (111) substrate", J. Appl. Phys. **109**, 113537 (2011).
10. **Youhua Zhu**, Arata Watanabe, Lin Lu, Zhitao Chen, and Takashi Egawa, "Characterization of GaN-Based Light Emitting Diodes Grown on 4-in. Si(111) Substrate", Jpn. J. Appl. Phys. (In press).

International Conferences:

1. **Y. H. Zhu**, Y. Sakai, J. C. Zhang, and T. Egawa, The 5th China International Exhibition & Forum on Solid State Lighting (CHINASSL2008), July 24-26, 2008, Shenzhen, China "Improved characteristics of InGaN LED on Si(111) using AlN/GaN multilayers".
2. J. C. Zhang, **Y. H. Zhu**, and T. Egawa, The 1st Japan-China-India Joint Workshop, Sept. 19, 2008, Nagoya Institute of Technology, Nagoya, Japan "AlInGaN UV LEDs grown by MOCVD".
3. J. C. Zhang, **Y. H. Zhu**, and T. Egawa,The 4th Asia-Pacific Workshop on Widegap Semiconductor, May 24-28, 2009, Zhang Jia Jie, Hunan, China, "The

emission mechanism and thermal behaviors of AlInGaN deep ultraviolet light-emitting diodes".

4. **Y. H. Zhu**, J. C. Zhang, and T. Egawa, The 4th Asia-Pacific Workshop on Widegap Semiconductor, May 24-28, 2009, Zhang Jia Jie, Hunan, China, "InGaN-based Light-emitting diodes on Si substrate using SiC intermediate layer".
5. J. C. Zhang, **Y. H. Zhu**, and T. Egawa, The 2nd China-Japan Joint Workshop on GaN-based Materials and Devices. Sept. 25, 2009, Beijing, China, "Study on electron overflow in AlGaN deep ultraviolet LEDs".
6. **Y. H. Zhu**, J. C. Zhang, and T. Egawa, The 2nd China-Japan Joint Workshop on GaN-based Materials and Devices. Sept. 25, 2009, Beijing, China, "InGaN blue LED grown on 3C-SiC/Si (111)".
7. Y. Sakai, **Y. H. Zhu**, and T. Egawa, The 1st International Symposium on Advanced Plasma Science and its Applications, March 8-11, 2009, Nagoya, Japan, "Demonstration of AlGaN-based deep-UV LEDs on AlN templates".
8. L. Lu, **Y. H. Zhu**, and T. Egawa, The 8th International Symposium on Semiconductor Light Emitting Devices (ISSLED2010), May 16-21, 2010, Peaking University, Beijing, China, "Effect of the thickness of n-GaN underlayer to InGaN-based multi-quantum well grown on Si(111) substrate".
9. **Y. Zhu**, A. Watanabe, L. Lu, Z. Chen, and T. Egawa, 2010 International Conference on Solid State Devices and Materials, September 22-24, 2010, Tokyo, Japan, High performance GaN-based light-emitting diodes grown on 4-inch Si (111)".

10. **Y. Zhu**, A. Watanabe, L. Lu, Z. Chen, and T. Egawa, The 3rd International Symposium on Advanced Plasma Science and its Applications, March 6-9, 2011, Nagoya, Japan, " Characterization of GaN-Based Light Emitting Diodes Grown on 4-in. Si(111) Substrate".
11. **Y. H. Zhu**, L. Lu, Z. T. Chen, and T. Egawa, The 5th Asia-Pacific Workshop on Widegap Semiconductor, May 22-26, 2011, Ise-Shima National Park, Mie, China, "Effect of n-GaN thickness on GaN-based Light-emitting diodes grown on 4-inch Si(111) substrate".
12. **Y. H. Zhu**, A. Watanabe, L. Lu, Z. T. Chen, and T. Egawa, The 4th International Joint Workshop on III-V Compound Semiconductors and Devices. Sept. 4, 2011, Xi'An, China, "Correlations of structural and optical property in InGaN-based light-emitting diodes with different n-GaN thickness grown on 4-inch Si(111)".